# MINERALOGICAL, PETROGRAPHICAL AND GEOCHEMICAL PROPERTIES OF ZEOLITE BEARING TUFFS IN NW ANATOLIA (TURKEY)

A THESIS SUBMITTED TO
THE GRADUATE SCHOOL OF NATURAL AND APPLIED SCIENCES
OF
MIDDLE EAST TECHNICAL UNIVERSITY

BY

SEVGİ ÖZEN

IN PARTIAL FULFILLMENT OF THE REQUIREMENTS
FOR
THE DEGREE OF MASTER OF SCIENCE
IN
GEOLOGICAL ENGINEERING

SEPTEMBER 2008

Approval of the thesis:

**MINERALOGICAL, PETROGRAPHYCAL AND GEOCHEMICAL PROPERTIES OF ZEOLITE BEARING TUFFS IN NW ANATOLIA (TURKEY)**

submitted by **SEVGİ ÖZEN** in partial fulfillment of the requirements for the degree of **Master of Science in Geological Engineering Department, Middle East Technical University** by,

Prof. Dr. Canan Özgen       _____
Dean, Graduate School of **Natural and Applied Sciences**

Prof. Dr. Vedat Doyuran       _____
Head of Department, **Geological Engineering**

Prof. Dr. M. Cemal Göncüoğlu       _____
Supervisor, **Geological Engineering Dept., METU**

Assist. Prof. Dr. Fatma Toksoy Köksal       _____
Co-Supervisor, **Geological Engineering Dept., METU**

**Examining Committee Members:**

Prof. Dr. Asuman G. Türkmenoğlu       _____
Geological Engineering Dept., METU

Prof. Dr. M. Cemal Göncüoğlu       _____
Supervisor, Geological Engineering Dept., METU

Prof. Dr. Zeki Çamur       _____
Geological Engineering Dept., METU

Prof. Dr. Selahattin Kadir       _____
Geological Engineering Dept., University of Osmangazi

Dr. Semih Gürsu       _____
Natural History Museum, MTA

**Date:**       03.09.2008

**I hereby declare that all information in this document has been obtained and presented in accordance with academic rules and ethical conduct. I also declare that, as required by these rules and conduct, I have fully cited and referenced all material and results that are not original to this work.**

Name, Last name : Sevgi ÖZEN

Signature        :

# ABSTRACT

## MINERALOGICAL, PETROGRAPHICAL AND GEOCHEMICAL PROPERTIES OF ZEOLITE BEARING TUFFS IN NW ANATOLIA (TURKEY)

ÖZEN, Sevgi

M.Sc., Department of Geological Engineering

Supervisor: Prof. Dr. M. Cemal Göncüoğlu

Co-Supervisor: Assist. Prof. Dr. Fatma Toksoy Köksal

September 2008, 210 pages

The purpose of this study is to understand the geological, petrographical, mineralogical and geochemical characteristics of analcime-bearing tuffs in the Biga Peninsula and to determine formation process of these tuffs.

The study area lies between Ayvacık and Küçükkuyu. The rock units are pre-Eocene basement rocks, Miocene Behram Volcanics (Arıklı Tuff, andesite, andesitic agglomerate), Pliocene volcanics, Miocene lacustrine sediments (Küçükkuyu Formation) and Quaternary alluvium. Analcimes which are found in Arıklı Tuff are the main objective of this study.

Detailed petrographical, mineralogical and geochemical studies were caried out on the Arıklı Tuff samples by using petrographical microscope, X-ray diffractometry, scanning electron microscopy, diffrential thermal analyses

inductively coupled plasma – mass spectrometry and optical emission spectrometry.

Fine-grained and coarse-grained analcime crystals in Arıklı Tuff were determined by their colorless, isotropic, trapezohedral and low relief. In addition to petrographic study, SEM and XRD methods also confirmed the presence of analcime.

Two modes of occurrences were determined by the petrographical and mineralogical studies; coarse-grained euhedral or anhedral crystals in cavities and pumice fragments and single crystals or clusters of fine-grained analcimes embedded in the matrix.

It was stated that there are two types of formation of analcime; alteration of volcanic glass and precipitation from alkaline solution based on petrographical and SEM studies. Geochemical methods, moreover, support the formation types.

# ÖZ

# KUZEYBATI ANADOLU'DAKİ (TÜRKİYE) ZEOLİT İÇEREN TÜFLERİN MİNERALOJİK, PETROGRAFİK VE JEOKİMYASAL ÖZELİKLERİ

ÖZEN, Sevgi

Yüksek Lisans, Jeoloji Mühendisliği Bölümü

Tez Yöneticisi: Prof. Dr. M. Cemal GÖNCÜOĞLU

Ortak Tez Yöneticisi: Yrd. Doç. Dr. Fatma Toksoy Köksal

Eylül 2008, 210 sayfa

Bu çalışmanın amacı, Biga Yarımadası'ndaki analsim içeren tüflerin jeolojik, petrografik, mineralojik ve jeokimyasal özeliklerini anlamak ve oluşum modellerini ortaya koymaktır.

Ayvacık-Küçükkuyu arasında bulunan çalışma alanı beş farklı birim içerir. Bunlar Eosen öncesi metamorfik temel, Behram Volkanikleri (Arıklı Tüfü, andesit, andesitik aglomera), Pliyosen Volkanikleri, Miyosen gölsel çökelleri ve Kuvaterner alüvyonudur. Arıklı Tüfü'nün içinde bulunan analcime bu çalışmanın asıl amacını oluşturmaktadır.

Arıklı Tüfü'ne uygulanan detaylı petrografik ve mineralojik çalışmalar X-ışınları difraktometresi, optik mikroskop, elektron mikroskobu, diferansiyel termal metod ve jeokimyasal çalışmalar ile yürütülmüştür.

Arıklı Tüfü'nün içinde bulunan ince ve kalın taneli analsim kristalleri renksiz, izotrop, trapezohedral şekil ve düşük rölyef özellikleri ile saptanmıştır. Petrografik çalışmalara ek olarak SEM ve XRD çalışmaları ile de analsim varlığı teyit edilmiştir.

Petrografik ve mineralojik çalışmalar ile iki oluşum şekli saptanmıştır; boşluklarda ya da pümisin içinde kalın taneli özşekilli ya da yarı özşekilli kristaller ve hamurun içinde gömülü olan tek ya da küme halinde bulunan kristallerdir.

Petrografik ve SEM çalışmalarının ışığı altında iki adet oluşum tipi belirlenmiştir. Bunlar volcanic camdan alterasyon ile oluşma ve alkali sulardan çökelme ile oluşum şeklidir. Jeokimyasal metodlar bu oluşum modellerini desteklemektedir.

Anahtar Sözcükler: analsim, tüf, volkanik cam, petrografi, Biga Yarımadası (Türkiye)

To My Parents

# ACKNOWLEDGMENTS

# TABLE OF CONTENTS

# LIST OF TABLES

**TABLES**

# LIST OF FIGURES

**FIGURES**

xvi

xvii

# ABBREVIATIONS

**Anl:** analcime

**Dol:** dolomite

**Phyll:** phyllosilicate mineral

**Kfs:** K-feldspar

**Qtz:** quartz

**Sme:** smectite

**Bio:** biotite

**VG**: volcanic glass

**PF**: pumice fragment

**GS:** glass shard

**RF:** rock fragment

**AD:** air-dry

**EG:** ethylene glycol

# CHAPTER 1

# INTRODUCTION

## 1.1. Purpose and Scope

Zeolites occur in many rock-types, of different ages and geologic settings. Most of the early work was on zeolites in cavities of basalt flows (Hay, 1978). Later work, however, showed that zeolite minerals were formed mainly by reactions in volcanic tuffs and tuffaceous sedimentary rocks in lacustrine environments. Zeolites were known for more than 200 years. However, it was after 1950s that detailed scientific work on their chemical and physical properties was started and their geological significance in tuffaceous sedimentary rocks was recognized. Analcime, a type of sodium zeolite, was noticed, when large amounts were discovered in the USA. Then, several investigations have been conducted to reveal properties of analcimes.

Although many studies have already been carried out on the mineralogical and chemical properties and occurrence of zeolites in NW Anatolia, the detailed examinations of analcimes in Küçükkuyu, Yeşilyurt and Arıklı areas of the Biga Peninsula are not available.

The purpose of this study is to examine the mineralogical-petrographical-geochemical features of analcime-bearing Neogene tuffs and to understand the analcime formation in Küçukkuyu-Yeşilyurt-Arıklı region. With these aims, geological, petrographical, mineralogical and geochemical studies were performed.

This Master's Thesis study, mainly based on mineralogy, petrography and geochemistry of the analcimes, was carried out to learn the analytical methods in studying zeolite minerals and to interpret the occurrence of analcimes in tuffs. For this, the tuffs were examined under optical microscope, analyzed by X-ray diffractometry, associated with differential thermal method and scanning electron microscopy. In addition, geochemical characteristics of the tuff samples were investigated to understand the behavior of mobile elements during diageneses and alteration.

## 1.2. Geographic Setting

The study area is located between Ayvacık and Küçükkuyu settlements to the southeast of Çanakkale. It covers an area of approximately 20 km$^2$ which is included in quadrangles i16-c3 and i17-d4 of the 1:25 000 topographic map of Turkey (Figure 1).

The main topographic features in the study area are ridges and valleys. Ridges are characterized by rugged morphology. Valleys trend in south-north direction. The highest elevations in the region are Kale Tepe (316 m), Çarşılı Tepe (451 m), Zindan Tepe (354 m) and Kocameşe Tepe (398 m). There are large stream networks in the area. Dereyol Dere is just near Arıklı, Öküz Dere is between Yeşilyurt and Nusratlı. The region is moderately forested and covered by olive-trees. It is easy to arrive the study area from Edremit to Küçükkuyu and Nusratlı along Edremit-Çanakkale Highway. The village and forest roads in the study area make most of the study area easily accessible.
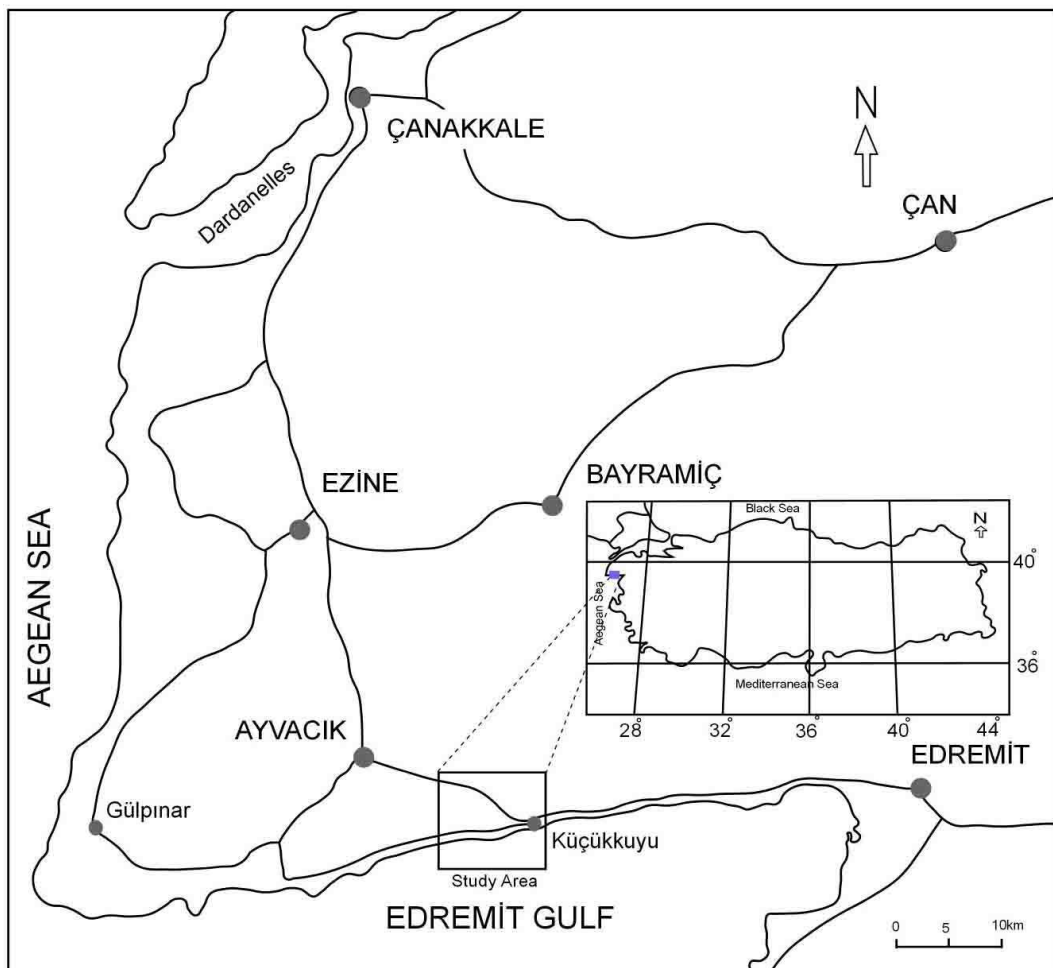
**Figure 1.** Location map of the study area.

## 1.3. Methods of Study

This study consists mainly of two stages as field and laboratory work.

### 1.3.1. Field Work

Field studies were done during the summer 2006 and were mainly concentrated on detailed sampling by the aid of the detailed 1/25 000 scaled geological map

prepared by Çelik et al. (1995). Approximately 90 samples were collected from different localities, including mainly pyroclastic rocks (Arıklı Tuff) in order to check for the presence of analcimes. As the other rock-types including the associated lavas were devoid of analcime and hence not the main object of the study, they were not studied in detail.

### 1.3.2. Laboratory Work

Laboratory work was mainly based on petrographical, mineralogical and geochemical analyses of the collected samples. Several analytical methods such as; petrography, X-ray diffractometry, scanning electron microscopy, differential thermometry, inductively coupled plasma – mass spectrometry (ICP-MS) and optical emission spectrometry (ICP-OES) were carried out to determine the mineralogy and to understand the processes responsible for analcime formation.

Petrographical study formed an important part of the laboratory work of the thesis. Thin sections were prepared in the Thin Section Preparation Laboratory of the Geological Engineering Department of the Middle East Technical University. A total of thirty-two thin sections was examined under a Nikon polarizing microscope in order to study the mineralogical, petrographical and textural features of the rocks. Mainly, thin sections of the Arıklı Tuff were examined under the microscope, since analcime formations, the main issue of this study, were restricted to these tuffs. Several photomicrographs were taken by using image analyzer system attached the Nikon camera in the Department of Geological Engineering of METU.

Twenty tuff samples were examined using X-ray diffractometry (XRD) at General Directorate of Mineral Research and Exploration. X-ray diffraction patterns were recorded using Rigaku D/Max-3C diffractometer with high power CuKα source operating at 40kV/30mA. XRD patterns were collected with a scan rate of 10

degree/min in the range of 0-70º for 20 tuff samples. Three tuff samples, on the other hand, were recorded with a scan rate of 10 degree/min in the range of 0-25º for detail clay analysis in the Department of Geological Engineering of METU by using Rigaku MiniFlex II diffractometer using CuKα radiation operating at 30kV/15mA.

Scanning electron microscope (SEM) was used to check the analcime presence and was utilized to examine the actual three-dimensional crystal relationships of minerals that were petrographically interpreted with Jeol 6400 scanning electron microscope in Metallurgical and Materials Engineering Department and Quanta 400F scanning electron microscope in the Central Laboratory.

Differential thermal analyses (DTA) and thermogravimetry (TG) analysis were carried out by Simultaneous Thermogravimetric Differential Thermal Analyses (SETARAM) in the Central Laboratory at METU.

Seventeen zeolite-bearing and three zeolite-free tuff samples were selected for geochemical analyses. Rock specimens of 50 to 60 g were broken with a hammer to centimeter-scale pieces and crushed into smaller pieces in an agate mortar. The agate mortar was carefully cleaned after each crushing to prevent cross-contamination of samples. After this crushing, approximately 20 g of tuff samples were again grind in an agate mortar. The powder was sieved using a 200 mesh-size sieve and the powder below 200 mesh was taken. After this, 20 g powder was weighted and sent for major, trace and REE analyses to the ACME Analytical Laboratories, Canada. Inductively Coupled Plasma-optical emission spectrometry (ICP-OES) was used for major elements and Inductively Coupled Plasma-mass spectrometry (ICP-MS) technique was used for trace elements and REE's in the analyses.

## 1.4. Previous Work

Previous studies are organized under three sections. The first section deals with the geology of the Biga Peninsula. The second section summarizes studies that were carried out on zeolites and the last section deals with the analcimes.

## 1.4.1. Previous Work on the Geology of the Biga Peninsula

Several researchers have examined the study area. From these Borsi et al. (1972) studied the volcanic units in terms of petrology and geochronology. They identified that the early-middle Miocene volcanism was calc-alkaline in character.

Bingöl et al. (1973) reported on the general stratigraphy and the tectonic features of the Biga Peninsula. According to these authors the Biga Peninsula consists from bottom to top of; pre-Permian Kazdağ Group, Early Triassic Karakaya Formation, Triassic clastics, Jurassic limestone and sandstone, Eocene and Neogene volcanics. Furthermore, they prepared a 1/25 000 scaled geological map of the area.

Öngür (1973) mainly studied the volcanic units, differentiated and named them in the western Biga Peninsula. Öngür (1973) mentioned that the volcanic activity was mainly concentrated on three centers. They were named as Ayvacık, Babakale and Assos volcanics. Öngür (1973) also stated that Ayvacık volcanics consists of Ayvacık lava, whereas the Babakale volcanics comprise an alternation of lava and breccia. Assos volcanic on the other hand constitutes of lavas, lahar and ignimbritic tuffs.

Ercan (1979) studied the geochemical features of Cenozoic volcanics in western Anatolia, Thrace and Aegean islands. He suggested that Cenozoic volcanics are

calc-alkaline and alkaline in character. The Cenozoic volcanic include andesitic-dacitic-rhyodacitic-rhyolitic lavas, tuffs and agglomerates.

Gevrek et al. (1984-1985) investigated the formation and distribution of hydrothermal alteration zones and their relationship with geothermal fluid circulation in volcanic rocks in the Biga area.

Siyako et al. (1989) studied the geology and hydrocarbon potential of the Tertiary basins in the Biga and Gelibolu Peninsulas. They grouped the end Mesozoic-Early Tertiary rocks into four lithostratigraphic units as Maastrichtian-early Eocene, middle Eocene-Oligocene, Miocene and Plio-Quaternary sediments. They observed that widespread calc-alkaline magmatism occurred in early-middle Miocene in the Biga and Gelibolu Peninsulas. They also pointed out the distribution of the volcanic rock-units, which were named as Taştepe, Ezine and Akçaalan volcanics in their geological map.

Okay et al. (1990) evaluated geology and tectonic evolution of the basement rocks of the region in detail. They recognized four distinct NE-SW trending tectonic zones in the Biga and Gelibolu peninsulas, which are Gelibolu, Ezine, Ayvacık-Karabiga and Sakarya zones. This MSc study is located in the Ayvacık-Karabiga zone of Okay et al. (1990).

Ertürk et al. (1990) investigated Cenozoic volcanic rocks of the Biga Peninsula petrographically and geochemically. According to these authors, volcanism started in Paleocene-Eocene and continued in Miocene time. Based on geochemical data they suggested that Paleocene-Eocene Akçaalan and early-middle Miocene Ezine volcanics are calc-alkaline and late Miocene Ezine and Taştepe volcanics are alkaline.

Ercan et al. (1995, 1996) studied Tertiary volcanism of the Biga Peninsula and Gökçeada, Bozcaada and Tavşan islands. They discussed the regional distribution

and geochemical characteristics of this volcanism that commenced in Eocene and continued until the end of upper Miocene. Volcanic rocks were organized into six main groups by these authors: Balıklıçeşme volcanics, Çan volcanics, Kirazlı volcanics, Behram volcanics, Hüseyinfakı volcanics and Ezine basalt. They studied volcanic rocks petrographically and geochemically, and made radiometric age determination by K/Ar method except those of Balıklıçeşme volcanics. The ages they reported were 34.3±1.2-23.6±0.6 Ma for Çan volcanics, 31.4±0.4 Ma for Kirazlı volcanics, 21.5-16.8 Ma for Behram volcanics, 15.3±0.3 Ma for Hüseyinfakı volcanics and 8.4±0.3 Ma for Ezine basalt. Moreover, Ercan et al. (1995, 1996) put forward that Eocene-middle Miocene volcanics are of calc-alkaline and upper Miocene volcanics are of alkaline nature.

Karacık and Yılmaz (1995) presented general geological features of the ignimbrite eruptions from the Ezine-Ayvacık area. They carried out a detailed field study and distinguished different volcanostratigraphic units. They divided the volcanic rocks into two main groups. These are the Ayvacık Volcanic Association and the Balabanlı Volcanics. The Ayvacık volcanics consist of rhyolite, rhyodacite lavas, pyroclastic-fall deposits, andesitic and trachyandesitic lavas. Balabanlı volcanics, on the other hand, consist of alternations of pyroclastic units, flows and detrital sediments. From these, Karacık and Yılmaz (1995) examined the petrography of Balabanlı volcanics in detail.

Ercan et al. (1996) made radiometric age determination using the K/Ar and Rb/Sr techniques from volcanic rocks having different volcanic episodes in western Anatolia. They stated that the oldest rock in this region is Selendi Volcanics (18,0±0,2 Ma) and the youngest one is Kula Volcanics (0.1-0.2 Ma). They also obtained geochemical data to contribute the petrological evolution of the regional volcanism.

Karacık and Yılmaz (1998) introduced the detailed stratigraphy of volcanic assemblages in the Ezine area. They also studied the geochemical and petrological features of volcanic rocks and proposed their source as "enriched mantle".

Ercan et al. (1998) revealed the Tertiary volcanism around the Sea of Marmara. They investigated the regional extension of the volcanic rocks, their ages, eruption episodes, petrochemical features, genetic explanations together with their relations with the adjacent sedimentary rocks.

Çelik et al. (1999) studied phosphate mineralization in the Ayvacık-Küçükkuyu area. Nodular phosphate formations with concentric shape, widespread in Neogene tuffs in this region were firstly described in this study. They analyzed more than 500 samples to study the mineralization in the tuffs. As one of the results of their analysis, they reported the presence of analcime in several tuff samples. They prepared the 1/25 000 and 1/5 000 scaled geological maps of the western Küçükkuyu area, which were used for field study in this thesis.

Okay and Satır (2000) provided new petrologic and isotopic data on a large area of metamorphic rocks (Çamlıca metamorphics) from the western Biga Peninsula. They showed that these rocks underwent eclogite-facies metamorphism in Late Cretaceous.

In the W and SW Biga Peninsula, Yılmaz et al. (2001) identified two distinct magmatic episodes: calc-alkaline association during the Oligocene-Early Miocene and alkaline one during the Late Miocene-Pliocene. They described major geochemical characters of these two magmatic associations. They also discussed the tectono-magmatic evolution of the southwestern part of Biga Peninsula.

Dönmez et al. (2005) allocated Eocene volcanic rocks into five different formations based on stratigraphy and lithology and mapped them in detail. They confirmed the presence of Eocene marine ignimbrites around Umurbey,

Balıklıçeşme, Çan and Bayramiç villages. They mapped these units and suggested a model of formation.

Çiftçi et al. (2004) studied Neogene stratigraphy of the Gulf of Edremit region, NW Turkey. They stated that Neogene units were characterized by lacustrine sedimentary rocks and volcanic rocks. Volcanic rocks represent seven distinctive volcanic episodes with different ages and these were intercalated with lacustrine sediments. They also evaluated the hydrocarbon possibilities in the region.

## 1.4.2. General Information and Previous Work on the Zeolites

The history of zeolites started by A. F. Cronsted, Swedish mineralogist in 1756 when he collected well-formed crystals from the Svappavari Copper Mine, Sweden. He named these minerals as zeolites from the Greek words "ξειν"= "to boil" and "λινος"= "stone" since these minerals eject water when heated and hence seems to boil (Mumpton, 1978; Gottardi, 1978; Gottardi and Galli, 1985). "A zeolite is an alumino-silicate whose framework structure which is $(Si,Al)O_4$ contains channels filled with water and exchangeable cations" (Gottardi, 1978). This important property, which is known as "ion- exchange capacity" is possible at low temperatures (100 ºC at the most) and water is lost at about 250 ºC and can be re-adsorbed at room temperature (Gottardi and Galli, 1985). The general chemical formula of zeolites is

$$(Na,K)_x(Mg,Ca,Sr,Ba)_y[Al_{x+2y}Si_{n-(x+2y)}O_{2n}].mH_2O \text{ (Gottardi, 1978)}$$
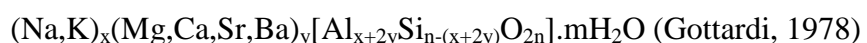
The most common naturally occurring zeolites in sedimentary rocks are analcime, clinoptilolite, heulandite, laumontite and phillipsite. Chabazite, erionite, mordenite, natrolite and wairakite, on the other hand, are in lower abundance (Hay, 1978).

"In recent years, zeolite minerals with attractive physical and chemical properties draw attention of commercial interest of many branches i.e. geological, mineralogical, chemical, industrial and agricultural. Natural zeolites can be used for many application aspects. For example they are used as filler in the paper industry, as ion exchangers in wastewater treatment, in the separation of oxygen and nitrogen from air, as lightweight aggregate and so on" (Mumpton, 1978).

Compositions of zeolites are listed in Table 1 with decreasing $Si/Al+Fe^{3+}$ and hydration values (Hay, 1978).

**Table 1.** Compositional features of common zeolites (Hay, 1978).

| Name | $Si/Al+Fe^{3+}$ | Dominant cations | $H_2O$ molecules per Al atom |
|---|---|---|---|
| Clinoptilolite | 4.0-5.1 | K>Na | 3.0-3.5 |
| Mordenite | 4.3-5.3 | Na>K | 3.2-3.5 |
| Heulandite | 2.9-4.0 | Ca, Na | 2.5-3.0 |
| Erionite | 2.9-3.7 | Na, K | 3.0-3.4 |
| Chabazite | 1.7-3.8 | Ca, Na | 2.7-4.1 |
| Phillipsite | 1.3-3.4 | K, Na, Ca | 1.7-3.3 |
| Analcime | 1.7-2.9 | Na | 1.0-1.3 |
| Laumontite | 2 | Ca | 2 |
| Wairakite | 2 | Ca | 1 |
| Natrolite | 1.5 | Na | 1 |

In this chapter, based on a review of previous studies only the geology of natural zeolites and zeolitic rocks will be overviewed for an introduction in the thesis study.

Cronstedt (1756) first recognized zeolite minerals in cavities and vugs of basalts in minor amounts. Mineralogical description of these minerals was the only primary studies of zeolites for a long time. Later, it was understood that zeolite occurrences are not restricted only to basalt cavities. A major early discovery was phillipsite in deep-sea sediments during explorations by the H. M. S. Challenger (Murray and Renard, 1891; Hay, 1978). Johannsen (1914) noted that fine-grained zeolites were found in the Eocene tuffs in Colarado, Wyoming and Utah. This early work was followed by reports of zeolites in saline-alkaline lake beds (Bradley, 1928; Ross, 1928). Several kinds of zeolites were next identified. Eskola (1936) established zeolite facies in very low-grade metamorphic rocks. Coombs (1971) studied this zeolite facies more in detail and he recognized vertical zoning of zeolites in sedimentary basins. This finding is very important due to interpretations of burial depth, pressure and temperature. Hay (1966) and Mumpton (1978) noticed the great abundance of zeolites in many lithologies and this led to several geological studies on the occurrence of zeolites. As a result of several geological-mineralogical studies, six main modes of geological occurrence of zeolites were established (Hay, 1966, 1970, 1977, 1978; Iijima and Utada, 1972; Iijima, 1980; Sheppard, 1973; Munson and Sheppard, 1974).

**1) Saline–alkaline lakes:** The most common occurrence is in saline-alkaline lake deposits through all of the occurrences. These zeolites were generally formed by reaction of volcanic glass with saline-alkaline solutions (Hay, 1966). Clinoptilolite, phillipsite and erionite generally form as a result of this reaction. These alkali zeolites may be transformed to analcime and analcime may also be transformed to K-feldspar resulting in a lateral zonation in the lakes (Hay, 1966; Sheppard and Gude, 1968; 1969a; Surdam and Sheppard, 1978; Iijima, 1980; Hay, 1978). Figure 2-a shows this zonation in saline alkaline lake deposits. Here from outer to the inner zones, salinity increases (Sheppard and Gude, 1968; Hay, 1978). Sheppard and Gude (1968) described an excellent example of such a zoning in the Cenozoic rocks in the Green River Formation.
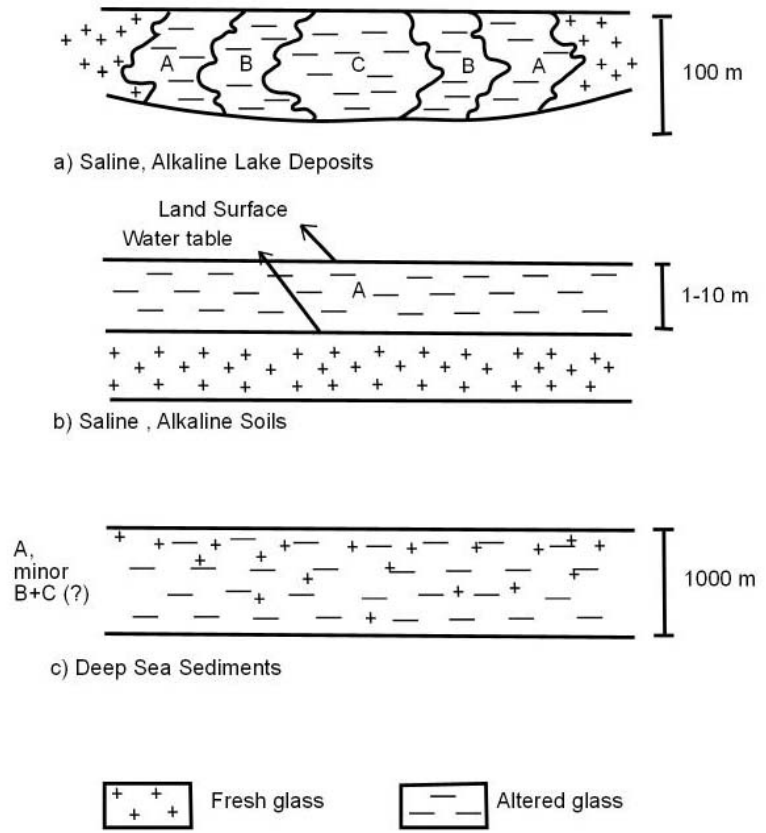
**Figure 2**. Diagrams showing patterns of authigenic zeolites and feldspars in tuffs of saline, alkaline lakes; saline, alkaline soils and deep-sea sediments. Zone A is characterized by alkali-rich zeolites without analcime, zone B by analcime and zone C by feldspars (After Hay, 1978).

**2) Zeolites of soils and land surfaces:** Zeolites also form from soils with suitable alkaline conditions, where pH is high enough (Hay, 1978). Hay (1966) stated that saline-alkaline soils only between land surface and water table altered to zeolites because rain contains sodium carbonate-bicarbonate circulating only in this region (Figure 2-b). Reaction rates of volcanic glass are the same as in saline-alkaline lakes (Hay, 1963b). Example of this type of occurrence is the San Joaquin Valley of California (Baldar and Whitting, 1968).

**3) Zeolites in marine sediments:** Zeolites occur in a wide variety of marine sediments (Hay, 1978; Iijima, 1980). A study of zeolites in marine sediments was first made by Murray and Renard (1891). However, most of the available information was gained by the Glomar Challenger expeditions during the Deep-Sea Drilling Program (DSDP). Phillipsite and clinoptilolite are the dominant zeolites in deep-sea sediments (Hay, 1978). Analcime exists not much, erionite and mordenite are rare. Zeolitization of this type forms by reaction of volcanic glass or poorly crystalline aluminosilicate material with sea-water at low temperature. Reaction rates are slow. No vertical or lateral zoning was established (Figure 2-c) (Hay, 1978).

**4) Zeolites of the open-system type:** The open-system type shows vertical zonation (Figure 3-a). When meteoric water circulates in deeper parts of vitric ash, the chemical composition of it was changed. The upper zone of ash contains fresh glass and montmorillonite. The lower zone contains clinoptilolite and underlying zone contains analcime with or without K-feldspar (Hay, 1963a, 1966; Walton, 1975; Hay, 1978). The example of open-system type is the Vieja Group of Texas (Walton, 1975).

**5) Hydrothermal zeolites:** These types of zeolites commonly occur in areas of volcanic activity due to high geothermal gradient (Hay, 1978). These may show well-defined zeolitic zonation. The example of this type zeolitization is Yellowstone Park in U.S.A. (Fenner, 1936) (Figure 3-b).

**6) Zeolites of burial diagenetic type:** Burial diagenetic type was established by Coombs (1971). Zeolitic burial diagenesis (very low grade metamorphism, Zeolite Facies) occurs in a thick sequence of strata with increasing depth (Hay, 1966; Hay, 1978; Iijima and Utada, 1966; Iijima, 1980). Burial diagenetic type zeolites show vertical zonations with increasing temperature with depth (Figure 3-c). From upper to lower, these zones are fresh glass, clinoptilolite and mordenite, analcime and heulandite and finally laumontite and albite (Hay, 1978).
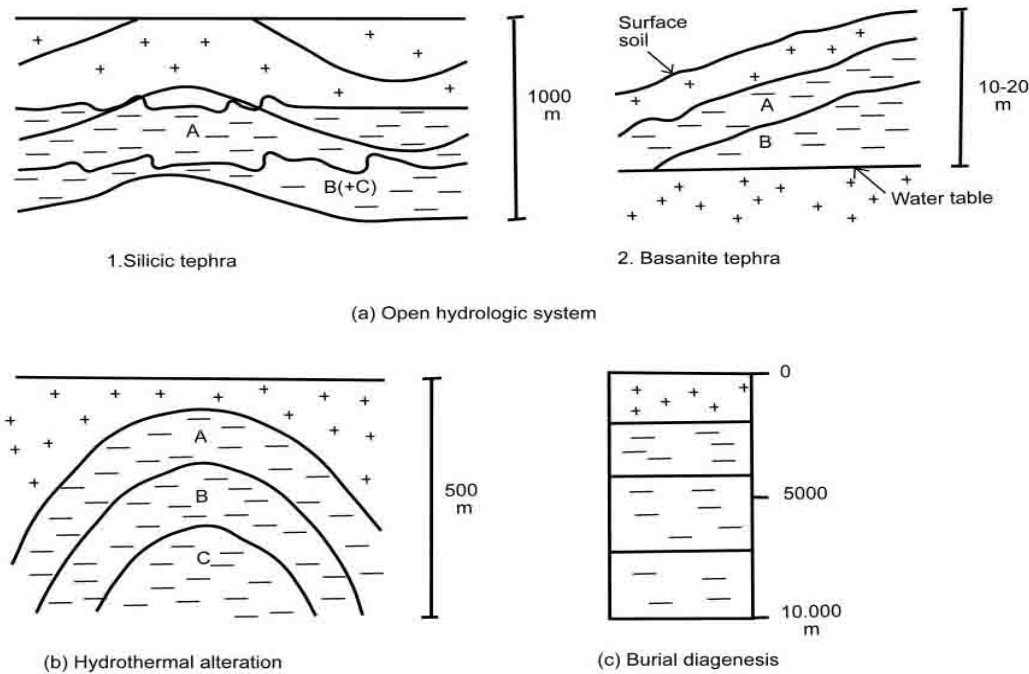
**Figure 3.** Diagrams showing patterns of authigenic zeolites and feldspars in tuffs where the zonation is of a) open-system type, b) hydrothermal-type and c) as a result of burial diageneses. Zone A is characterized by non-analcime alkali-rich zeolites, zone B by analcime or heulandite and zone C by K-feldspar in (a1) by albite with of without laumontite in (b) and (c). Symbols are the same as Figure 2 (After Hay, 1978).

### 1.4.3. General Information and Previous Work on the Analcimes

Analcime has been known for a long time, but the interest to them changed rapidly in the last 30 years. Haüy (1801) proposed the name "analcime" from the Greek word "forceless" because of its poor ability in acquiring frictional electricity (Gottardi and Galli, 1985).

The symmetry of analcime was firstly determined as isometric by Taylor (1930). Coombs (1955), on the other hand, showed some differences from cubic

15

symmetry. Later, it was noticed by Mazzi and Galli, (1978) that there are at least two different symmetries. Hazen and Finger (1979) confirmed the differences from cubic structure. They proved not only cubic symmetry but also tetragonal, orthorhombic or even monoclinic or triclinic one. The detail morphology of analcimes will be given in the Chapter 4.3. (SEM analyses).

Analcime is a common authigenic silicate mineral in volcaniclastic rocks. It is a less hydrous and less siliceous zeolite and its dominant cation is $Na^+$, as can be seen in Table 1. Its chemical formula is

$$Na_{16}Al_{16}Si_{32}O_{96}.16H_2O \text{ (Hay, 1978)}$$
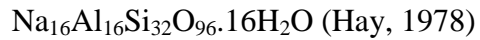
Analcime was firstly reported in tuffs of the Green River Formation of Wyoming by Bradley (1928) and in the Big Sandy Formation of Wikieup, Arizona by Ross (1928). Bradley (1928) called attention to the large amount of occurrence of analcime in the Green River Formation. These studies lead to greater emphasis on recognition of occurrence of analcime. Then, several researchers have conducted studies to reveal their valuable mineralogical, chemical and physical properties, their occurrences in tuffaceous sedimentary rocks and their potential applications of industrial and agricultural technology.

Analcime is a common authigenic silicate mineral in sediments and sedimentary rocks. It occurs in the same geologic settings as other zeolites, mentioned above. Saline-alkaline lake deposits are the most common ones of these occurrences and analcimes are mainly found in these occurrences.

Ross (1928) made a detailed study on the crystal form, optical properties and chemical compositions. Later, Ross (1928) also tried to interpret the formation of analcime. The material Ross initially studied contained glassy ash. Even though this kind of material must alter to bentonite, bentonite was not observed in his samples. Thus, Ross (1928) explained the formation of analcime based on reaction

between concentrated sodium salts and glass ash. Bradley (1928) described similar occurrences of analcimes. Later, High and Picard (1965) stated that analcime was formed from alteration of volcanic ash by water, rich in dissolved salts. Both volcanic ash and the water supplied the necessary $Na^+$ ions for the analcime. Later, Iijima and Utada (1966), Iijima (1980) also supported the idea that formation of analcime was from volcanic glass. Surdam and Sheppard (1978), however, suggested that analcime does not form directly from glass, but it forms with the alteration of a precursor alkaline zeolites. In addition to alkali zeolites (Surdam and Sheppard, 1978; Surdam and Parker, 1972), gels (Surdam and Eugster, 1976) and clay minerals (Brobst and Tucker, 1973; Keller, 1952; Hay and Moiola, 1963) derived from volcanic glass causes the formation of analcime. Sheppard (1971), Van Houten (1962), Hay (1966) and Wu (1970) said that analcime might precipitate directly from saline-alkaline lake water.

The studies on the formation of analcime and other zeolites in Turkey have started in the 1970's. One of the earliest studies was Ataman and Beseme (1972) in the region of Bahçecik, Gölpazari and Göynük. Later, analcime rocks in the Anatolian Tertiary Basins and their geologic positions were studied by Ataman and Gündoğdu (1981). They confirmed that Tertiary and especially Neogene successions owe some geological series with analcime as principal rock-forming mineral. Analcime-rich zones in the Tertiary Basins are Bahçecik-Gölpazarı-Göynük (Paleogene), Nallıhan-Çayırhan-Beypazarı-Mihalıçcık (Neogene), Polatlı-Mülk-Oğlakçı-Ayaş (Neogene), Kalecik-Çandır-Şabanözü (NW of Ankara) (Neogene) and Ahiboz (SE of Ankara) (Neogene) (Ataman and Gündoğdu, 1981).

Analcimes were also studied in detail by Ataman (1977). Zeolite occurrences in Anatolia comprising Ankara-Polatlı, Bigadiç, Şaphane, Gediz, Emet and Gördes regions were examined and analcime and clinoptilolite were detected in high amounts. Ataman (1977) stated that west Anatolia is an important region for the

formation of zeolites in Neogene and that zeolites can be formed by not only precipitation but also alteration of acidic tuffs.

Esenli et al. (2005) studied zeolitization of tuffaceous rocks in the Keşan region, Thrace. Vitreous tuffs of dacitic composition of Oligocene age altered to zeolites including mordenite, clinoptilolite-heulandite and analcime. Since there is a marked vertical zonation in zeolites, they suggest that the chemical environment was controlled by different hydrological systems. They further put forward that the conditions in open hydrological system changed to the closed lacustrine environment. Analcime formation was determined directly from volcanic glass as heulandite-clinoptilolite and mordenite.

Çelik et al. (1999) prepared an exploration report for phosphate rich beds in the region between Ayvacık and Küçükkuyu, where the present MSc study was performed. They prepared geological maps of 1/25 000 and 1/5 000 that was used in the present study. They investigated more than 500 rock samples petrographically and mineralogically by optical microscope and XRD method. Although the aim of their study was to determine the phosphate rich beds, they also observed analcime occurrences and plotted them on their 1/5 000 map. There is no further information about analcimes but only their locations.

# CHAPTER 2

# GEOLOGY OF THE STUDY AREA

## 2.1. Regional Geology

The basement of Biga Peninsula comprises Paleozoic-Early Mesozoic metamorphic rocks (Bingöl et al., 1973). These metamorphic rocks are unconformably overlain by Jurassic-Cretaceous sedimentary sequence, represented by sandstones, oolitic limestones containing chert nodules and sandy limestones that are exposed in the eastern part of the Biga Peninsula (Bingöl et al., 1973; Ercan, 1996). Two tectonic slivers of Cretaceous age, Çetmi Ophiolitic Mélange and Denizgören Ophiolite, overthrust the metamorphic basement. Upon these units, Eocene marine sedimentary rock units together with volcanics consisting of andesitic and dacitic lavas and tuffs were deposited. In the Biga Peninsula, a new volcanic period made up of andesite, dacite, trachy-andesite, rhyodacite starts at early Oligocene, and the volcanism was effective during the whole Oligocene. These volcanic rocks generally alternate with sedimentary rocks. There is an extensive calc-alkaline volcanism in Early-Middle Miocene and granodioritic plutons of Oligocene-Miocene age in the region (Okay et al., 1990). Rocks of Early-Middle Miocene volcanism are dacitic, rhyodacitic, andesitic, latitic lavas and tuffs. Moreover, terrestrial sediments accompany these rocks. Upper Miocene volcanics, firstly trachy-andesitic lavas, and then alkaline olivine basalts form in the last period of Tertiary volcanism. Pliocene detrital sedimentary rocks are found beneath the Quaternary alluvium (Figure 4).
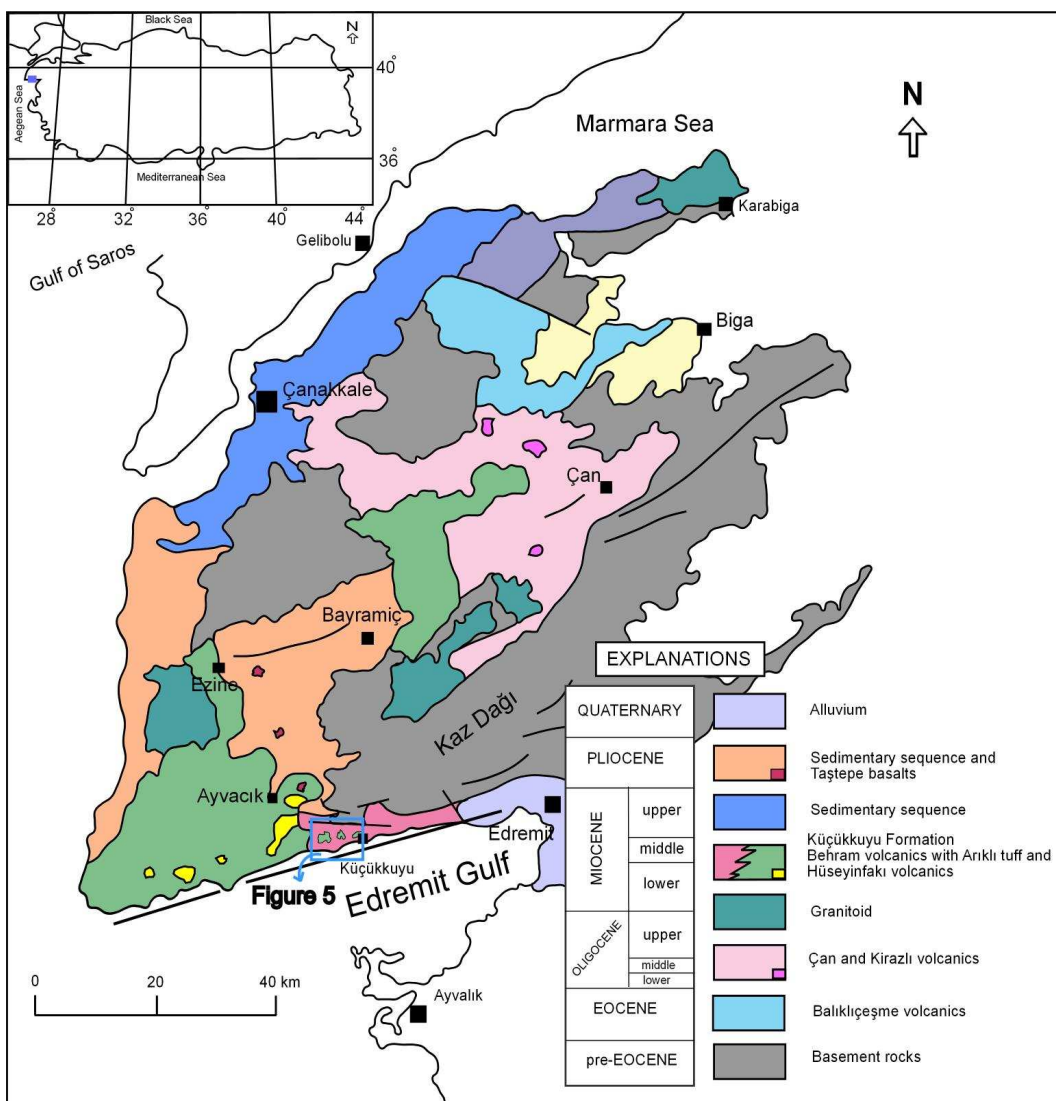
**Figure 4.** Simplified geologic map of the Biga Peninsula (Modified from Siyako et al., 1989; Okay et al., 1990; Ercan et al., 1995).

In the western part of the Biga Peninsula pre-Liassic, metamorphic rocks form the basement. These rocks include the Çamlıca Metamorphics, the Karadağ Metamorphic assemblage and the Denizgören Ophiolite, which were described in detail by Okay et al. (1990). In the east and southeast of the Biga Peninsula, the pre-Liassic basement rocks include the Kazdağ Metamorphics, the Karakaya

Complex and the Çetmi Ophiolitic Mélange (Bingöl et al., 1973; Gözler 1986; Okay et al., 1990; Ercan et al., 1995).

The Kazdağ Complex is tectonically overlain by the Çetmi Ophiolitic Mélange in the west and Permo-Triassic Karakaya Complex in the east. The Çetmi Ophiolitic Mélange is a volcano-sedimentary complex, which consists of spilitic basic volcanic lavas and pyroclastic flows, Upper Triassic, Upper Jurassic-Early Cretaceous and Upper Cretaceous limestone blocks and shales (Okay et al., 1990). The Karakaya Complex consists of feldispathic sandstone, quartzite, conglomerate, and siltstone, which is intercalated with spilitic basalt, mudstone and radiolarian chert. The Karakaya Complex cropping out widely in the eastern part of the Biga Peninsula also contains exotic blocks of Permian and Carboniferous limestone (Bingöl et al., 1973). Okay and Göncüoğlu (2004), reviewed the geological features of this unit in detail. The Kazdağ Group is unconformably overlain by the Jurassic-Cretaceous sedimentary sequence (Bingöl et al., 1973). Çetmi ophiolitic melange is thrust upon the Jurassic–Cretaceous sediments.

In the Biga Peninsula, the period of Upper Cretaceous-Early Eocene is represented by the Fıçıtepe Formation, comprising conglomerates with thin coal seams, sandstones and shales and Akçaalan Volcanics, containing andesites and andesitic tuffs (Siyako et al., 1989). Previous work stated that the volcanism (Balıklıçeşme volcanic) started in Eocene (Gözler 1986; Ercan et al., 1995; İşseven et al., 1995) (Figure 4). There is a significant transgression in Middle Eocene resulting in the deposition of shallow marine Soğucak Limestone (Siyako et al., 1989) while the Eocene volcanism is still active (Ercan et al., 1995; 1998). The Ceylan formation, consisting of mainly of turbidites overlies the volcanic rocks but also includes two acidic tuff levels alternating with turbidites (Ercan et al., 1995). They are determined as Upper Eocene in age by Siyako et al. (1989).

Starting from Lower Oligocene, the region was uplifted (Ercan et al., 1995) and passed into terrestrial environment. Andesitic, dacitic and rhyodacitic lavas, tuffs and agglomeras occur in the area of Çan and southeast of Çanakkale. The Middle-Upper Oligocene volcanics are called Çan volcanics by Ercan et al. (1995) (Figure 4). However, Siyako et al. (1989) called them as Early Miocene Doyran volcanics (Table 2). They further put forward that all the Oligocene sediments were eroded in the Biga Peninsula. In the last stage of Oligocene volcanism, the nature of volcanism changed. The volcanics, represented by trachy-andesitic and basaltic dykes and lava flows are called Kirazlı volcanics (Figure 4). They are Late Oligocene in age (Ercan et al., 1995; 1998). In the Biga Peninsula, Oligocene volcanic rocks are observed to be intercalated with sedimentary rocks.

**Table 2.** Correlation chard of Tertiary volcanics in the Biga Peninsula.

| Çelik et al., 1999 | | Karacık and Yılmaz, 1995 | | Ercan et al., 1995 | | | Siyako et al., 1989 | | | Çiftçi et al., 2004 | | |
|---|---|---|---|---|---|---|---|---|---|---|---|---|
| Pliocene | Basalt and basaltic agglomerate | MIOCENE | | MIOCENE | upper | Ezine Basalt | plio-Quaternary | | Taştepe Basalt | MIOCENE | upper | Basalt |
| MIOCENE | Andesitic agglomerate / Tuff / Lacustrine sediments / Andesite / Andesitic agglomerate | | middle / lower | Ayvacık + Balabanlı volcanics | | middle | Hüseyinfakı volcanics | | upper | Ezine volcanics | | middle-lower | Küçükkuyu Formation Arıklı Tuff | I-VI volcanic episodes |
| | | | | | lower | Behram volcanics | MIOCENE | | | | | |
| | | | | OLIGOCENE | upper | Kirazlı volcanics / Çan volcanics | | middle | Küçükkuyu Formation Arıklı Tuff | Doyran volcanics | | |
| | | | | | middle / lower | | | lower | | | | |
| | | | | EOCENE | | Balıklıçeşme volcanics | | | | | | |

22

During Lower-Middle Miocene extensive calc-alkaline volcanism occured in the Biga Peninsula (Figure 4). Andesitic, dacitic, rhyodacitic, latitic lavas, tuffs and agglomerates covered vast areas and granodioritic plutons were emplaced. The age of these plutons are confirmed to be between Oligocene-Miocene, based on the isotopic age determinations by Siyako et al. (1989).

Lower-Middle Miocene volcanism spreading over wide areas in the Biga Peninsula is named as the Behram volcanics (Ercan et al., 1990) (Figure 4). The Behram volcanics alternate with lacustrine sandstone, marl, claystone and limestone respectively. This volcanism, starting between 21.5 and 16.8 Ma (Lower-Middle Miocene) according to the radiometric age determination by Borsi et al. (1972) and Ercan et al. (1995), are stated to be the Middle-Upper Miocene Ezine volcanics by Siyako et al. (1989). In addition to these names Karacık and Yılmaz (1995) named the same rocks as Balabanlı and Ayvacık volcanics (Table 2).

In the area studied, basaltic and trachyandesitic dykes and lava flows cutting Behram volcanics are called Hüseyinfakı volcanics (Ercan et al., 1995) (Figure 4). Hüseyinfakı volcanics occur as small outcrops to the south of the Biga Peninsula and the datings yielded Middle Miocene age (Ercan et al., 1995). Between Ezine and Ayvacık, to the west of Biga Peninsula, alkali olivine basaltic lavas known as the Ezine basalts are observed (Ercan et al., 1995). These are the last products of the Tertiary volcanism. Ezine basalts having small outcrops towards west are called as Plio-Quaternary Taştepe basalts by Siyako et al. (1989) and Ertürk et al. (1990) (Figure 4). Depending on radiometric age determination, however, Ercan et al. (1995) states Upper Miocene age for these rocks (Table 2).

The Plio-Quaretnary units in the study area are represented by fluvial sediments and lacustrine carbonates including conglomerates, sandstones and shales. They are called as Bayramiç Formation by Siyako et al. (1989). During the Quaternary alluvium and terrace deposits were formed in the study area.

## 2.2. Geology of the Study Area

### 2.2.1. General

The study area comprises four main rock units. These are the ophiolitic basement rocks, volcanic unit, lacustine sediments and alluvium (Figure 5). The Çetmi Ophiolitic Melange forms the basement of the study area and it is unconformably overlain by volcanics and detrital sediments. The mélange, representing the regional basement is not observed in the mapped area but some very small outcrops are seen just at the northern margin in the previous studies (Çelik et al., 1999).

The main rock-types of the volcanic unit in the study area are tuff, andesitic tuff, andesitic agglomerate, basalt and basaltic agglomerate. From these tuffs, the zeolite-bearing ones will be investigated in detail in this study. The studied volcanic unit is unfortunately named by different authors by varying names: Ezine Volcanics by Siyako et al. (1989), Behram Volcanics by Ercan et al. (1995), Ayvacık and Balabanlı volcanics by Karacık and Yılmaz (1995) (Table 2). From these, we followed the nomenclature of Ercan et al. (1995).

Overall, the volcanic activity continued during the deposition of lacustrine sediments in the study area and hence volcanics alternate with Miocene sedimentary rocks. Repeated volcanic activity must have delivered volcanic material to lacustrine basins that interrupted the shale-sandstone sedimentation. By this, it can be deduced that volcanic eruptions were realized in several phases
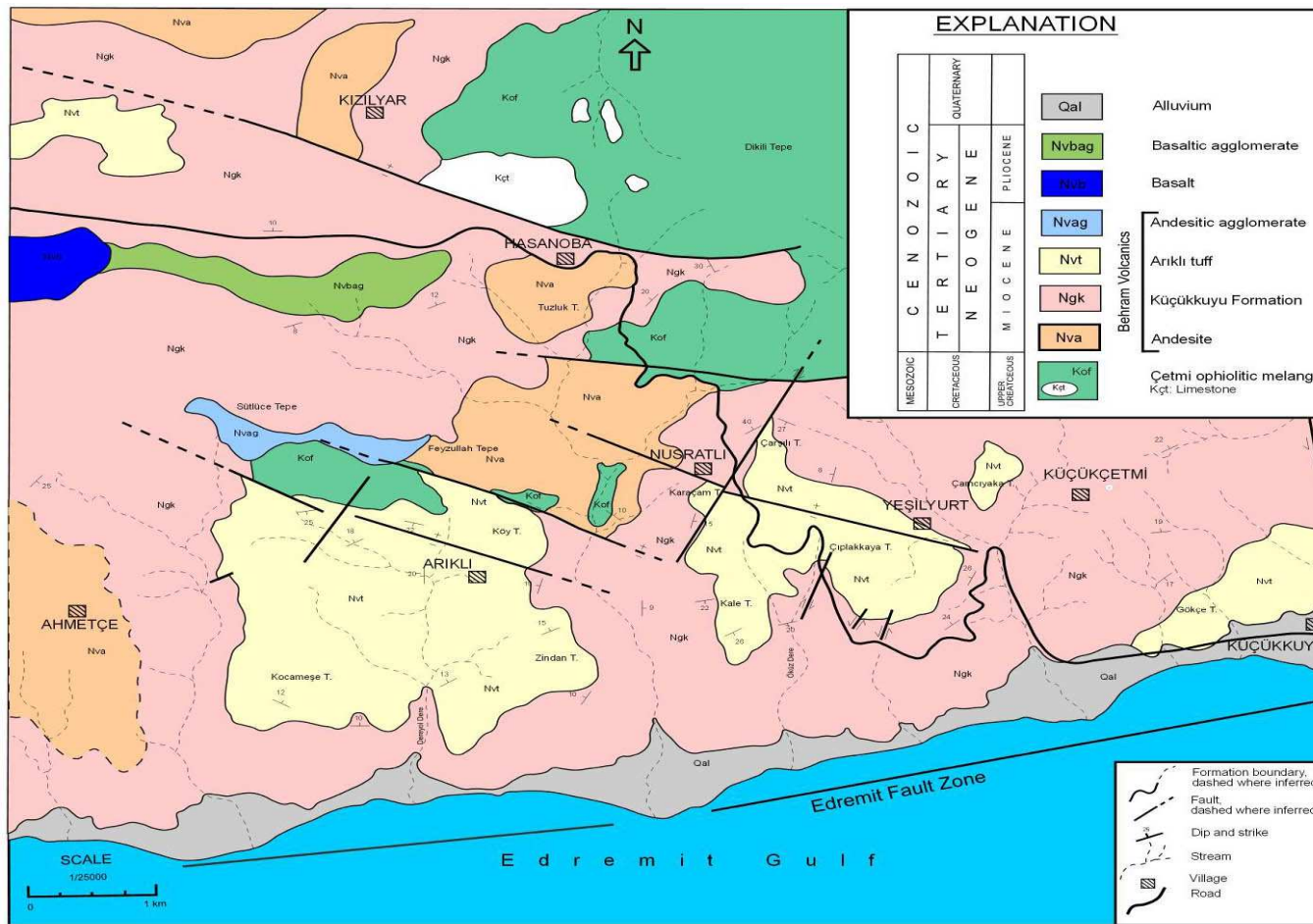
**Figure 5.** Simplified geological map of the studied area (after Çelik et al., 1999).

in the region. This is also emphasized by Çiftçi et al. (2004), who identified seven different volcanic episodes in the study area. Lacustrine clastic sediments are laterally and vertically transitional to the tuffs. Quaternay alluvium on the other hand, forms the uppermost unit.

In the following section, only the stratigraphy of the Neogene units will be briefly described, based on the studies of Siyako et al. (1989), Çelik et al. (1999), Çiftçi et al. (2004) and our own observations.

## 2.2.2. Neogene Sediments and Volcanic Rocks in Küçükkuyu Area

Neogene sediments and volcanics cover a large area in the western Biga Peninsula. Volcanic rocks, which are named as Behram volcanics by Ercan et al. (1995) commence already on the basement of the Neogene sequences. Behram volcanics are intercalated with a thick package of sedimentary rock, which are collectively known as the Küçükkuyu Formation. This name was first used by İnci (1984).

### 2.2.2.1. Küçükkuyu Formation (Ngk)

In the study area, Neogene sediments of the Küçükkuyu Formation are studied mainly by Saka (1979); Siyako et al. (1989) and Çiftçi et al. (2004). The Küçükkuyu Formation is represented by turbiditic lacustrine sediments that is coeval with volcanism. The age of Küçükkuyu Formation is Early Miocene based on radiometric age data (İnci, 1984).

The formation unconformably overlies the earlier sediments with a basal conglomerate at the bottom. It includes an alternating sequence of conglomerate, sandstone, claystone, mudstone and shale. A typical view of the Küçükkuyu Formation is shown in Figures 6 and 7. The Küçukkuyu Formation is well-

bedded and yellow, yellowish brown, whitish grey and greenish brown in color in the field. Dominant rock-types in the outcrops of the Küçükkuyu Formation are claystone, mudstone and shale. Conglomerate and sandstone are observed only in few locations in the field.

Shale, mudstone and claystone appear almost of the same light brown to beige color. Shale, one of the main rock-types of the formation exposes in different areas in the study area. The best exposure of shale mainly lies along the Küçükkuyu-Ayvacık road, to the southwest of Yeşilyurt and east of Nusratlı. The thicknes of bedding in shale changes from laminae (circa 1mm) to 2 cm and beige to brown in color.



**Figure 6**. A view of sedimentary succession with shales and mudstones of the Küçükkuyu Formation (Ngk), southeast of Yeşilyurt.

**Figure 7**. Photograph illustrating Küçükkuyu Formation (Ngk) with well-bedded, yellowish brown siltstones and shales, northeast of Nusratlı.

The thickness of the shale packages in the succession may reach up to 2m. However, the most typical occurrence is a thinly bedded rock with darker colors (Figure 8). Folding is frequent in the unit. e.g. the road junction Küçükkuyu-Arıklı and Yeşilyurt (Figure 9). Thin beds of dark brown to pale brown silty claystones alternate with shales. The matrix is probably carbonate. The color of mudstones is darker than shale and claystones which is brown in color. Claystones, mudstones and shale beds are typically laminated. Iron oxide staining along the bedding surfaces gives the rock a darker color.
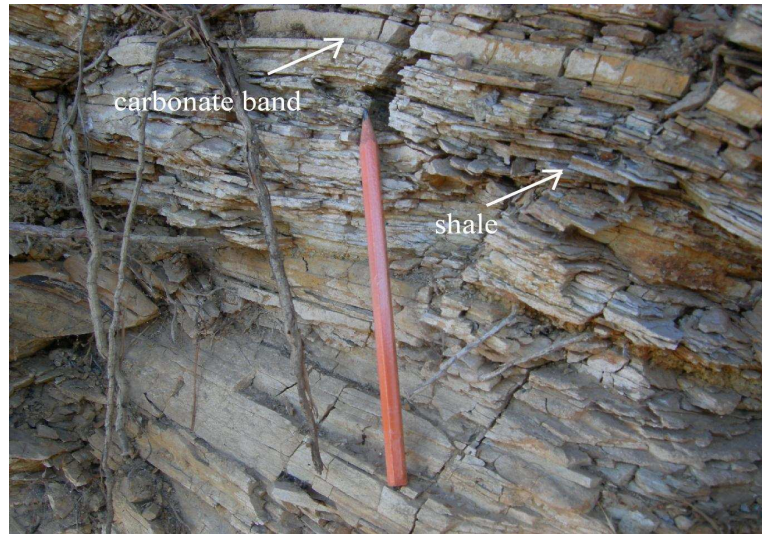
**Figure 8.** A view from Küçükkuyu Formation (Ngk) showing alternation of thin-
bedded and dark-coloured shale with carbonate bands, northeast of Karaçam
Tepe.



**Figure 9**. Photo showing small scale folding in Küçükkuyu Formation (Ngk),
road junction of Küçükkuyu-Arıklı and Yeşilyurt.

Conglomerate and sandstone, on the other hand, crop out only at the road that east of Tuzluk Tepe and the road around the Hasanoba. Except in these two localities, conglomerate and sandstone can not be observed in the field. Pebbles of conglomerate are beige, white, black, light brown to dark grey in color and they include mainly volcanic clasts such as andesite and mainly basalt. These pebbles with radious of 1-3 cm in diameter are rounded or poorly angular. Pebbles of the conglomerate are bounded with the matrix of very fine-grained clastic material (Figure 10).



**Figure 10**. Conglomerate sequence with well to moderately rounded, poorly sorted pebbles of basalt and andesite in the Küçükkuyu Formation (Ngk). The pebbles are bound with fine-grained clastic matrix, east of Tuzluk Tepe.

Sandstones are dark brown to grey in color and 2-5 m in thickness. They are compact and more resistant to alteration and are characterized by differential erosion. The clastic rocks of the Küçükkuyu Formation disconformably overlie the lower andesitic lavas of the Behram Volcanics at the south of Hasanoba and it is overlain by Arıklı Tuff of the east of Nusratlı. However, it was observed in

several places that they are intercalated with tuffs (Figure 11). The age of Küçükkuyu Formation is determined as Early-Middle Miocene based on the palynological data (Çiftçi et al., 2004).
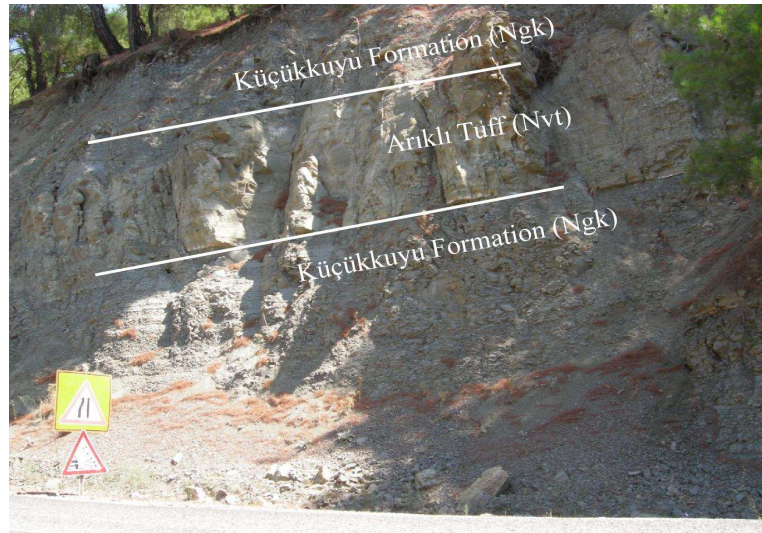


**Figure 11.** Photograph showing alternation of the Küçükkuyu Formation (Ngk) and Arıklı Tuff (Nvt) northwest of Çarşılı Tepe.

#### 2.2.2.2. Behram Volcanics

Early-Middle Miocene volcanics are named as Behram Volcanics by Siyako et al. (1989). Behram volcanics include andesite, andesitic tuff, andesitic agglomerate and dacitic-rhyolitic Arıklı Tuff which is the main objective of this study.

#### 2.2.2.2.1. Andesite (Nva)

Andesites within the Behram Volcanics are generally observed in the form of massive lavas. The andesites are slightly dark-grey to pinkish grey in color. But,

31

the color locally turns to light grey and brownish grey probably due to intense weathering and alteration along the road to the north of Nusratlı (Figure 5). It has porphyritic texture with the plagioclase and biotite phenocrysts, coarse enough to be recognized by naked eye. The unit locally shows slight difference in its granularity.

Andesites of Behram Volcanics mainly expose as massive lava-flows to the north of Arıklı and west of Nusratlı, south of Hasanoba, around the Ahmetçe and northwest of Kızılyar (Figure 5).

In the south of Hasanoba, the andesite unit of Behram volcanics is underlain by the clastic rocks of the Küçükkuyu Formation. According to Çelik et al. (1999), the clastic rocks are Middle Miocene in age. This age is based on its stratigraphic position with respect to the Küçükkuyu sediments.

### 2.2.2.2.2. Arıklı Tuff (Nvt)

The dacitic-rhyolitic tuffaceous rocks within Behram volcanics are named as Arıklı Tuff by Çiftçi et al. (2004). The Arıklı Tuff represents the main pyroclastic products and covers mainly the southern part of the study area (Figure 5).

Arıklı Tuff includes massive and bedded rocks. Figure 12 shows the occurrence of massive form and Figure 13 shows the occurrence of bedded tuffs. The petrographic study showed that the bedded Arıklı tuff includes dolomitic bands, as it will be explained in the petrography chapter. Dolomite dominates towards the transition of Küçükkuyu Formation and Arıklı Tuff. The thickness of the single beds varies from laminae to 1m, but is usually 2 to 5 cm.

**Figure 12.** Photograph illustrating massive Arıklı (Nvt) Tuff, which is fine grained, compact, dark yellow to light orange in color.



**Figure 13.** Photo showing bedded tuff, which is at the transiton between lake deposits and tuffs, southeast Karaçam Tepe.

Samples of Karaçam Tepe, Kale Tepe, Çıplakkaya Tepe and samples around the Arıklı and Yeşilyurt are yellow to orange in color. Tuffs in the south of Çarşılı Tepe are usually white to light yellow in color. Tuffs in the south of Küçükkuyu, on the other hand, are white to whitish green in color when fresh and light brown in color in altered zones. Sporadically distributed nodules with 2-7 cm radius occur in the Arıklı Tuff near the south of Çarşılı Tepe and between Kale Tepe and Karaçam Tepe (Figure 14). These are usually concentric and silisic in composition. However, some of them are dark in color and have highly altered manganiferous rims (Çiftçi et al., 2004). Some tuffs display brown bands, which are due to late stage staining with Fe- oxide.



**Figure 14.** Photograph showing a close up view of the nodules in Arıklı tuff (Nvt), in Çarşılı Tepe.

The mineral and rock fragments of the Arıklı Tuff are less than 2 mm in diameter, so that the Arıklı Tuff can be classified as fine-tuff based on its grain-size (Fisher and Schmincke, 1984). Arıklı Tuffs are fairly hard and compact in general. Along the road of east of Karaçam Tepe, however, very fragmental tuffs were observed

(Figure 15). In addition, along the road to west of Küçükkuyu, tuffs are generally highly altered and have breccoidal appearance due to the Neotectonic Edremit Fault Zone to the south of Kaz Dağları along the Northern coast of the Edremit Bay (Figure 16).



**Figure 15.** Photograph illustrating brecciated Arıklı Tuff (Nvt) along the road east of Karaçam Tepe.

Arıklı Tuff is mainly exposed around three different areas. These are in the vicinity of Arıklı Village (Kocameşe Tepe, Zindan Tepe, Köy Tepe), between the Yeşilyurt and Nusratlı villages (Kale Tepe, Çıplakkaya Tepe, Çarşılı Tepe, Karaçam Tepe) and north of Küçükkuyu town (Gökçe Tepe) (Figure 5).

**Figure 16.** A view of breccoidal appearance of Arıklı Tuff (Nvt) due to the
Neotectonic Edremit Fault Zone, along the road of west of Küçükkuyu.

Arıklı tuff is locally overlain by andesitic agglomerate in the west of study area. It
lies conformably over the shale-siltstone alternation of the Küçükkuyu Formation
to the southeast of Nusratlı (Figure 17). The age of Arıklı Tuff is Early-Middle
Miocene (Çiftçi et al. 2004).

**Figure 17.** Photograph showing the faulted boundary between Arıklı Tuff (Nvt) and shale-siltstone alternation of the Küçükkuyu Formation (Ngk), southeast of Nusratlı.

Arıklı Tuff in the region, mainly in Yeşilyurt, Nusratlı and Arıklı villages, is widely used as building stones because of its homogenity and very large amount. The unit is the main point of interest in this MSc theses, as it bears considerable amount of analcime.

### 2.2.2.2.3. Andesitic Agglomerate (Nvag)

Andesitic agglomerates unit of the Behram Volcanics occur as blocks in a restricted area from Feyzullah Tepe to Sütlüce Tepe (Figure 5). It has usually a purple color (Figure 18). The blocks of andesites are angular and varying dimensions from 1 cm to 10 cm in diameter. The matrix is wholly composed of andesitic ash.

**Figure 18.** A close up wiev of andesitic agglomerate (Nvag). Pink, angular blocks of agglomerate are embedded in andesitic ash matrix (green).

### 2.2.2.3. Pliocene Basalt and Basaltic Agglomerate (Nvb, Nvbag)

Pliocene basalts and basaltic agglomerates in the study area are named as Taştepe basalt by Siyako *et al.* (1989). These are exposed to the northwest of the study area. Even though basaltic lavas can not be observed in field, basaltic agglomerates were examined in the field just beside the Küçükkuyu-Ayvacık road west of Hasanoba (Figure 5). Basaltic agglomerates include angular and rounded blocks and are of grey and black in color (Figure 19).

**Figure 19.** A close up view of basaltic agglomerate (Nvbag) with black rounded
to poorly angular basalt blocks, west of Hasanoba.

### 2.2.3 Quaternary Alluvium (Qal)

Alluvium exposing along the coast of Edremit Gulf comprises of loose material of
pebble, sand and clay. They are Quaternay in age (Çelik et al., 1999).

# CHAPTER 3

# PETROGRAPHY

## 3.1. Introduction

For petrographical purposes, a total of 32 thin sections were prepared out of 90 samples, collected from different localities of the study area within the Arıklı Tuff. Among them, 13 samples are from Çarşılı Tepe (ÇT), 3 samples from Karaçam Tepe (KÇ), 2 samples from Kale Tepe (KL), 6 samples from Çıplakkaya Tepe (ÇPT), 2 samples from Yeşilyurt village (YÇT), 3 samples from Arıklı village (A) and 3 samples from fresh road cuttings to the west of Küçükkuyu (KK).

Arıklı Tuff consists of dust, ash and minor amount of clasts. Microscopical study reveals that the fragments range in size from 0.01 mm to 0.06 mm, so the Arıklı tuff can be classified as fine tuff (dust tuff) based on grain size (Fisher and Schmincke, 1984) (Table 3). The sample location map is given in the Figures 20 and 21.

**Table 3.** Granulometric classification of pyroclasts and of unimodal, well-sorted pyroclastic deposits (Fisher and Schmincke, 1984).

| Clast size | Pyroclast | Pyroclastic deposit | |
|---|---|---|---|
| | | Mainly unconsolidated: tephra | Mainly consolidated: pyroclastic rock |
| 64 mm | Block, bomb | Agglomerate, bed of blocks or bombs or block or bomb tephra | Agglomerate, pyroclastic breccia |
| | Lapillus | Layer, bed of lapilli or lapilli tephra | Lapillistone |
| 2 mm | Coarse ash grain | Coarse ash | Coarse (ash) tuff |
| 1/16 mm | Fine ash grain (dust grain) | Fine ash (dust) | Fine (ash) tuff (dust tuff) |
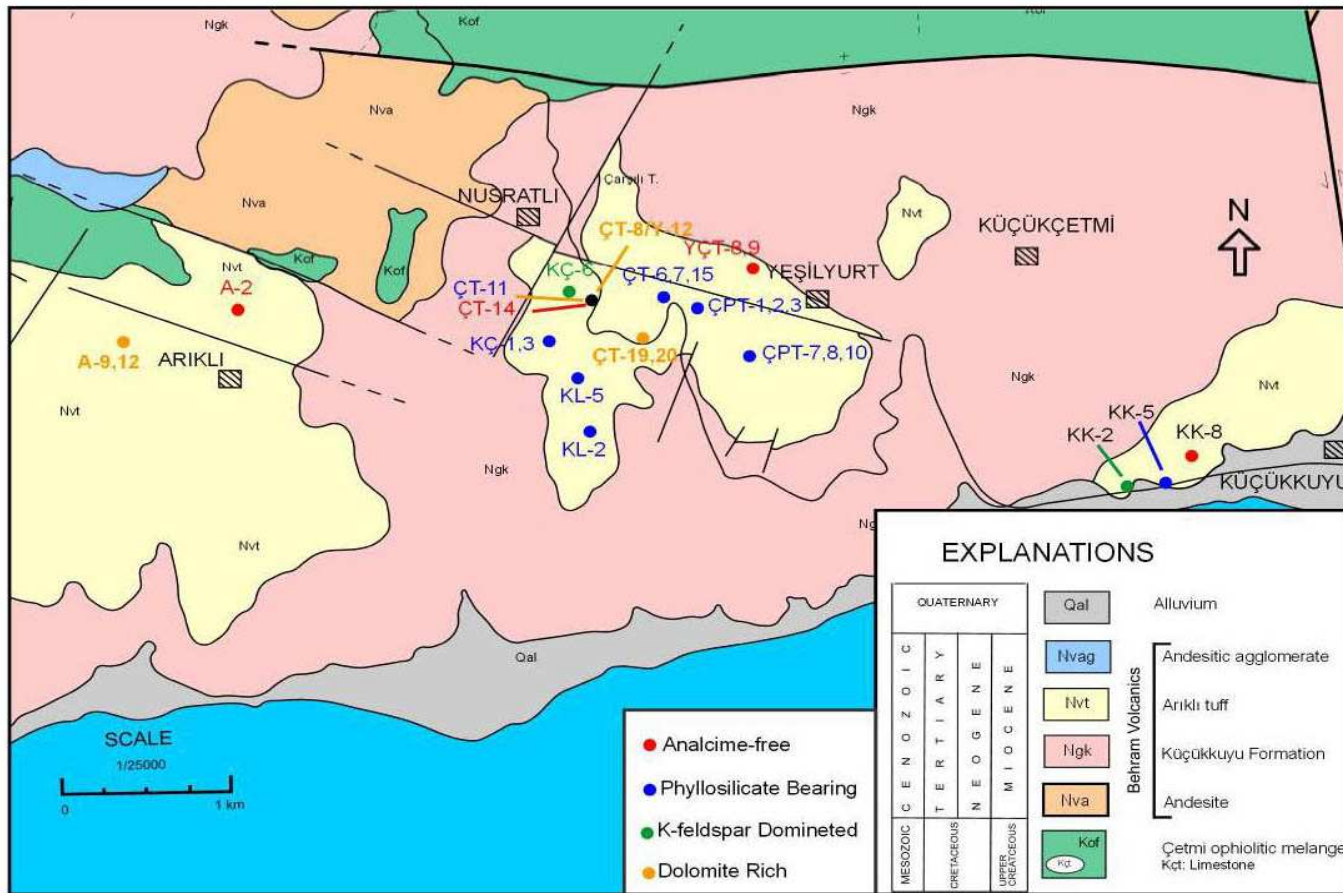
**Figure 20**. Sample location map of the Arıklı-Yeşilyurt-Küçükkuyu district, Ayvacık, Çanakkale (only petrographically and geochemically analysed samples) (after Çelik et al., 1999).
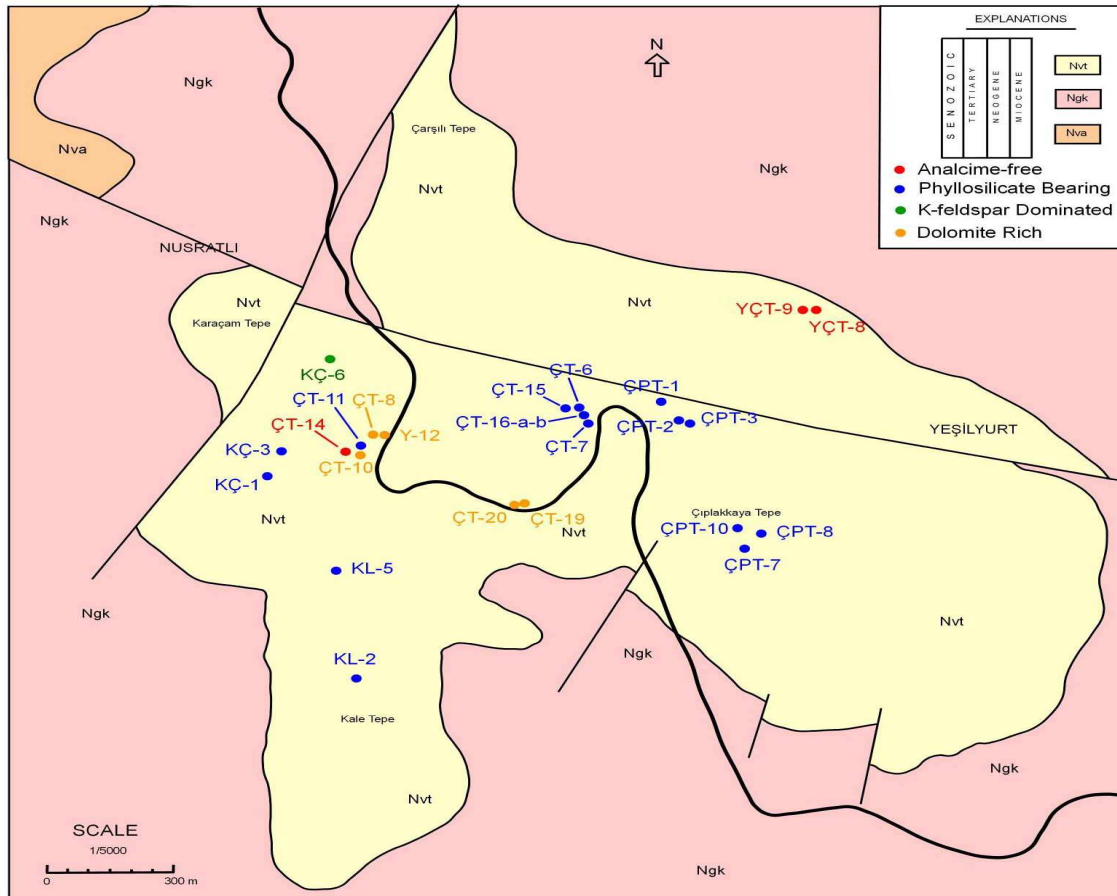
**Figure 21.** Sample location map of the Yeşilyurt, Ayvacık, Çanakkale (only petrographically and geochemically analysed samples) (after Çelik et al., 1999).

Variation in the primary minerals of each of the altered tuffs is a little. Generally, all tuff samples comprise quartz, minor amount of biotite, plagioclase and sanidine. Glass shards, pumice fragments and rarely rock-fragments make up the lithic components. The matrix is composed of tiny flakes of phyllosilicate minerals, dolomite and K-feldspar. These secondary minerals are of varying amounts in the matrix. Table 4 shows the visual estimation of phnenocrysts, lithic fragments and authigenic minerals.

**Table 4.** Phenocryst, lithic fragment and authigenic mineral percentages in phyllosilicate minerals-bearing Arıklı Tuff.

| | PHYLLOSILICATE MINERALS BEARING VITRIC TUFFS | | | | | | | | |
|---|---|---|---|---|---|---|---|---|---|
| | primary minerals | | lithic fragments | | | authigenic minerals | | | |
| | quartz | biotite plagioclase sanidine+opaque | pumice fragment | glass shard | Rock fragment | analcime | dolomite | phyllosilicate minerals | K-feldspar |
| ÇT-6 | 2 | 2 | 6 | none | <1 | 35 | none | 45 | ~20 |
| ÇT-7 | 5 | 4 | <1 | none | 1 | 35 | 2 | 45 | ~20 |
| ÇT-11 | 4 | 3 | <1 | none | 1 | 30 | none | 45 | ~20 |
| ÇT-15 | 3 | 2 | <1 | none | 1 | 20 | none | 30 | 20 |
| ÇT-16-A | 2 | 2 | 2 | none | 2 | 20 | 3 | 30 | 25 |
| ÇT-16-B | 2 | 2 | 4 | none | 3 | 25 | none | 30 | 30 |
| ÇT-17 | 3 | 2 | <1 | none | 1 | 15 | 4 | 55 | 20 |
| YÇT-8 | 3 | 2 | 1 | none | <1 | none | none | 70-80 | 5 |
| ÇPT-1 | 4 | 5 | 1 | none | 2 | 30 | 5 | 20 | 35 |
| ÇPT-2 | 4 | 3 | 5 | none | None | 30 | none | 15 | 30 |
| ÇPT-3 | 4 | 2 | <1 | none | None | 35 | 1 | 15 | 35 |
| ÇPT-7 | 5 | 6 | 1 | none | 3 | 30 | none | 30 | 35 |
| ÇPT-8 | 5 | 2 | 1 | none | <1 | 30 | none | 30 | 25 |
| ÇPT-10 | 3 | 2 | 3 | none | 1 | 20 | none | 45 | 30 |
| KÇ-1 | 5 | 5 | 4 | none | 1 | 20 | none | 35 | 25 |
| KÇ-3 | 4 | 3 | 3 | none | 1 | 25 | none | 30 | 25 |
| KK-5 | 3 | 3 | 6 | 10-15 | 2 | 20 | none | 45-55 | 10 |
| KL-2 | 4 | 2 | 2 | none | <1 | 30 | none | 20 | 35 |
| KL-5 | 10 | 7 | 8 | none | 2 | 25-30 | none | 20 | 30 |

**Table 4.** (continued)

| | | primary minerals | lithic fragments | | | authigenic minerals | | | |
|---|---|---|---|---|---|---|---|---|---|
| DOLOMITE RICH VITRIC TUFFS | | | | | | | | | |
| | quartz | biotite plagioclase sanidine+opaque | pumice fragment | glass shard | rock fragment | analcime | dolomite | phyllosilicate minerals | K-feldspar |
| A-9 | 3 | 2 | 10 | none | 1 | 20 | 60 | <3 | 20-25 |
| A-12 | 5 | 2 | 15-20 | none | <1 | 20 | 65-70 | <3 | 15-20 |
| ÇT-8 | 2 | 1 | 15 | none | none | 40 | 60-65 | <3 | none |
| DOLOMITES | | | | | | | | | |
| Y-12 | 1 | <1 | none | none | none | 20 | 70 | <3 | not observable |
| ÇT-10 | 1 | <1 | none | none | none | 20 | 70 | <4 | not observable |
| ÇT-19 | 2 | <2 | none | none | none | 20 | 70 | <5 | not observable |
| ÇT-20 | 2 | <3 | none | none | none | 20 | 70 | <6 | not observable |
| | K-FELDSPAR DOMINATED VITRIC TUFFS | | | | | | | | |
| | | primary minerals | lithic fragments | | | authigenic minerals | | | |
| | quartz | biotite plagioclase sanidine | pumice fragment | glass shard | rock fragment | analcime | dolomite | phyllosilicate minerals | K-feldspar |
| A-2 | 2 | 1 | 15 | none | <1 | none | 25 | none | 70 |
| KK-2 | 7 | 3 | 25 | 25 | 1 | 10 | none | none | 75-80 |
| KK-8 | 6 | 2 | 10 | none | none | none | none | none | 75-80 |
| KÇ-6 | 3 | 2 | 10 | none | <1 | 10 | none | 15 | 70 |
| YÇT-9 | 10 | 3 | 2 | none | 1 | none | none | 20 | 70 |

Well-preserved glass shards are not recognized in most of the thin sections except KK-2 and KK-5, as alteration has caused destruction of glass to zeolites and other diagenetic minerals. However, ghost forms of irregular glass fragments with irregular shape can be still identified. Hence, even if glass is rarely preserved as such because of alteration, most samples were named as vitric tuff based on the presence of other glassy material which is pumice fragments. The triangular diagram of Pettijohn (1957) was used for nomenclature and classification of tuffs (Figure 22).



**Figure 22.** Nomencluture and classification of tuffs (Pettijohn, 1957).

The primary composition of the vitric tuff can not be exactly determined only by petrographic observations. This is due to the later mineralogical changes. Still, it can be said that the tuffs have rhyolitic to rhyo-dacitic character according to the abundances of the pheno- and micro-phenocrysts as seen on Table 5 (Raymond, 1995). This naming is also confirmed by the chemical analysis of the same samples and will be discussed in Chapter 5.

**Table 5.** Mineralogical classification of common volcanic rocks (Raymond, 1995).

| | | | Other phenocrysts or grains | | | | | |
|---|---|---|---|---|---|---|---|---|
| | | | Alkali-feldspar ∓ biotite | Plagioclase ∓ alkali-feldspar ∓ biotite | Hornblende ∓ plagioclase | Pyroxine | Olivine | Olivine + pyroxine + plagioclase |
| Porphyritic texture | Essential phenocrysts or grains | Quartz ∓ feldspar | *f*-Rhyolite | *f*-Dacite | | | | |
| | | Feldspar only | *f*-Trachyte | *f*-Andesite | | | *f*-Basalt | |
| | | Feldspathoids ∓ feldspar | *f*-Phonolite | *f*-Feldspathoidal andesite<br>Light feldspar | | *f*-Feldspathoidal basalt (Dark feldspar) | *f*-Basanite | |
| | | None | *f*-Biotite felsite | | *f*-Andesite | | *f*-Basalt | |
| Aphanitic texture | No visible grains Glass<50% | | Felsite (Light colored) | | | Mafite (Dark colored) | | |
| | Glass>50% | | Obsidian | | | | | |

Although all tuffs have similar type of phenocrysts, their authigenic mineral assemblages are variable. By this feature, petrographically thin sections are separated into three groups on the basis of these authigenic mineral content visible/dominant in the matrix. These groups are allocated as; phyllosilicate minerals-bearing, dolomite-rich and K-feldspar dominated vitric tuffs (Table 4). Phyllosilicate-bearing tuffs are the most common ones through all the samples.

### 3.1.1. Phyllosilicate Minerals-Bearing Vitric Tuffs

The first group of tuffs is named as phyllosilicate minerals-bearing tuffs, since they include more than 20% phyllosilicate minerals in the matrix. Rock fragments and phenocrysts are embeded in a matrix that includes authigenic micrometer-size flakes of clay minerals showing cryptocrystalline texture. Phyllosilicate formation is also noticed in most of the other tuff samples, but in less amounts.

According to the grain size classification of Fisher and Schmincke (1984), these tuffs are classified as fine tuffs (Table 3). Nineteen of the samples fall in this group. One of them were taken around the region of Yeşilyurt, six of them were from Çıplakkaya Tepe south-west of Yeşilyurt, two of them from Karaçam Tepe south of Nusratlı, seven of them were from the south of Çarşılı Tepe, one of them from Küçükkuyu road and two of them from the Kale Tepe (Figures 20 and 21).

Generally, this group of tuffs contains quartz, minor amounts of biotite, plagioclase and sanidine as phenocrysts, and zeolite (analcime), phyllosilicates (smectite), K-feldspar and carbonate (dolomite) as authigenic minerals and rock fragments and pumice fragments. Their matrix is composed of phyllosilicate minerals which are smectites as determined by the detailed clay analysis explained in the XRD section of Chapter 4. Apart from phyllosilicate minerals, the matrix contains some dolomite and K-feldspar.

### 3.1.1.1. Primary Minerals

Phenocrysts in the tuffs consist of quartz, minor amount of biotite, plagioclase, sanidine and opaque minerals (Table 4). The phenocryst content ranges from 4 to 17% but is generally about 5-7% in samples ÇPT-3, ÇT-17, KK-5 etc. KL-5 has the highest amount of primary minerals (17%).

Quartz is the major component of the phenocrysts. The percentage of quartz ranges from 2% to 10% but is approximately 4% on the average. Grains of quartz are anhedral and clear. Minor amounts of plagioclase, sanidine, biotite and opaque minerals, which make up 2-7% of phenocrysts are also seen. Plagioclase grains are idiomorphic and display polysynthetic twinning. Biotite crystals are brown pleocroic. They have euhedral to subhedral crystal outlines. Mainly all biotites are flaky and occur as fine-grained crystals.

Sanidine crystals generally occur as small phenocryts having euhedral to subhedral crystals outline.They undergone alteration.

Opaque minerals are generally anhedral in crystal outline. Some of them, however, are thought to be pyrite due to their typical subhedral shape.

### 3.1.1.2. Glassy Material

The glassy material mainly consists of pumice fragments and glass shards. They are differentiated on the basis of their structure and appearance. Glass shards can be easily recognized with their typicall Y- and V-shape structure (Fisher and Schmincke, 1984). Pumice fragments, however, contain vesicles and they are larger than the glass shards (Fisher and Schmincke, 1984). Pumice fragments are the dominant vitric constituents, whereas glass shards are only found in the sample KK-5. Pumice sizes vary from 500μ to 5 mm in diameter. The pumice fragments commonly make up about ~2% of the constituents in thin-section and are variably rounded. In some samples (e.g. ÇT-7) it is less than 1% and some samles (KK-5, ÇT-6) contain 6-8% pumice fragments (Table 4). Pumice fragments are generally porous (Figure 23-a), which are filled by phyllosilicate minerals and analcime (Figure 23-b). They were also filled by dolomite in lesser amount. A few subhedral K-feldspar in pumice was observed in samples KL-5 and KK-5. It is difficult to separate pumice fragments, which are not porous, from

the matrix. A dark rim stained by very fine Fe-oxide may help to differentiate them (Figure 23). Analcime, phyllosilicate minerals and K-feldspar coexist inside the pumice fragments in sample KK-5.
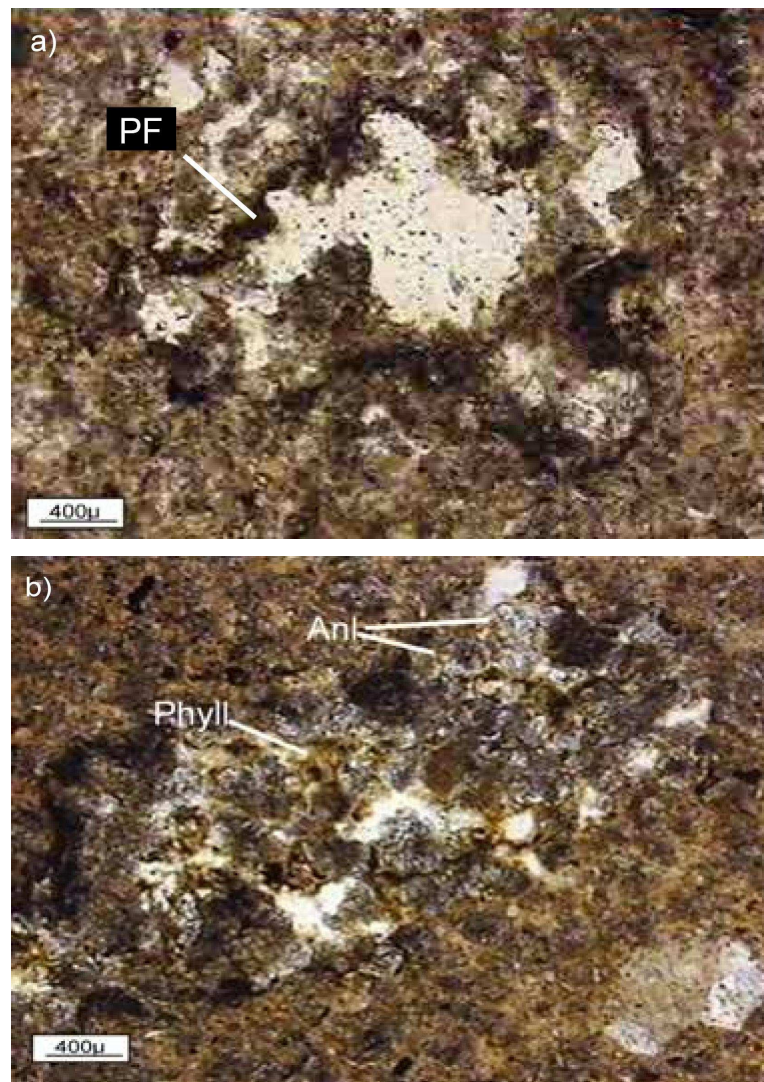


**Figure 23.** Photomicrographs showing a) porous pumice fragment dark rim stained by Fe-oxide (ÇPT-7, PPL), b) pumice fragment filled by phyllosilicate minerals and analcime (ÇPT-6, PPL), (Anl: analcime, Phyll: phyllosilicate mineral, PF: pumice fragment).

Another glassy type material in the studied samples is glass shards, which are very well-preserved in the sample KK-5 (Figure 24). Glass shards represent about 10-15% of the rock.
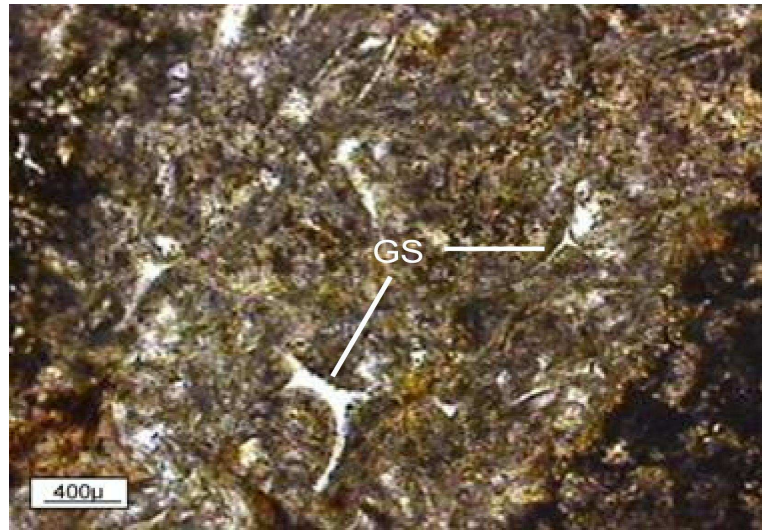


**Figure 24.** Photomicrograph showing glass shards (KK-5, PPL), (GS: glass shard).

### 3.1.1.3. Rock Fragments

Rock fragments form a portion of not more than 3% of whole tuff-samples. In some of the studied tuff samples, no rock fragments could be detected. In some cases, it is very difficult to determine the type of rock of the fragments because of alteration. However, in many cases their textures help to recognize them as fragments of volcanic origin, as seen in Figure 25. Some of these volcanic rock fragments resemble the biotite-andesites, which are stratigraphically below the tuffs.

52
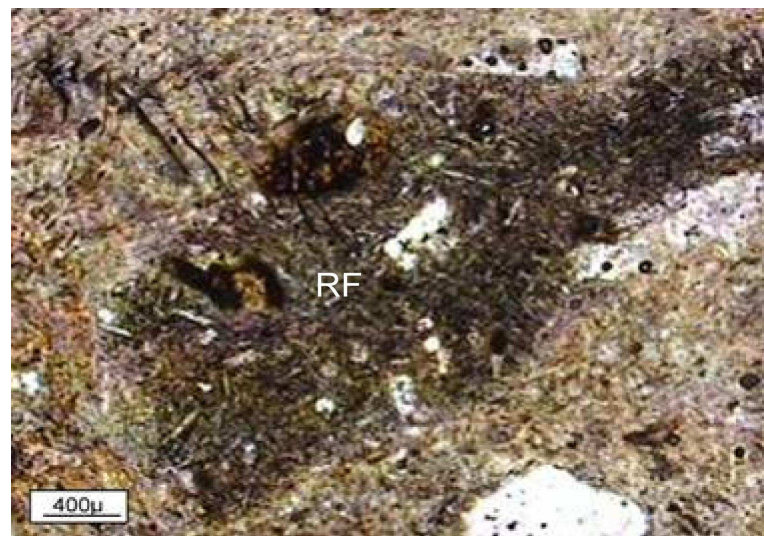
**Figure 25.** Photomicrograph displaying altered rock fragment of volcanic origin (KL-2, PPL), (RF: rock fragment).

### 3.1.1.4. Diagenetic Minerals

Mainly several parts of the tuffs, for example pumice fragments, ash material in matrix and also vesicules except the phenocrysts show formation of diagenetic minerals. These are analcime, phyllosilicate minerals, K-feldspar and dolomite, which are considered as secondary and authigenic.

The terms diagenetic, authigenic and secondary were used according to the Glossary of Geology (Bates & Jackson, 1980). Diagenetic minerals are formed by "….pertaining to or caused by diagenesis". Secondary minerals are "….minerals formed later than the rock enclosing it, usually at the expense of an earlier-formed primary minerals, as a result of weathering, metamorphism or solution". Lastly, authigenic minerals are minerals "….formed or generated in place and came into existence at the same time of the rock".

*3.1.1.4.1. Analcime*

In some thin sections the grain size is large enough to determine analcimes by petrographic study. However, it was in many cases necessary to identify the analcime by X-ray powder diffraction because of the minute grain size of most of the material. In thin sections, such coarse-grained analcime crystals are easily recognizable by their typical optical properties (Table 6). They are colorless, have low relief (Figure 26-a), isotropic (Figure 26-b) and euhedral. In addition to these, although diagnostic optical properties could not be determined because of minute size in many cases, some predictions about existence of analcime in the matrix can be made by high magnification. Two modes of occurrence are noticed for the formation of analcime. These are;

1) Coarse-grained euhedral or anhedral crystals in cavities and pumice fragments
2) Clusters or single crystals of fine-grained analcimes embedded in the matrix

The analcimes in the cavities and pumice fragments are approximately 100μ to 1 mm in size and under the petrographic microscope, these coarse grains of analcime are easily recognized with their optically isotropic character. The most striking point is that these coarse-grained, euhedral to anhedral analcime crystals were concentrated in pumice fragments or cavities, as seen in Figures 26 and 27.

**Table 6.** Optical properties of analcime.

| | |
|---|---|
| color | colorless |
| relief | low |
| pleochroism | no |
| cleavage | not seen/very poor |
| birefrincenge/interference color | isotropic |
| crystal system | cubic |
| morphology | trapezohedral |
| group | zeolite |
| interference figure/optic sign | isotropic |
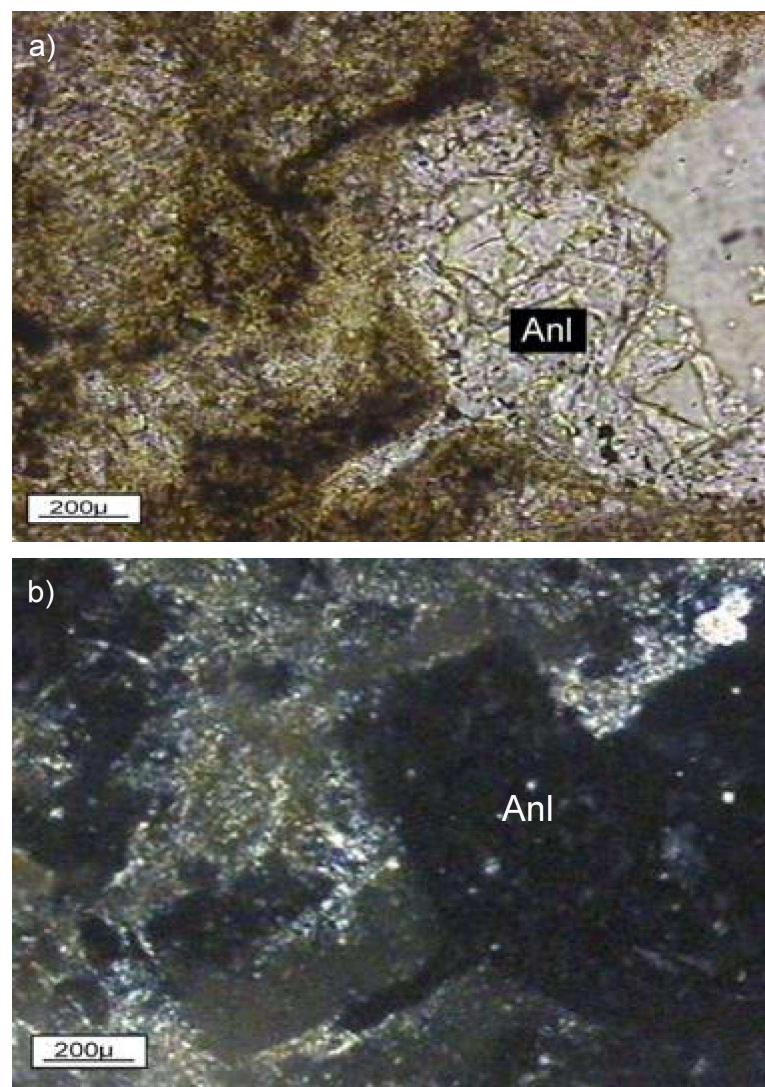
**Figure 26.** Photomicrographs showing optical properties of subhedral analcime crystal in cavity a) low relief (ÇT-6, PPL), b) isotropic character (ÇT-6, XPL), (Anl: analcime).
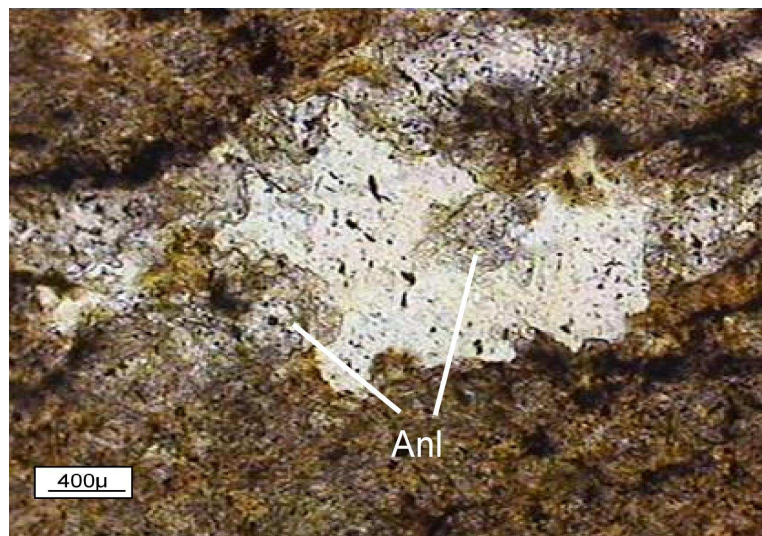
**Figure 27.** Photomicrograph showing euhedral to anhedral analcime crystals in pumice fragment (ÇPT-2, PPL), (Anl: analcime).

In addition to analcimes formed in the pores of the tuff, there are also some small analcime crystals or group of crystals or clusters, which can be identified by their typical optical properties within the matrix (Figure 28). Some of them, on the other hand, can be only observable with their low relief and isotropic properties under high magnification (x40) because of very minute size (Figure 29). It was considered that these very fine-grained and cryptocrystalline analcimes are scattered throughout the matrix, even not directly observable but identified by XRD analyses.
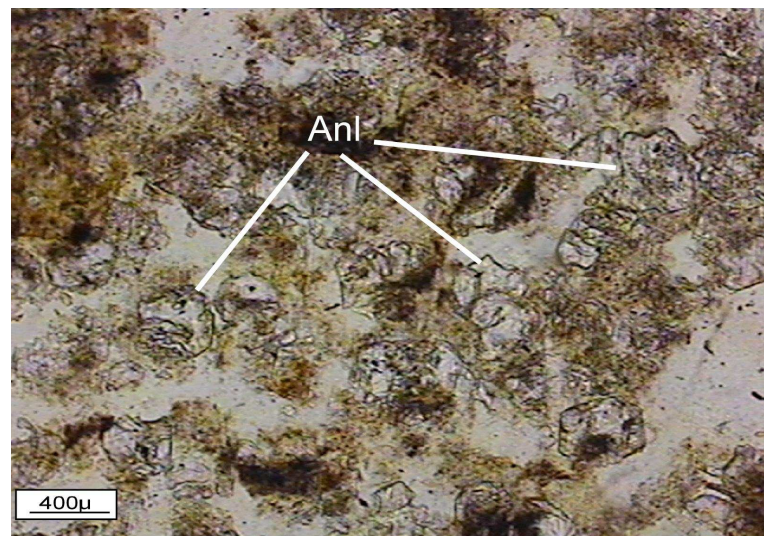
**Figure 28.** Photomicrograph showing colorless and low relief analcime clusters within the matrix (KL-5, PPL), (Anl: analcime).
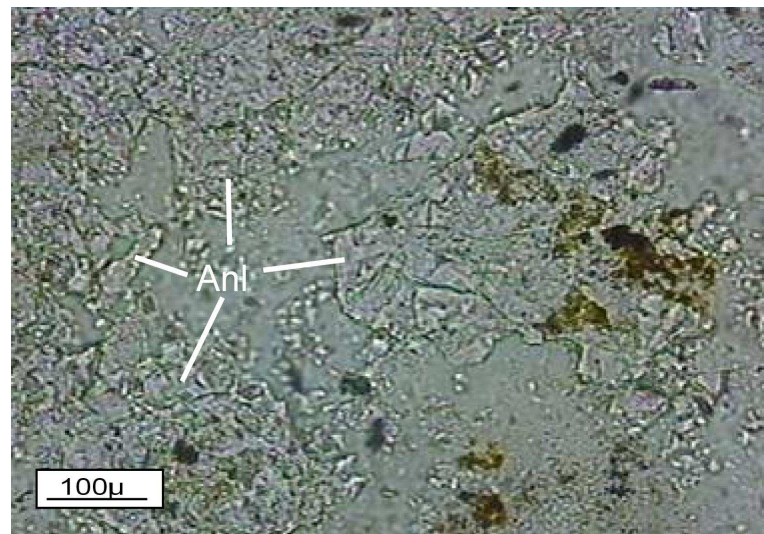


**Figure 29.** Photomicrograph showing very small analcime crystals in the matrix (ÇT-6, PPL), (Anl: analcime).

Some small analcime crystals identified by their low relief and colorless properties (Figure 30-a) in plane polarized light. Most of these clusters are black

and display euhedral morphology in crossed polars (Figure 30-b). These analcimes are differentiated from phyllosilicate minerals in matrix easily because of observable colorless and low relief properties. Even when analcime could not be directly identified in some other parts of matrix in plane polarized light (Figure 31-a) by more carefull examination, in crossed nicols scattered black, mainly circular clusters embedded inside the phyllosilicate matrix were observed (Figure 31-b). Most tuff samples, mainly fine-grained ones show this feature in the matrix. An exact determination of these minerals in the clusters is optically difficult because optical properties are not observable even by high magnification (X40). These are probably correspond to very small analcime crystals in the matrix. However, these isotropic clusters with questionable analcime are very similar to those we observed crossed polars in samples KL-5 in Figure 30. The identification of this type of minerals as analcime by optical means is reliable, only when controlled by XRD and SEM studies. Even if the presence of cryptocrystalline analcime in the matrix can be recognized, the exact percentage of analcime in the rock can only be roughly estimated. Therefore, the percentage of analcime given in Table 4 is only conjectural.
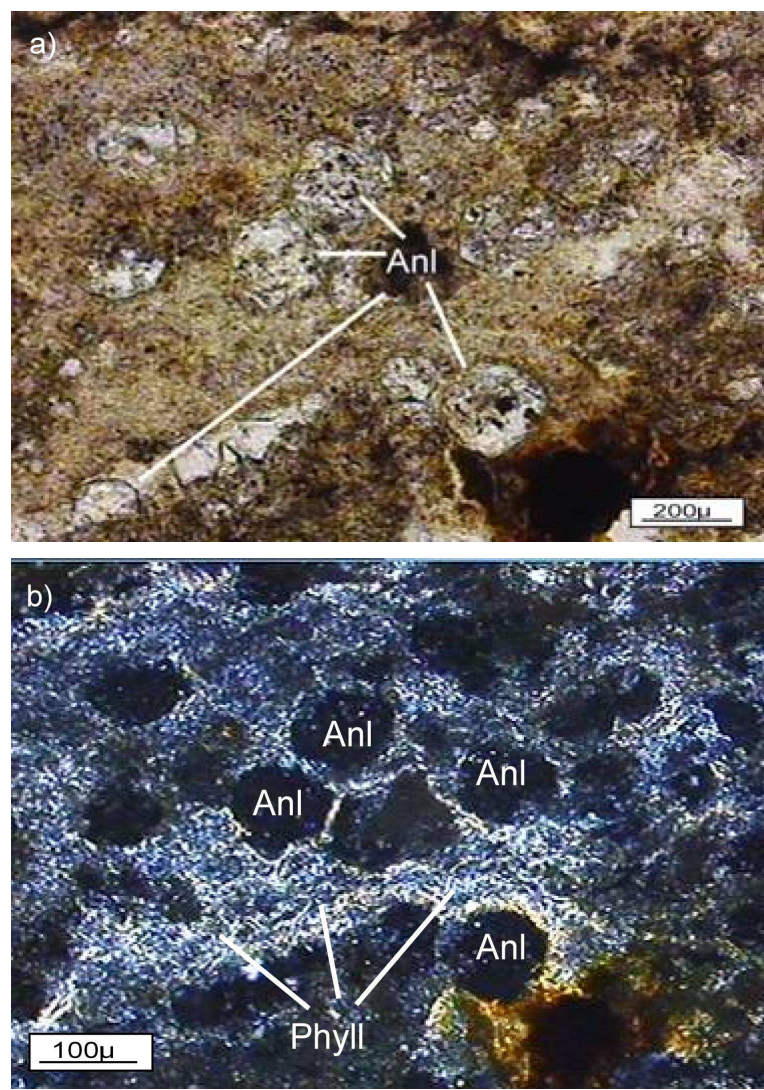
**Figure 30.** Photomicrographs showing analcime clusters in the matrix surrounded by phillosilicates a) (KL-5, PPL), b) (KL-5, XPL), (Anl: analcime, Phyll: phyllosilicate mineral).
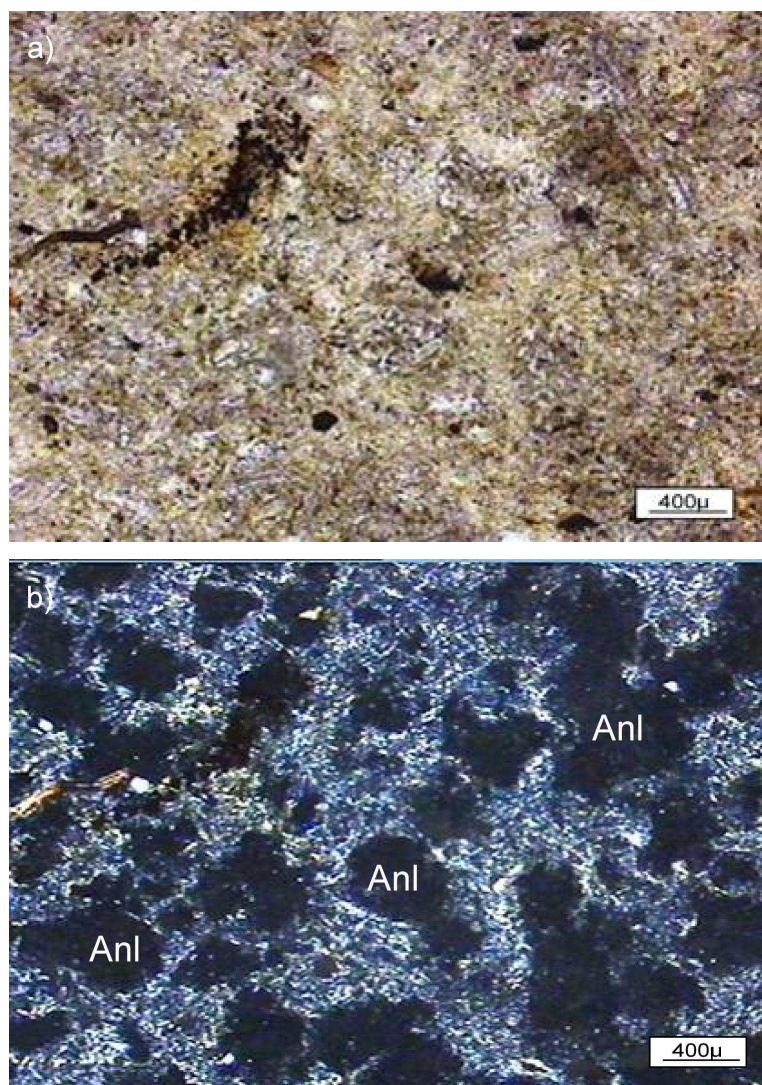
**Figure 31**. Photomicrograph showing analcime clusters in matrix a) (ÇT-6, PPL), b) (ÇT-6, XPL), (Anl: analcime).

### 3.1.1.4.2. Dolomite

Dolomite is found as a secondary mineral in the studied tuffs. Actually, it is difficult to distinguish dolomite from calcite in thin sections because of their similar optical properties. Hence the existence of dolomite can be proven by XRD studies. The dolomites in the studied samples have high birefringence and display

variable relief. Disseminated, anhedral dolomite grains are up to 1 mm in diameter. They are found in pumice fragments, in cavities or in the matrix (Figure 32). Dolomites were found in less amount in this group of tuff, usually not more than 5% and some samples do not include dolomite (e.g. sample KÇ-1) (Table 4).
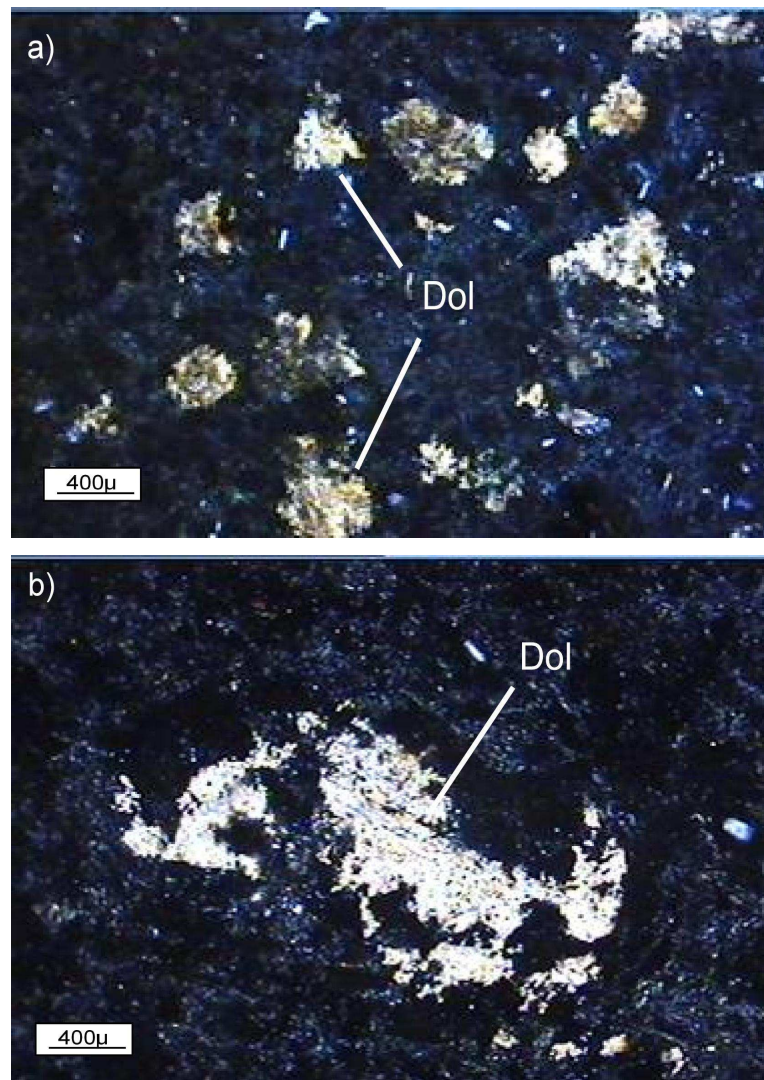


**Figure 32.** Photomicrograph showing dolomite crystals a) in matrix (ÇPT-1, XPL) b) in pumice fragment (ÇT-17, XPL), (Dol: dolomite).

### 3.1.1.4.3. Phyllosilicate Minerals

The presence of authigenic phyllosilicate minerals all thin sections of this group of the studied tuffs is used as a criteria for discrimination. Because phyllosilicate minerals occur as fine-grained aggregates, their optical properties are difficult to determine. Most of the time, phyllosilicate minerals can be distinguished by their characteristic flaky appearance (Figure 33) which are characterized by parallel extinction. In thin sections, they are generally light yellow to brownish yellow in color. Their length is about 5μ. Phyllosilicate minerals occurring as tiny crystals in the cryptocrystalline matrix make up about 30-40% of the rock (Table 4). Phyllosilicate minerals were also found in pumice fragments together with analcime (Figure 34-a) and K-feldspar (Figure 34-b).

As it is the case with the zeolites, the type of the phyllosilicate minerals can not be exactly determined by optical methods. Hence, the detailed identification of the phyllosilicate minerals as smectite is realized by the analyses of XRD, SEM and DTA methods.
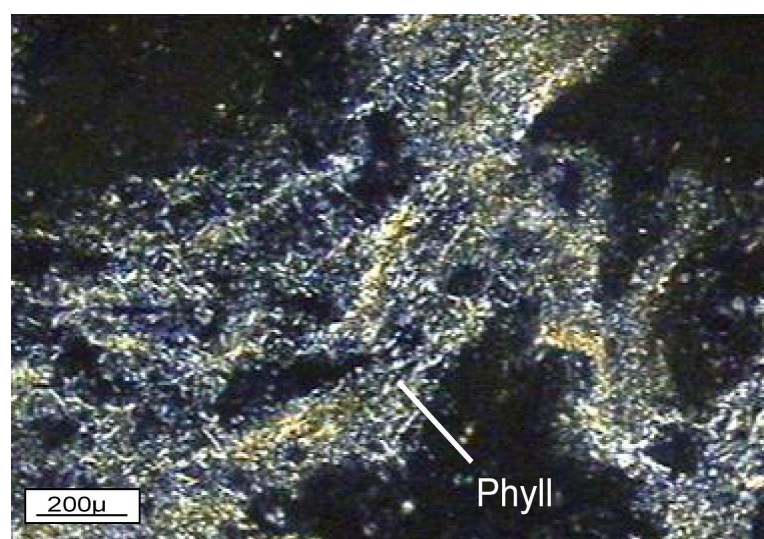


**Figure 33.** Photomicrograph of phyllosilicate minerals with flaky appearance (ÇPT-7, XPL), (Phyll: phyllosilicate minerals).
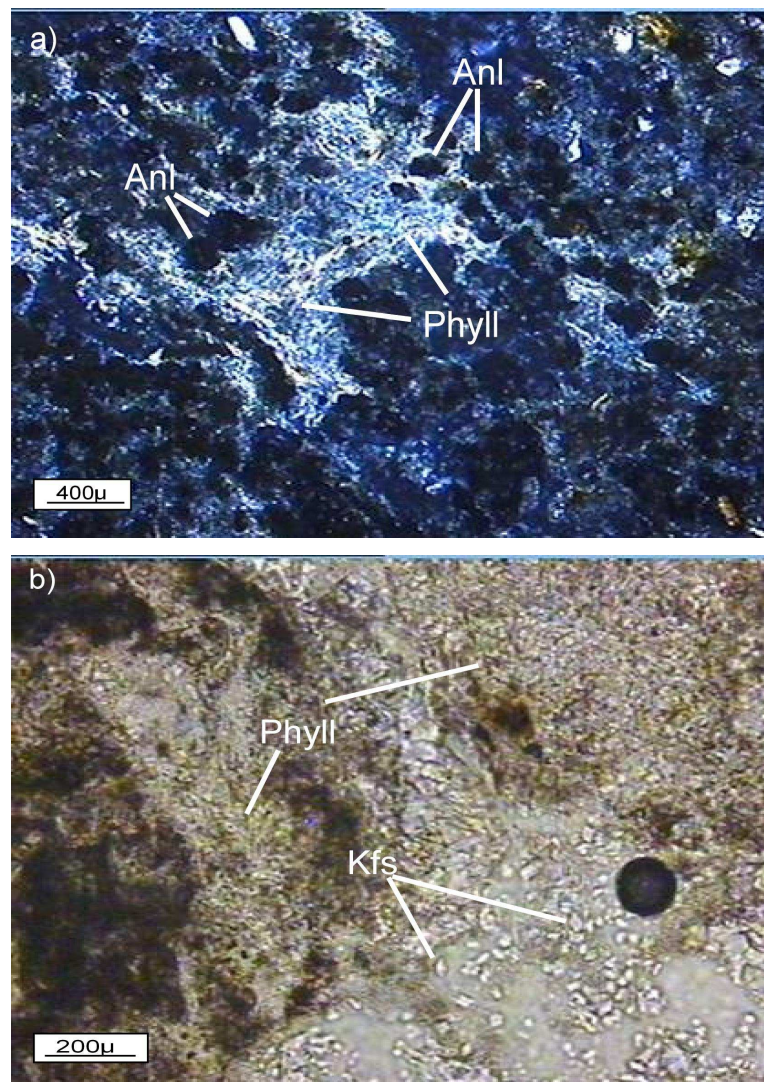
**Figure 34.** Photomicrograph of phyllosilicate minerals together with a) analcime and b) K-feldspar a) (KL-5, XPL), b)(KL-5, PPL), (Phyll: phyllosilicate mineral, Anl: analcime, Kfs: K-feldspar).

### 3.1.1.4.4. K-feldspar

The authigenic K-feldspar minerals occur as very small prismatic crystals under high magnification (X40). They were found in matrix together with phyllosilicate minerals and analcime (Figure 35). Only few optical properties of K-feldspars are

visual in thin sections because of very minute grain size. Still, low birefringence is the main identification property (Figure 36). In addition, K-feldspars are easily differentiated by their low relief, colorless feature and mainly prismatic shape (Figure 37).
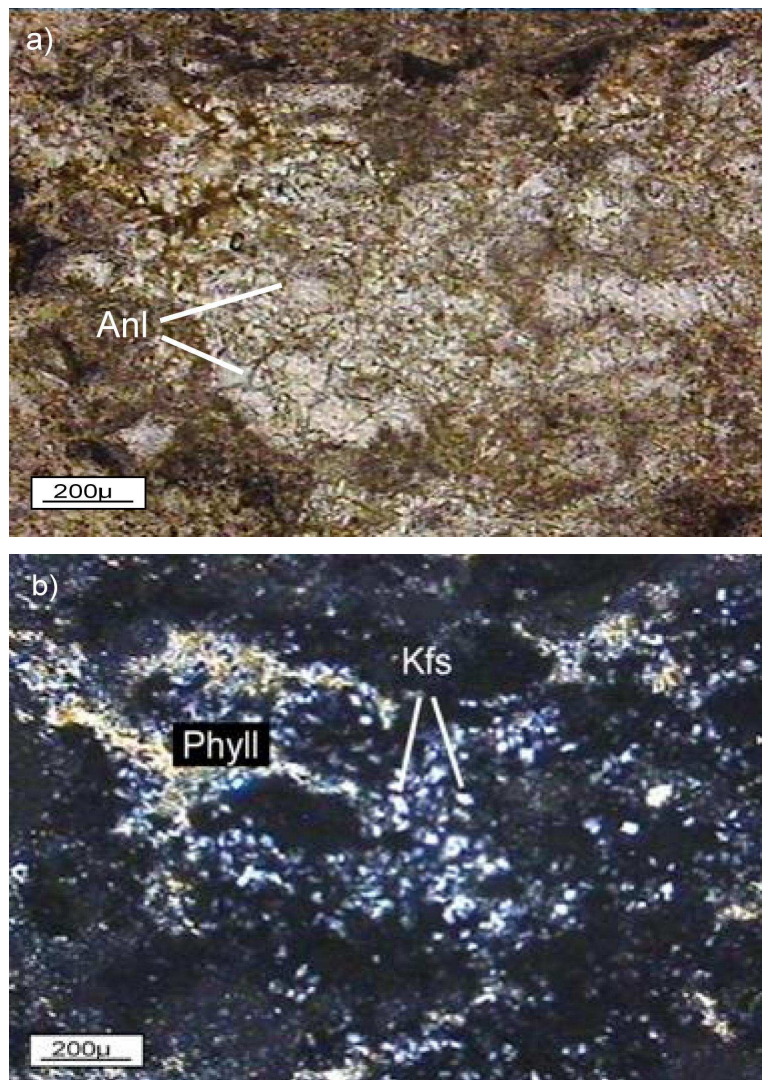


**Figure 35.** Photomicrograph of K-feldspar together with analcime and phyllosilicate (KK-5, PPL) b) (KK-5, XPL), (Anl: analcime, Phyll: phyllosilicate mineral, Kfs: K-feldspar).

These minerals were determined as K-feldspars based on SEM study which will be given in Chapter 4. Authigenic K-feldspar minerals exist in all samples and usually makes up about 25%. These K-feldspars usually embedded in the matrix.
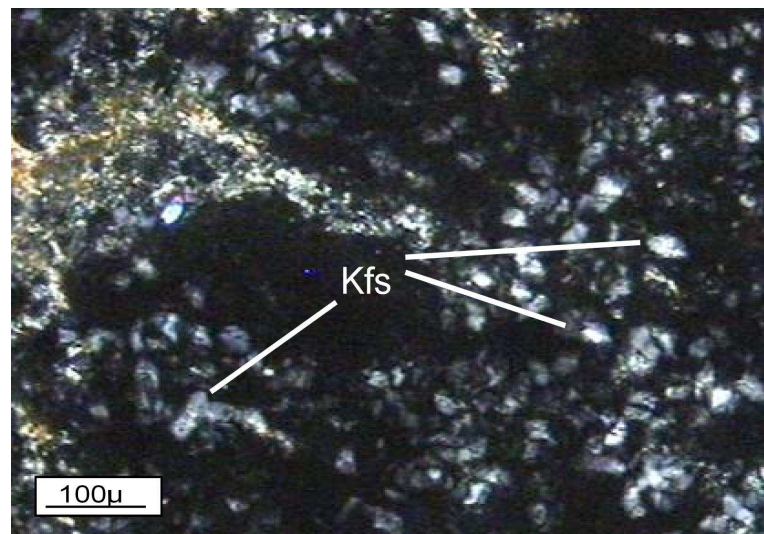


**Figure 36.** Photomicrograph showing low birefrincent K-feldspar (KK-5, XPL), (Kfs: K-feldspar).
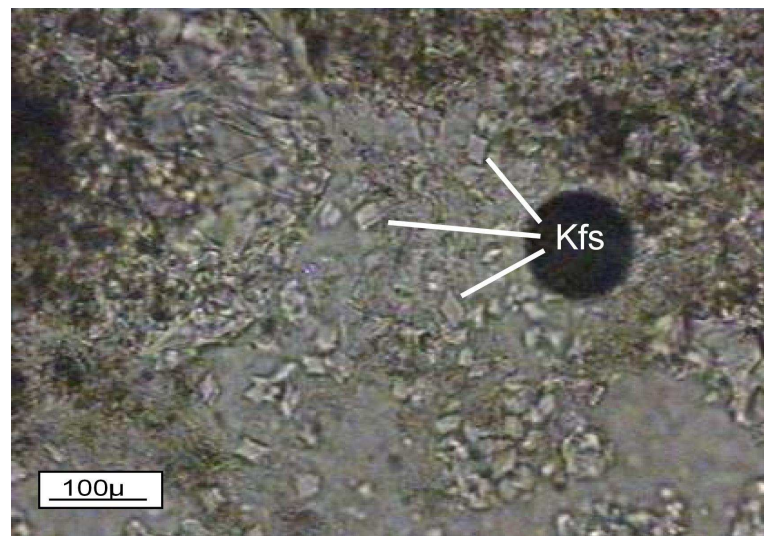
**Figure 37.** Photomicrograph of K-feldspar with prismatic in shape (KL-5, PPL), (Kfs: K-feldspar).

### 3.1.2. Dolomite-Rich Vitric Tuffs and Dolostone

### 3.1.2.1. Dolomite-Rich Vitric Tuffs

Based on the dominance of authigenic dolomite in the matrix, a part of the studied rocks (7 samples) is grouped as dolomitic vitric tuffs. Another group of dolomite-dominated rock was found at the transition between the lake deposits and tuffs. It is actually a sedimentary rock with very fine tuffaceous material and named as dolostone.

The vitric tuffs of this group are similar to the first group in their mineralogical characters. However, the phenocryst content is lower than the first group of tuffs. The rock comprises mainly quartz, minor biotite, plagioclase, sanidine, rock fragments and pumice fragments. Tuff samples were named as vitric tuff according to Pettijohn (1957). These dolomitic vitric tuffs consist of phenocrysts, ash and lithic fragments. Microscopical study reveals that pyroclasts range in size

67

0.01 mm to 0.06 mm, so these tuffs can be classified as fine tuff (Fisher and Schimincke, 1984) (Table 3).

Three samples of this group are A-9, A-12 and ÇT-8. Samples A-9 and A-12 are from the Arıklı region (Figures 20 and 21). Sample ÇT-8, however, was taken from the outcrops to the south of Nusratlı. Because samples of A-9 and A-12 were taken from locations very close to each other in the field, the thin sections show little differences in percentage of phenocryts and other compounds. Both of them contain pumice fragments. The pumices are generally 50μ-1mm in size and of angular shape. These broken pumices contain well-developed analcime crystals.

This group of tuffs contains quartz, minor amount of biotite, plagioclase and sanidine as primary minerals. Most of the vitric material is altered to one or more of the authigenic aluminosilicate minerals. These are zeolite (analcime), carbonate (dolomite), K-feldspar and phyllosilicates (smectite). Pumice fragments and rock fragments are also found. Glass shards are not observed.

### 3.1.2.1.1. Primary Minerals

Dolomitic tuffs have the same type of phenocrysts, which are quartz, biotite, plagioclase and sanidine with respect to clayey tuffs. The percentage of phenocrysts ranges from 2 to 5%. The amount of phenocrysts in sample ÇT-8 is low (2%), and samples A-9 and A-12 have 3-5% phenocrysts (Table 4). The most abundant silicate mineral is quartz, which occurs as single crystals. It is anhedral in shape. Plagioclase exhibits albite twinning. Euhedral to subhedral biotite is brown pleochroic and show mottled extinction. Small phenocrysts of sanidine having euhedral to subhedral crystal shape are colorless and show low birefrincence.

### 3.1.2.1.2. Glassy Material

Only pumice fragments constitute glassy material. No glass shards are differentiated in this second group. Pumice fragments are angular and some are porous. Pumice fragments in ÇT-8 and A-12 are cracked and highly angular. Euhedral analcimes are found in these pumice fragments (Figure 38). The pumice fragments are more abundant than those in the phyllosilicate group. They are commonly make up about 15-20% of the constituents (Table 4). Generally, all non-porous pumice fragments underwent dolomitization as seen in Figure 39.
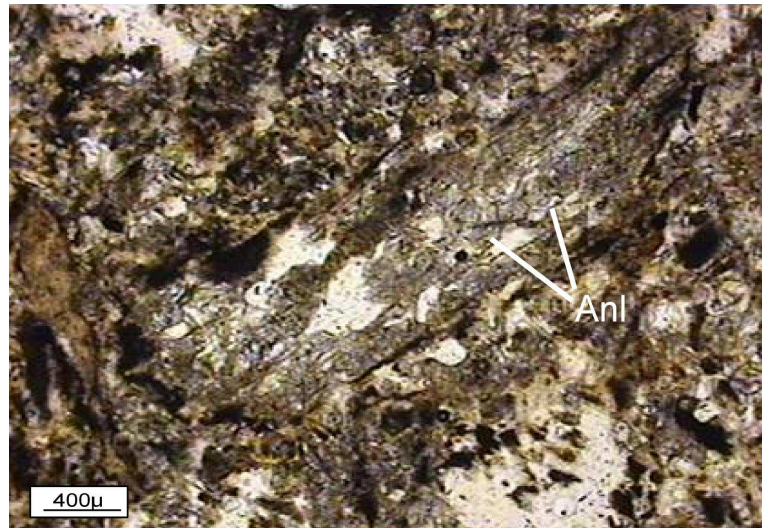


**Figure 38.** Photomicrograph showing porous pumice fragment and euhedral analcime crystals in it (ÇT-8, PPL), (Anl: analcime).
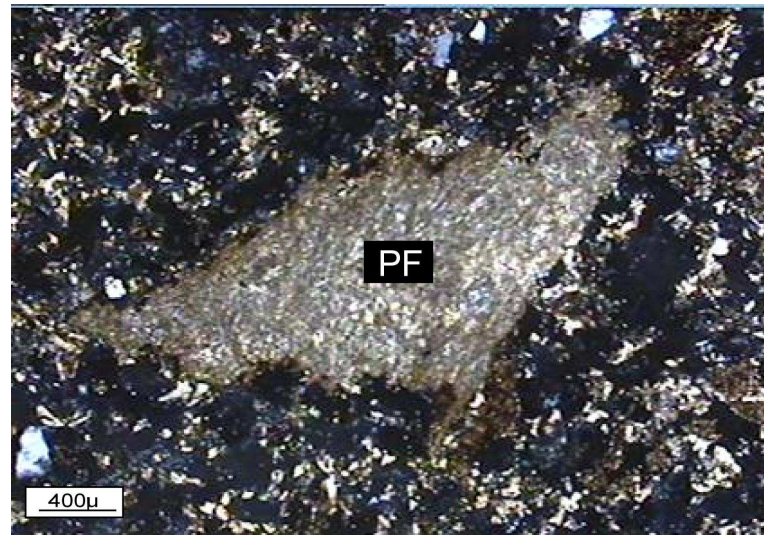
**Figure 39.** Photomicrograph showing wholly dolomitizied pumice fragment (A-12, XPL), (PF: pumice fragment).

### 3.1.2.1.3. Rock Fragments

Since rocks fragments have undergone high alteration, it is difficult to determine their type. However, based on ghost textures, clasts of porphyritic volcanic rocks with flow-texture can be identified as andesitic lavas. Rock fragments form a portion of only 1% of whole tuff-samples (Table 4).

### 3.1.2.1.4. Diagenetic Minerals

Even if the primary minerals are the same, dolomitic vitric tuffs are different in their authigenic mineral assemblages. In the matrix, they are represented by analcime, dolomite, phyllosilicate mineral and K-feldspar.

*3.1.2.1.4.1. Analcime*

Petrographically these analcimes in dolomite rich vitric tuffs are completely the same as with analcimes in clayey tuffs. They are colorless, have low relief (Figures 40 and 41), isotropic and often demonsrate euhedral (Figure 41) morphology.

Similar modes of occurrence are accepted to the tuffs with clayey (phyllosilicate-rich) matrix. Two modes of occurrence are noticed for formation of analcime just like phyllosilicate minerals dominated ones. These are;

1) Coarse-grained euhedral or anhedral crystals in cavities and pumice fragments
2) Clusters or single crystals of very fine analcimes embedded in the matrix

Colorless analcimes founding in cavities and pumice fragments are easily differentiated with low relief and isotropic character. Analcimes are mostly euhedral in pumice fragments (Figure 41). Size of analcime crystals are usually 100-200µ in diameter.
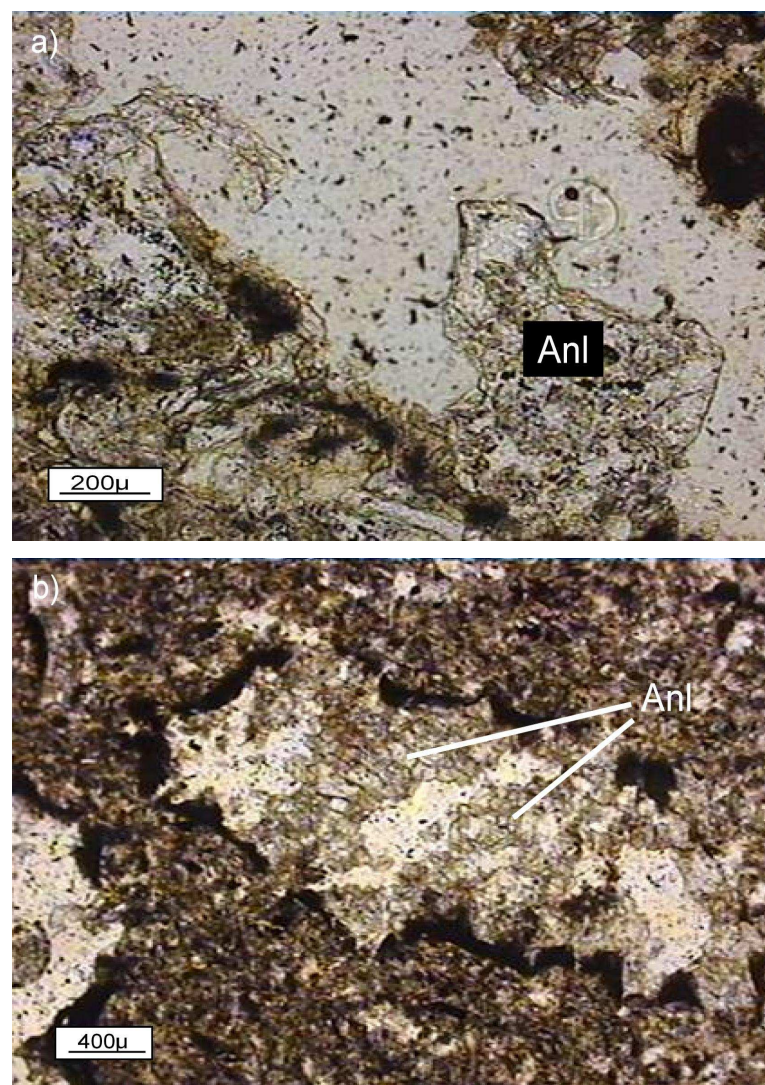
**Figure 40.** Photomicrograph showing analcime crystal a) in cavity (A-12, PPL), and b) in pumice fragment (ÇT-8, PPL), (Anl: analcime).
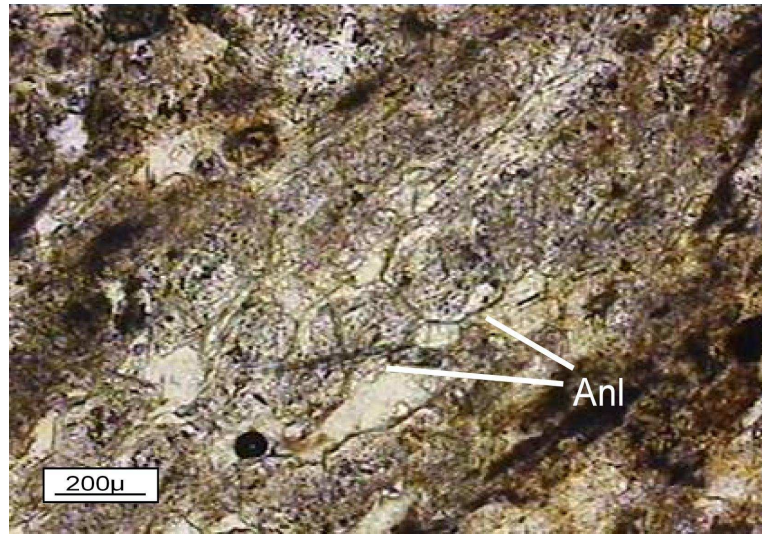
**Figure 41.** Photomicrograph showing euhedral analcime crystal in pumice fragment (A-12, PPL), (Anl: analcime).

Analcimes in the cavities as well as in pumice fragments are found within the matrix like the previous two types. They occur as small crystals and cryptocrystalline aggregates making up a part of the matrix in these tuffs (Figure 42). This group of tuffs usually includes 20-30% analcime (Table 4).
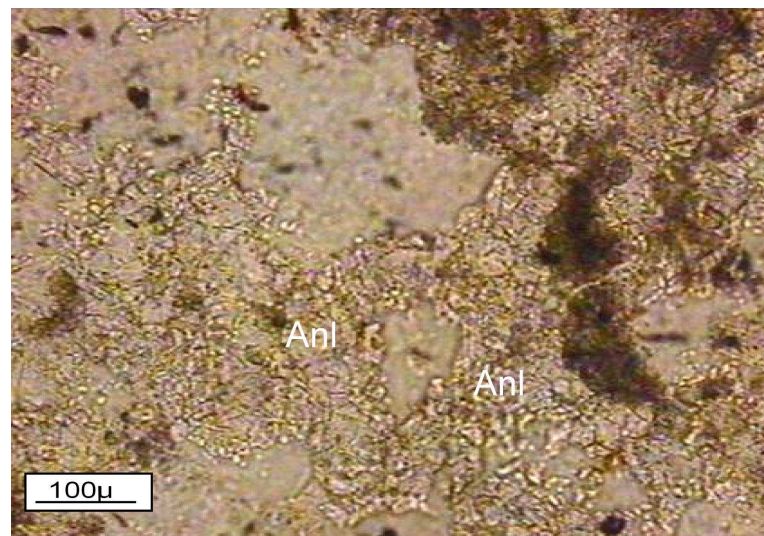
**Figure 42.** Photomicrograph showing cryptocrystalline aggregates of analcime crystals in the matrix (A-9, PPL), (Anl: analcime).

### 3.1.2.1.4.2. Dolomite

Dolomite is dominant in all of the examined samples. Mostly it occurs as aggregates of anhedral crystals (Figure 43). They make up about 60-70% of the rocks. High birefringent dolomite crystals are bigger in A-9 and A-12 than in ÇT-8. Changing relief can be observed when stage is rotated. Dolomite is found in the matrix as well as in the cavities. It is clearly a late product. Diatoms observed in ÇT-8 indicate lacustrine environment (Figure 43).
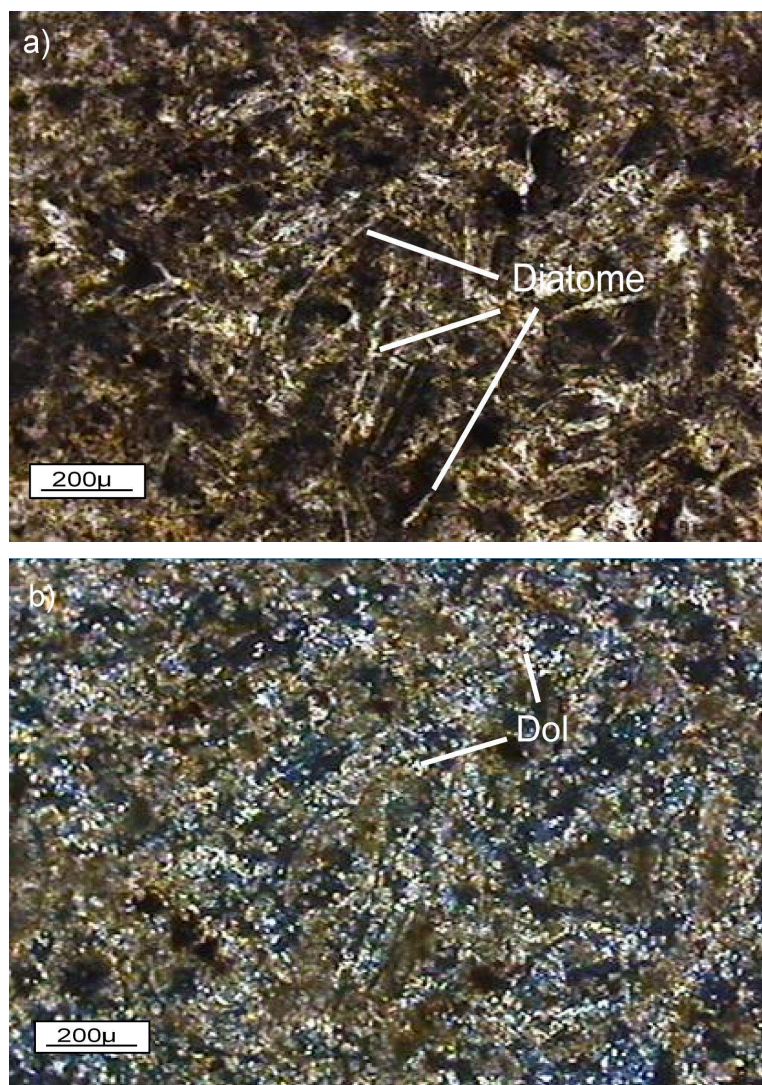
**Figure 43.** Photomicrograph of dolomite a) (ÇT-8, PPL), b) (ÇT-8, XPL), (Dol: dolomite).

### 3.1.2.1.4.3. Phyllosilicate Minerals and K-feldspar

K-feldpar and phyllosilicate minerals in this type of tuffs were not easily identified by optical methods because of their very minute size. Even in high magnifications, it is difficult to differentiate them from other constituents. In the matrix, only the low birefringent tiny minerals can be identified. Based on SEM

data, it can be said that the colorless tiny prismatic minerals observed together with dolomite in the matrix are K-feldspars and they are 15-20% in amount. The phyllosilicate minerals, on the other hand are characterized by parallel extinction but very small amount, not more than 3%. Another important point is that the K-feldspars in this group are not euhedral and they are found only in matrix and not in pumice fragments.

### 3.1.2.2. Dolostone

These rocks were separated from dolomitic tuff group as they do not include pumice fragments or glass shards. In thin sections, the rock mainly consists of tiny dolomites and euhedral analcimes in the cavities (Figures 44 and 45). Dolomites have very minute grain size. Therefore they can only be differentiated by their high birefrincence. Only four samples, namely Y-12, ÇT-10, ÇT-19 and ÇT-20 fall under this group.
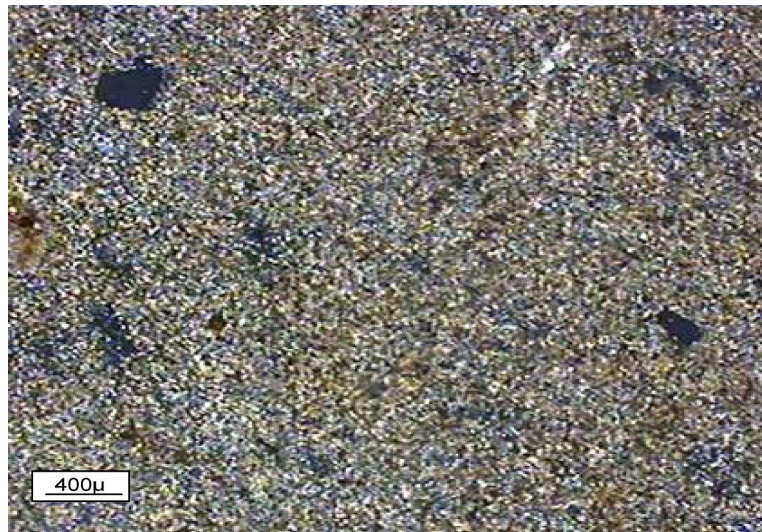


**Figure 44.** Photomicrograph of tiny dolomite crystals (ÇT-10, XPL).

Quartz was found as fine clasts in both thin sections. Plagioclase and biotite clasts are of trace amounts in the studied samples. So, primary minerals constitute less than 2% (Table 4). K-feldspar in this type of tuffs can not be identified by optical methods because of their very minute size. Hence, their percentage is can not be given. There are no phyllosilicate minerals in the studied samples.

Analcime occurs in these rocks as well-developed euhadral, subhedral or anhedral crystals in cavities (Figures 45 and 46). Well-developed analcime crystals show euhedral shape in best morphology (Figure 45). In addition, euhedral or anhedral analcime crystals in cavities were detected by petrographical study, whether analcime is formed in the matrix or not it can not be determined with this method.
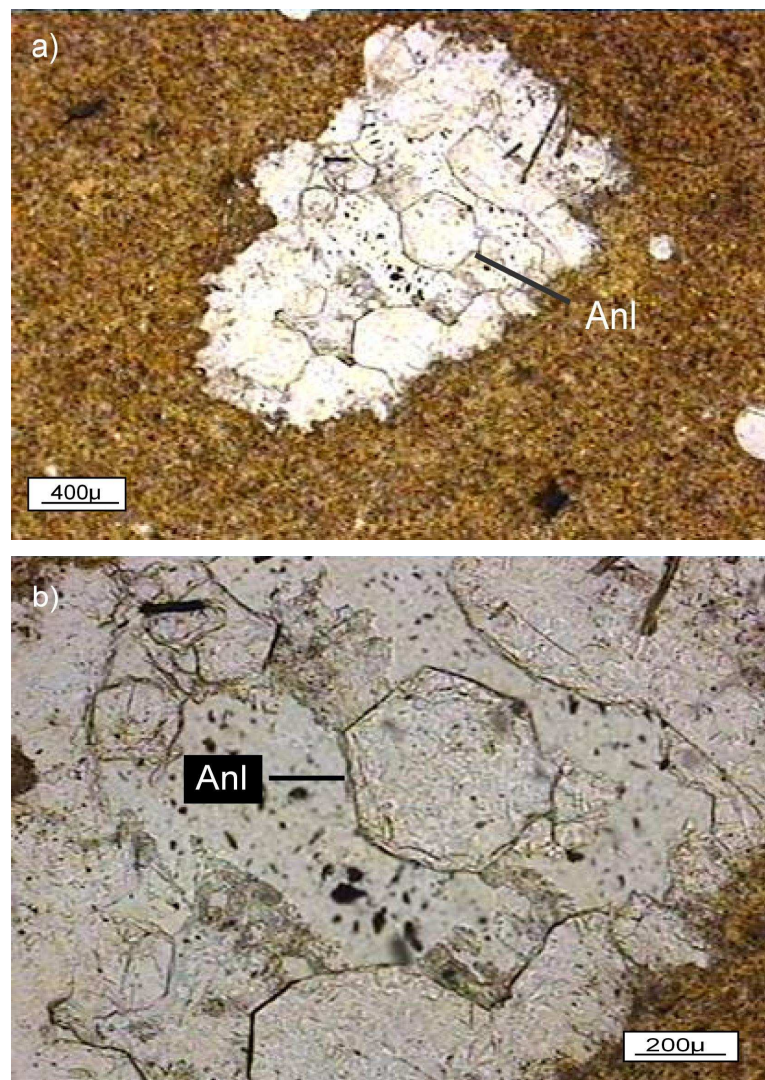
**Figure 45.** Photomicrographs showing euhedral analcime crystals showing idiomorphic morphology in cavity a) (ÇT-10, PPL), b) (ÇT-10, PPL), (Anl: analcime).
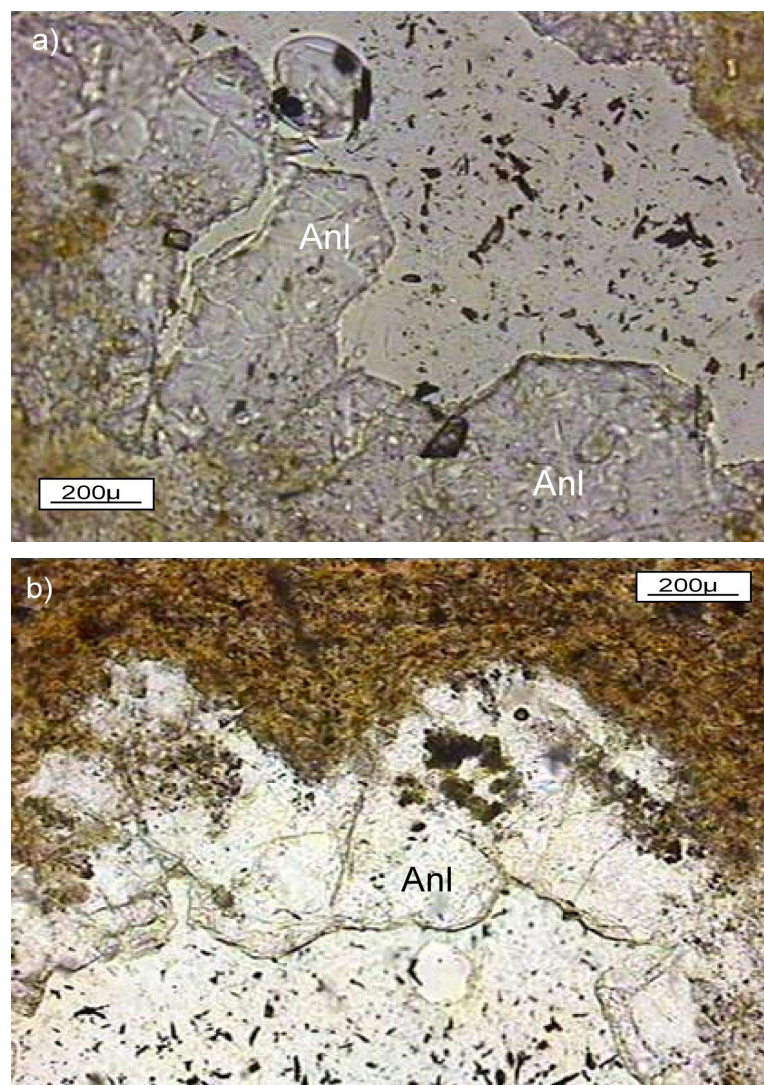
**Figure 46.** Photomicrographs showing a) subhedral and b) anhedral analcime crystals a) (ÇT-10, PPL), b) (ÇT-10, PPL), (Anl: analcime).

### 3.1.3. K-feldspar-Dominated Vitric Tuffs

While studying this group of tuffs in thin section, it is recognized at first sight that phenocrysts, rock fragments and glass shards are embedded in a matrix that consists wholly of cryptocrystalline minerals (Figure 47). These colorless minerals have white interference color with low birefrengence. These minerals are

also found in clayey and dolomitic tuffs in smaller amounts, but, here the amount of them are very high. Consequently, these samples were evaluated as different group. Even though most of them are cryptocrystalline, there are larger ones compared to the sizes of other two types.

This group of tuffs can be named as vitric tuff by existence of glass shards and pumice fragments (Pettijohn, 1957). They are classified as fine tuffs, as the grain size varies between 0.01 and 0.06mm (Fisher and Schimincke, 1984) (Table 4). The pyroclastic grains consist mainly of quartz, minor plagioclase, sanidine, biotite, rock fragments, glass shards and pumice fragments.

The colorless cryptocrystalline minerals that replace the matrix are too small for the examination of their optical properties. Therefore, these minerals were studied by SEM and designated as K-feldspars. A detailed account of this designation will be discussed in Chapter 4.

Thin sections of five samples from this group were studied in detail: KK-2, KK-8, A-2, KÇ-6 and YÇT-9 namely. Samples KK-2 and KK-8 are from Küçükkuyu, A-2 is from Arıklı, KÇ-6 is from the Karaçam Tepe, to the south of Nusratlı and YÇT-9 is from southwest of Yeşilyurt. Samples KK-2 and KÇ-6 are rich in analcime, whereas no analcime could be identified in samples A-2, KK-8 and YÇT-9 (Table 4).

Generally, this group of tuffs contains quartz, biotite and minor amounts of plagioclase, sanidine as phenocrysts, and zeolite (analcime), phyllosilicate (smectite), K-feldspar and carbonate (dolomite) as authigenic minerals, locally unaltered volcanic glass and rock fragments.
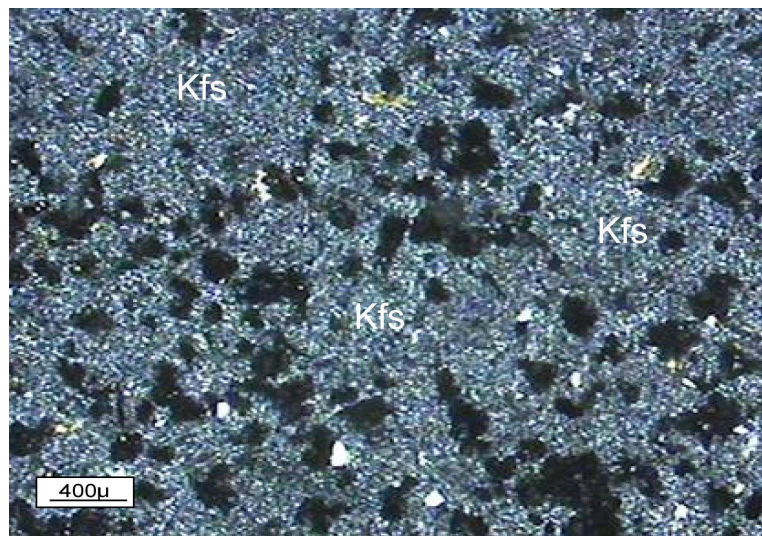
**Figure 47.** Photomicrograph showing cryptocrystalline K-feldspars embedded in matrix (KK-8, XPL), (Kfs: K-feldspar).

### 3.1.3.1. Primary Minerals

The phenocrysts are the same as those mentioned in the other tuffs. The percentage of phenocrysts ranges from 3% to 13%. YÇT-9 has high amount of primary minerals (13%) with respect to the other tuffs. KK-8 and KK-2 have more primary minerals (8%) than KÇ-6 (5%) (Table 4). Quartz is found more than other two tuff groups. It constitutes 2% to 10% of the whole rock (Table 4). Clear, colorless quartz crystals with low birefrincence have subhedral outlines. These are generally small in size. Minor amounts of plagioclase, sanidine and biotite which make 2% of phenocrysts are also seen. Plagioclase typically exhibits polysynthetic twinning. Fine grained biotite crystals are brown in color and show brownish pleochroism. Some biotite crystals demonstrate well-developed cleavages. Colorless sanidine crystals generally occur as small phenocryts having a euhedral to subhedral crystals outline. They underwent slight alteration and low birefringence.

### 3.1.3.2. Glassy Material

The vitric material consists mainly of pumice fragments and glass shards. The size of the pumices varies from 500μ to 1mm in diameter. Pumice fragments are usually elongate, and some of them are vesicular. These can be easily differentiated with a dark rim of very fine grained Fe-oxide as seen in the Figure 48. In addition to these, larger pumice fragments have usually different internal textures than those in the matrix. This is mainly due to the presence of euhedral K-feldspars in the pumice fragments that contrasts with the very fine-grained anhedral ones in the matrix. The pumice fragments in this group commonly make up about 10-15% of the rock, more than that in phyllosilicate mineral-bearing tuffs (Table 4).
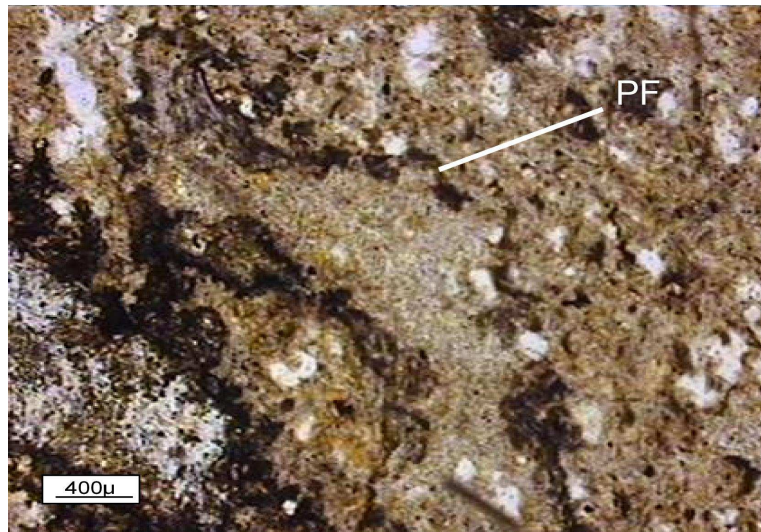


**Figure 48.** Photomicrograph of pumice fragments with dark rim of Fe-oxide (A-2, PPL), (PF: pumice fragment).

The other type of the glassy material in the samples is glass shards, which are very well preserved in the sample KK-2. Glass shards comprise about 25% of the rock.

Well-preserved glass shards indicate that this tuff was exposed to relatively low alteration. As seen in the Figure 49, the glass shards are lath and Y-shaped, which is a typical feature of them. As seen in the Figure 50, some glass shards were partly replaced by a cryptocrystalline unisotropic mineral that resembles K-feldspars rather than analcimes.
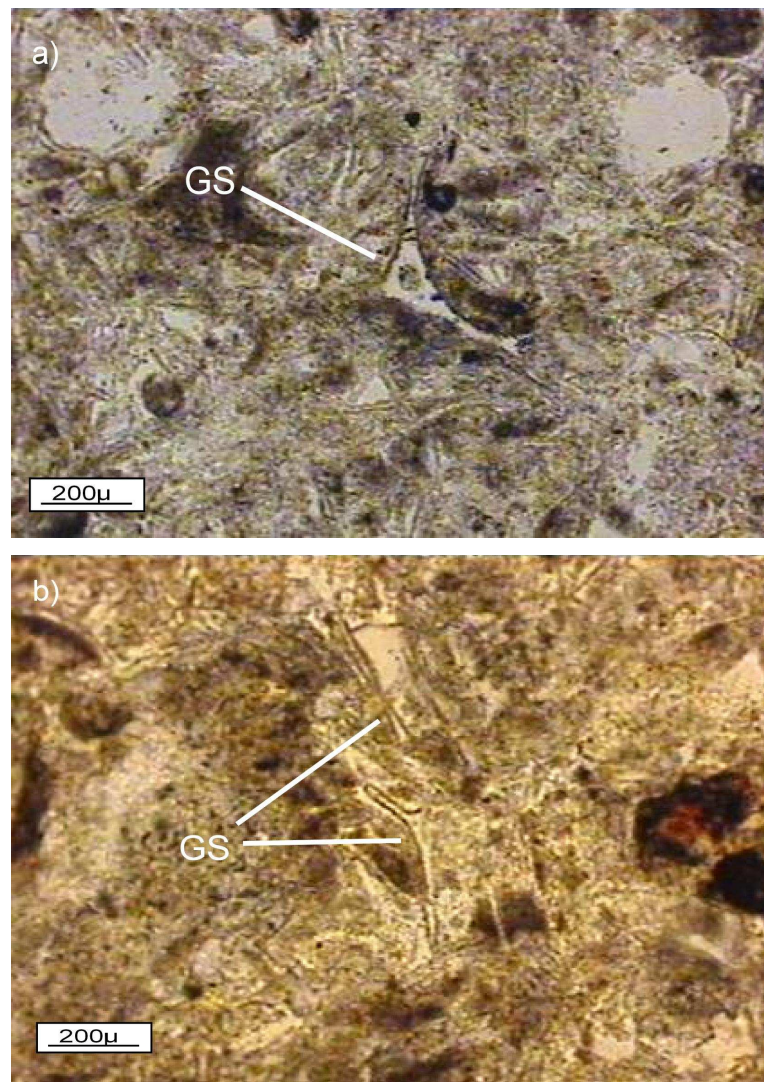


**Figure 49.** Photomicrographs showing lath and Y-shape of glass shards a, b: (KK-2, PPL), (GS: glass shard).
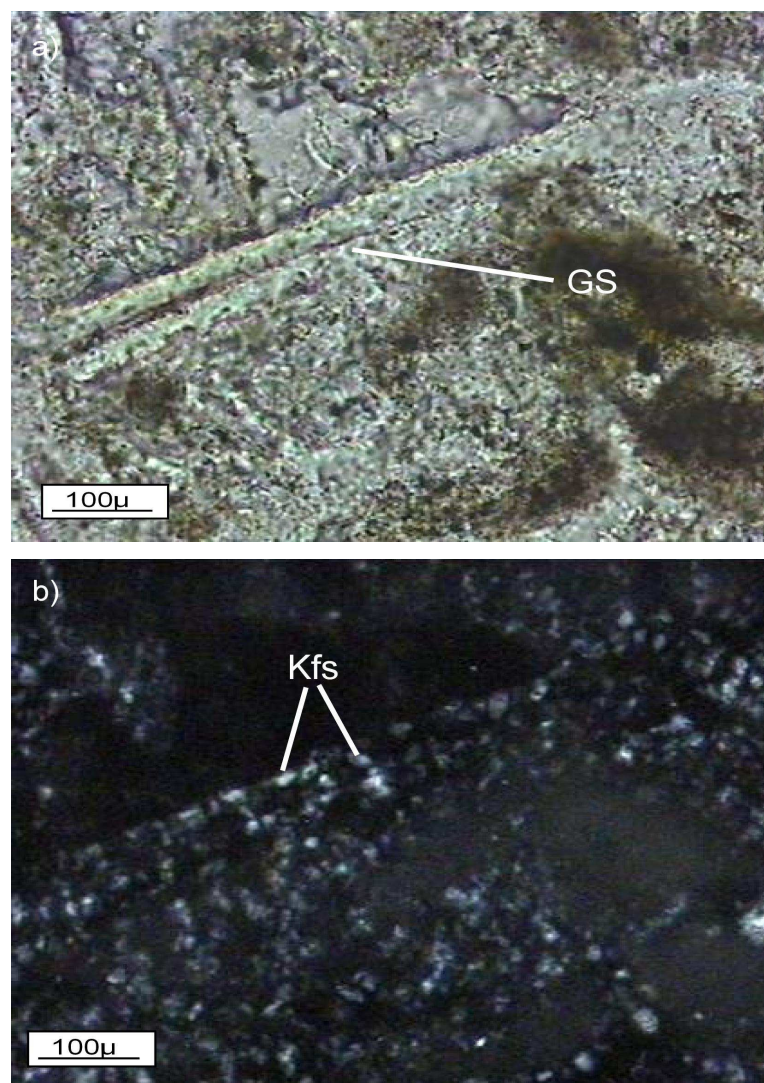
**Figure 50.** Photomicrograph showing glass shard replaced by K-feldspar a) (KK-2, PPL), b) (KK-2, XPL), (GS: glass shard, Kfs: K-feldspar).

### 3.1.3.3. Rock Fragments

Rock fragments are found in limited amounts and make up not more than 1% of the studied samples (Table 4). Alteration causes the difficulty for determination of the type of fragments. Still, it can be said that these are volcanic in origin based on their textures (Figure 51).
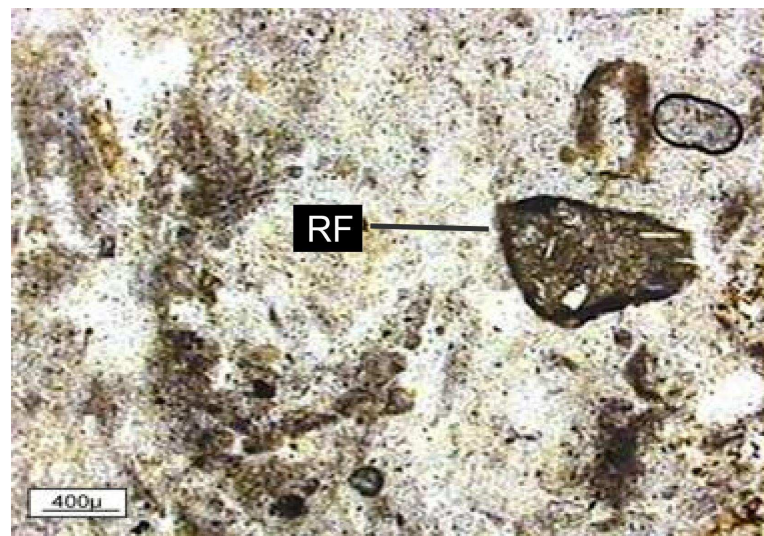
**Figure 51.** Photomicrograph showing rock fragment with volcanic origin (KK-2, PPL), (RF: rock fragment).

### 3.1.3.4. Diagenetic Minerals

The type of diagenetic minerals exists in these tuffs is the same as former two types. However, the amount of analcime is less than the other two types. Morever, 3 tuff samples (A-2, KK-8, YÇT-9) do not include analcime.

#### 3.1.3.4.1. Analcime

Except A-2, KK-8 andYÇT-9, other samples (KK-2, KÇ-6) of this type of tuffs altered to analcime. Although these five tuff samples resemble each other petrographically, KK-2 and KÇ-6 contain analcime. In thin sections, such coarse-grained analcime crystals are easily recognizable by their typical optical properties (Figure 52). They are colorless, have low relief (Figure 53) and isotropic property. Two modes of occurrence are noticed for the formation of analcime like former two groups.

Analcimes in pumice fragments and cavities are very rare. Euhedral analcime can not be detected in pumice fragments. Usually these are anhedral in shape but subhedral ones were detected as seen in Figure 52. Analcimes in pumice fragments and cavities are approximately 100μ in diameter and they are differentiated with their low relief and isotropic properties.
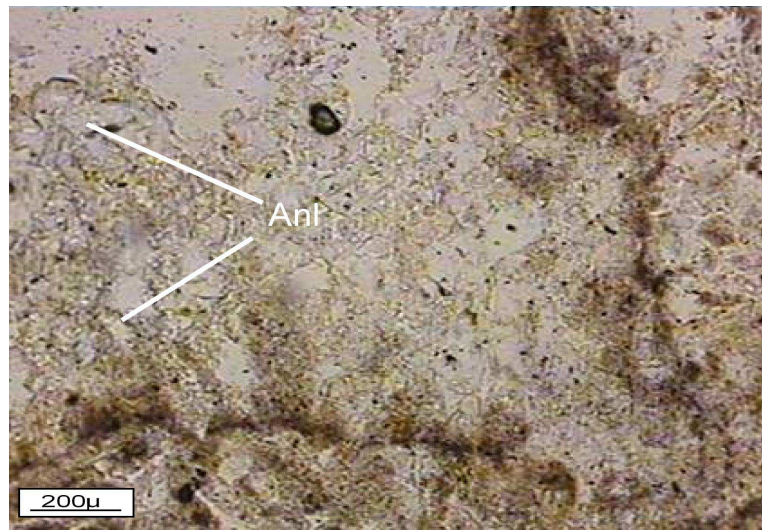


**Figure 52.** Photomicrograph showing subhedral analcime crystals in pumice fragment (KK-2, PPL).

Next to analcimes in cavities and pumice fragments, some are also observed in the matrix. Analcimes in the matrix are more than analcimes in pumice fragments. Figure 53-a shows a large analcime crystal in the matrix, however they usually occur as small crystals (Figure 53-b).
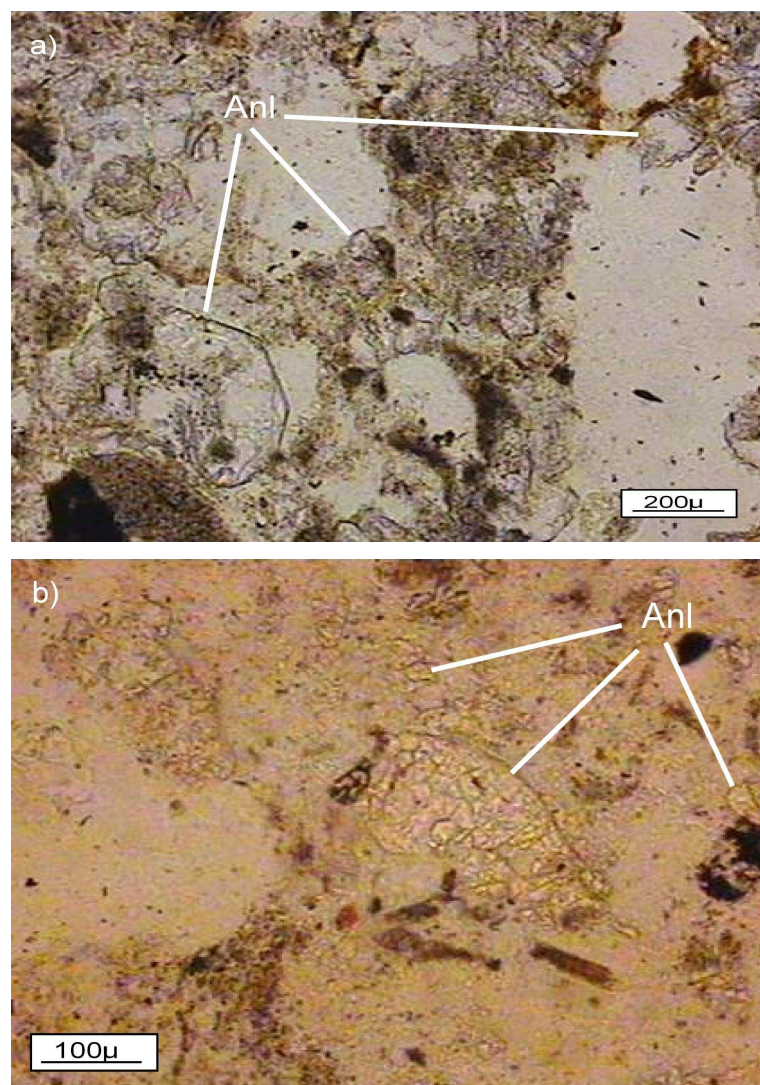
**Figure 53.** Photomicrograph showing a) coarse-grained (KK-2, PPL) b) very fine-grained analcime crystals in matrix (KK-2, PPL), (Anl: analcime).

The percentages of analcime in KK-2 and KÇ-6 are approximately 10% (Table 4).

### 3.1.3.4.2. Dolomite

Dolomite was found only in the sample of A-2, either in cavities or in the matrix. Dolomite makes up approximately 25% of the rock. It is a secondary mineral like

other two groups of tuff. Dolomite can easily be differentited with its high birefrincence and usually exhibits changing relief when microscope stage is rotated (Figure 54).
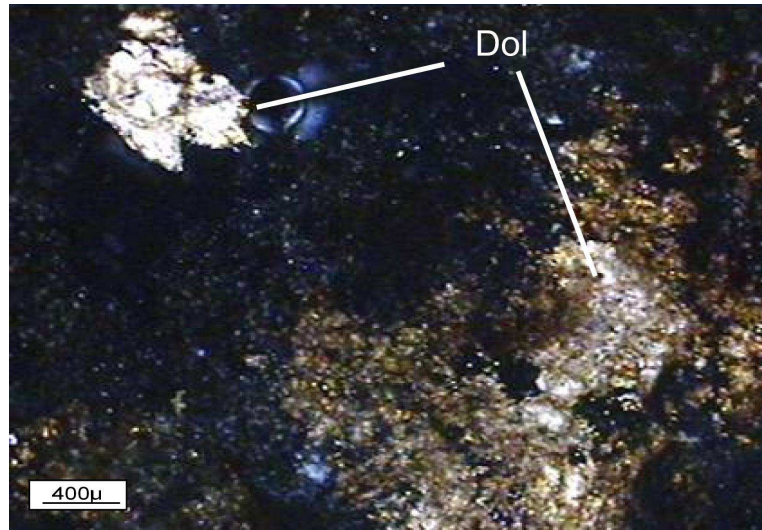


**Figure 54.** Photomicrograph showing high birefrincent of dolomite (A-2, XPL), (Dol: dolomite).

### 3.1.3.4.3. Phyllosilicate Minerals

Phyllosilicate mineral was found in samples KÇ-6 and YÇT-9 15% in amount. Sample A-2 contains less than 3%. Samples KK-2 and KK-8, on the other hand, contain no phyllosilicate mineral in the matrix (Table 4). Because KK-2, KK-8 and A-2 lack in phyllosilicate, the texture of these tuffs and the first group of tuff are completely different as seen in Figure 55. In sample KL-5 (Figure 55-a), (phyllosilicate–bearing vitric tuff), phyllosilicate minerals cover all parts of the thin section. In sample KK-2, (K-feldspar dominated vitric tuff), however, low

birefringent K-feldspars are seen (Figure 55-b). Figure 56 shows phyllosilicate mineral together with K-feldspar in the pumice fragment.
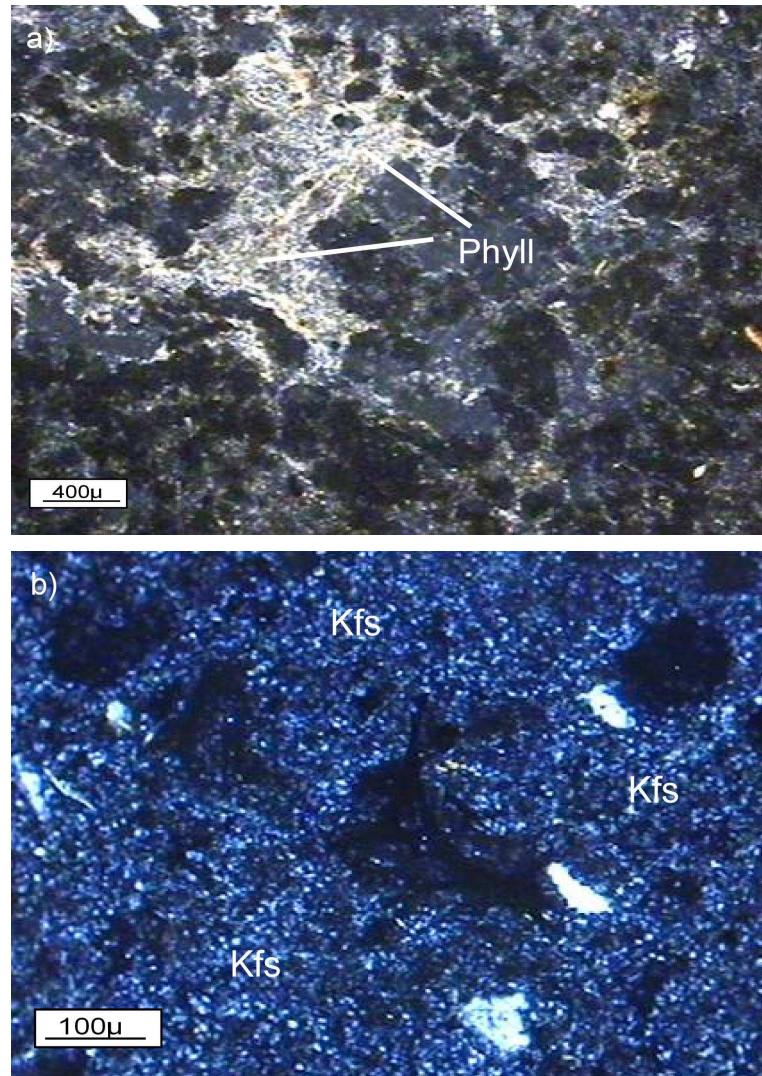


**Figure 55.** Photomicrographs showing a) appearance of phyllosilicate mineral–bearing tuff (KL-5, XPL) and b) appearance of K-feldspar dominated tuff (KK-2, XPL), (Phyll: phyllosilicate mineral, Kfs: K-feldspar).

Phyllosilicate minerals are recognized with flaky appearance in crossed polars with greenish yellow color. K-feldspar can be easly differentiated with low birefrincence as seen in Figure 56.
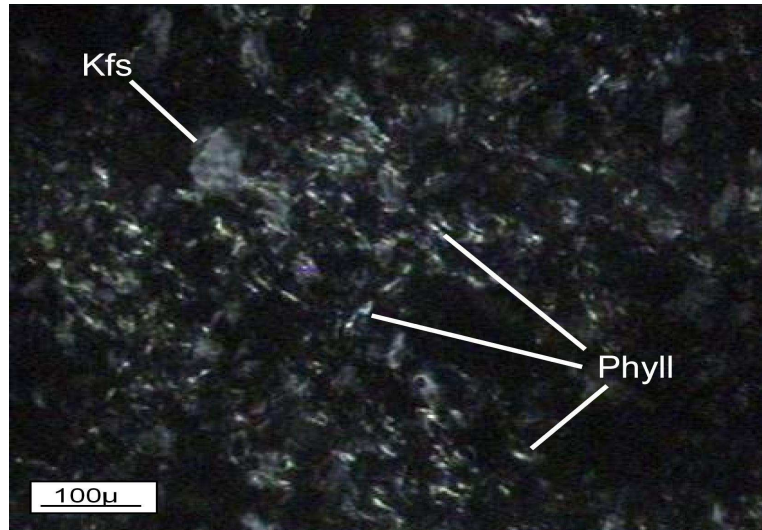


**Figure 56.** Photomicrograph of K-feldspar and phyllosilicate in pumice fragment (KÇ-6, XPL), (Kfs: K-feldspar, Phyll: phyllosilicate).

### 3.1.3.4.4. K-feldspar

K-feldspars make up 70-80% of the studied samples (Table 4). These white minerals are not only found in the matrix but also in the pumice fragments. The point that must be taken into account is that K-feldspars are anhedral in the matrix, but euhedral in pumice fragments. In the sample of KK-2, K-feldspars can be easly seen as prismatic shape (Figure 57). The K-feldspar that can easily be distinguished in the matrix with white interference color might be of diagenetic origin.
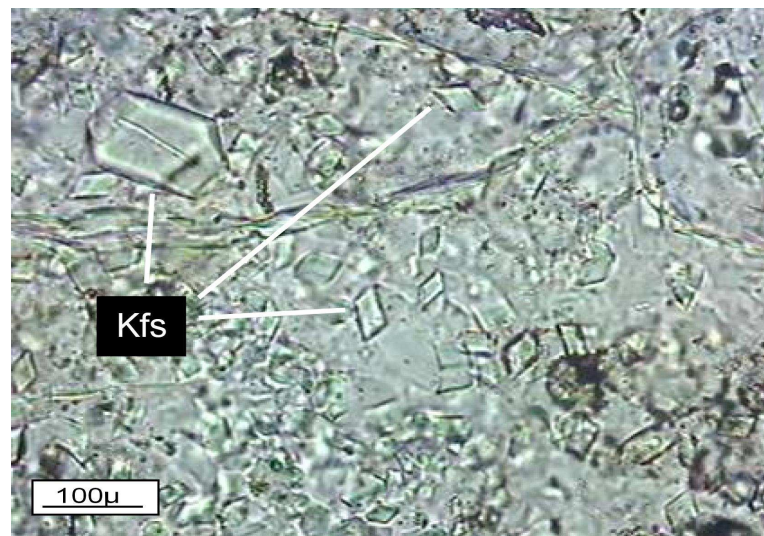
**Figure 57.** Photomicrograph showing prismatic K-feldspar in pumice fragment (KK-2, PPL), (Kfs: K-feldspar).

In general, small minerals with low birefringence were recognized as K-feldspars, based on optical properties and SEM studies. In sample A-2, on the other hand, K-feldspar-like low birefringent minerals grow into the void space (Figure 58).
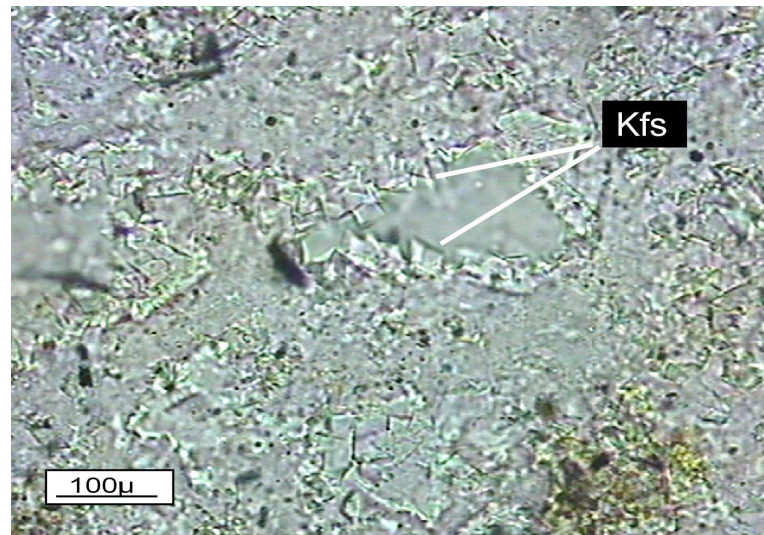


**Figure 58.** Subhedral K-feldspar crystals (A-2, PPL), (Kfs: K-feldspar).

The sample of ÇT-14 is different then the others since it is crystal tuff. It contains quartz, biotite, orthoclase, plagioclase and sanidine as phenocrysts, phyllosilicate minerals and K-feldspar as authigenic minerals, rock fragments and pumice fragments as lithic components. It does not contain analcime. Phenocrysts content ranges from 35% to 40%. Grains of quartz are anhedral and clear. Plagioclase grains display polysynthetic twinning. Biotite crystals are brown pleochroic and display cleavage. All biotites occur as coarse-grained laths. Orthoclase crystals occur as coarse-grained phenocrysts having euhedral to subhedral crystal outline. They have undergone alteration. The glassy material is represented by pumice fragments, which make up about 1% of the constituents. Rock fragments form 3% of whole sample. The matrix is composed of phyllosilicate minerals and K-feldspar as authigenic minerals. Phyllosilicate minerals can be distinguished by their flaky appearance, which are characterized by parallel extinction. Phyllosilicate minerals make up about 30-40% of the rock. The authigenic K-feldspar minerals occur as very small crystals under high mignification (X40). K-feldspars are easily differentiated by their low birefringence.

# CHAPTER 4

# MINERALOGY

## 4.1. Introduction

This chapter focuses on the mineralogical and morphological characteristics of the analcimes that were determined by optical microscopy methods. In addition to them, further investigation of mineralogical identification was performed by powder X-ray diffraction (XRD) and scanning electron microscope (SEM). These analyses are supported by differential thermal analysis (DTA).

## 4.2. X-Ray Diffractometric Analyses

### 4.2.1. Theoretical Background

When the atomic planes of crystals exposed to beams of X-rays, they give different reactions while beams leave the crystal. This event is called as X-ray diffraction.

Determination of minerals was made by matching $d$-spacings and $2\theta$ angles. A systematic procedure was used by ordering the $d$-spacings in terms of their intensity, beginning with the most intense peak ($I_{rel}$). Identification of crystalline compounds can be obtained by comparing the acquired pattern with the International Center for Diffraction Data (ICDD) database. Table 7 shows for XRD datas such as $d$-spacing, $2\theta$ and intensity of minerals. Therefore, examined

my samples by comparing XRD peaks in the graph. For this thesis, main interest was analcime and some other very fine grained minerals, which could not be identified by classical microscopy methods.

**Table 7.** 2θ angles (CuKα), interplanar spacing (*d*) and relative intensity (*I*rel) of minerals (Anl: analcime, Dol: dolomite, Qtz: quartz, Kfs: K-feldspar, Sme: smectite, AD: air-dry, EG: ethylene glycol, heating to 300 ℃ and 550 ℃) (Ferraris et al., 1972).

| | | | | | | |
|---|---|---|---|---|---|---|
| Anl | $I_{rel}$ | 100 | 80 | 70 | 50 | 40 |
| | *d-* | 3.43 | 5.61 | 2.92 | 2.5 | 4.85 |
| | 2θ | 25.97 | 15.79 | 30.5 | 35.77 | 18.29 |
| Dol | $I_{rel}$ | 100 | 30 | 30 | 15 | 10 |
| | *d-* | 2.89 | 2.19 | 1.79 | 2.01 | 2.67 |
| | 2θ | 30.94 | 41.22 | 51.14 | 45.1 | 33.56 |
| Qtz | $I_{rel}$ | 100 | 35 | 17 | 12 | 12 |
| | *d-* | 3.34 | 4.26 | 1.81 | 2.46 | 2.28 |
| | 2θ | 26.68 | 20.85 | 50.2 | 36.52 | 39.52 |
| Kfs | $I_{rel}$ | 100 | 55 | 55 | 50 | 30 |
| | *d-* | 3.33 | 3.79 | 4.24 | 3.23 | 3.47 |
| | 2θ | 26.77 | 23.54 | 20.9 | 27.61 | 25.67 |
| Sme | method | random | AD | EG | 300ºC | 550ºC |
| | *d-* | 5.73 | 5.93 | 5.19 | 8.75 | 9.02 |
| | 2θ | 15.14 | 14.87 | 16.72 | 10.15 | 9.88 |

## 4.2.2. Preparation of Samples

The samples were prepared following the procedure of Jackson (1975).

### 4.2.2.1. Preparation of Random Powder Bulk Samples

Random powder of the bulk sample was used for characterization of the whole rock mineralogy. Nearly 10 gr of each tuff sample was ground to a fine (<63μm) powder in an agate mortar. The powder was set on the glass slide assuring a flat

upper surface. It is important to completely cover the glass slide to avoid the XRD beams of the glass slide itself. Than, the glass slide was fixed in the diffractometer device.

**4.2.2.2 Preparation of Oriented Clay Samples**

Preparation of samples for detailed clay analyses is a little different than the random analyzes. In this method, the powdered tuff sample was brought into suspension in distilled water for extraction of the clay minerals from other fine grained non-clay minerals. The suspension was stirred with automatic mixer and it waited for 8 hours. Separation of clay fraction (<2mm) was obtained by the settling time methods based on Stokes Law (Jackson, 1975). At the end of this period, the upper part of the suspension was pipetted and filled in to tubes. The tubes were then centrifuged and 4 glass slides were covered by clay fraction. The 4 glass slides were allowed to dry in air. One of these was saturated by ethylene glycol at 60 ºC during 8 hours, two of these were heated to 300ºC and 550ºC, respectively for 1 hour and the last one was air-dried sample.

**4.2.3. X-Ray Diffractometry Data**

The XRD analysis was performed to confirm the presence of certain minerals mainly analcime. Although petrographic studies showed that the presence of analcime in Arıklı Tuff samples, X-ray diffraction analysis was the best way for identifying analcime because of the small grain size.  Some minerals observed by optical microscope may have very small reflections or even can not be detected by XRD in some samples. For example, biotite is present almost all of the Arıklı Tuff as seen by optical microscope, but abundance of biotite is very low (usually less than 3%) (Table 4). Therefore it showed small reflections or no reflection and it can be said that the biotite peak was close to the detection limit (C) or not detected (N) as shown in Table 8.

30 samples, collected from Arıklı Tuff were analyzed by XRD. Patterns of all of the analyzed samples are in general similar to each other. The mineralogical composition of the tuffs, as determined by XRD analysis, is given in Table 8.

**Analcime**

The characteristic peak of analcime was found on the XRD patterns in 25 samples. Representative XRD pattern of analcime-bearing tuffs (samples KL-5, KK-5) are shown in Figure 59. The most distinctive reflections of the Arıklı Tuff are 2θ of 25.97, 15.79, 30.50, 35.77 and 18.29 with *d*-spacing of 3.43, 5.61, 2.92, 2.50 and 4.85 °A, respectively (Table 7). No other zeolite type was obtained from the XRD analysis. Five Arıklı Tuff samples (YÇT-9, A-2, ÇT-14, KK-8 and YÇT-8) do not show analcime peaks. XRD patterns of analcime–bearing and analcime free tuffs were given in Figure 60. While sample KÇ-6 displays the main analcime peaks of *d*-spacing of 3.43, 5.61and 2.92 °A, sample YÇT-9, on the other hand, does not exhibit any of analcime peaks.

**Table 8.** XRD mineralogy of Arıklı Tuff samples determined by powder XRD (Symbols: P = present, N = not detected, C = close to detection limit, S = small amount, Qtz = quartz, Anl = analcime, Kfs = K-feldspar, Dol = dolomite, Sme = smectite, Bio = biotite).

|         | Qtz | Anl | Kfs | Dol | Sme | Bio |
|---------|-----|-----|-----|-----|-----|-----|
| ÇT-6    | S   | P   | P   | N   | P   | C   |
| ÇT-11   | S   | P   | P   | N   | C   | N   |
| ÇT-8    | S   | P   | N   | P   | C   | N   |
| A-12    | S   | P   | P   | P   | C   | N   |
| A-9     | S   | P   | P   | P   | C   | N   |
| KL-5    | S   | P   | P   | N   | C   | C   |
| KK-5    | S   | P   | P   | N   | P   | N   |
| ÇPT-3   | S   | P   | P   | N   | C   | C   |
| ÇPT-2   | S   | P   | P   | N   | C   | C   |
| KÇ-1    | S   | P   | P   | N   | N   | C   |
| ÇT-17   | S   | P   | P   | N   | P   | C   |
| ÇPT-1   | S   | P   | P   | N   | C   | N   |
| ÇPT-7   | S   | P   | P   | N   | C   | N   |
| ÇT-15   | S   | P   | P   | N   | C   | N   |
| ÇT-7    | S   | P   | P   | N   | C   | N   |
| ÇT-16-A | S   | P   | P   | N   | C   | C   |
| KK-2    | S   | P   | P   | N   | N   | N   |
| ÇT-10   | S   | P   | P   | P   | C   | C   |
| KÇ-6    | S   | P   | P   | N   | C   | N   |
| KL-2    | S   | P   | P   | N   | C   | C   |
| ÇT-19   | S   | P   | P   | N   | N   | N   |
| KÇ-3    | S   | P   | P   | N   | C   | N   |
| ÇPT-8   | S   | P   | P   | N   | N   | N   |
| ÇPT-10  | S   | P   | P   | N   | N   | C   |
| Y-12    | S   | P   | P   | P   | N   | C   |
| ÇT-14   | S   | N   | P   | C   | P   | P   |
| YÇT-8   | S   | N   | P   | N   | P   | C   |
| A-2     | S   | N   | P   | P   | N   | N   |
| KK-8    | S   | N   | P   | N   | N   | N   |
| YÇT-9   | S   | N   | P   | N   | N   | C   |
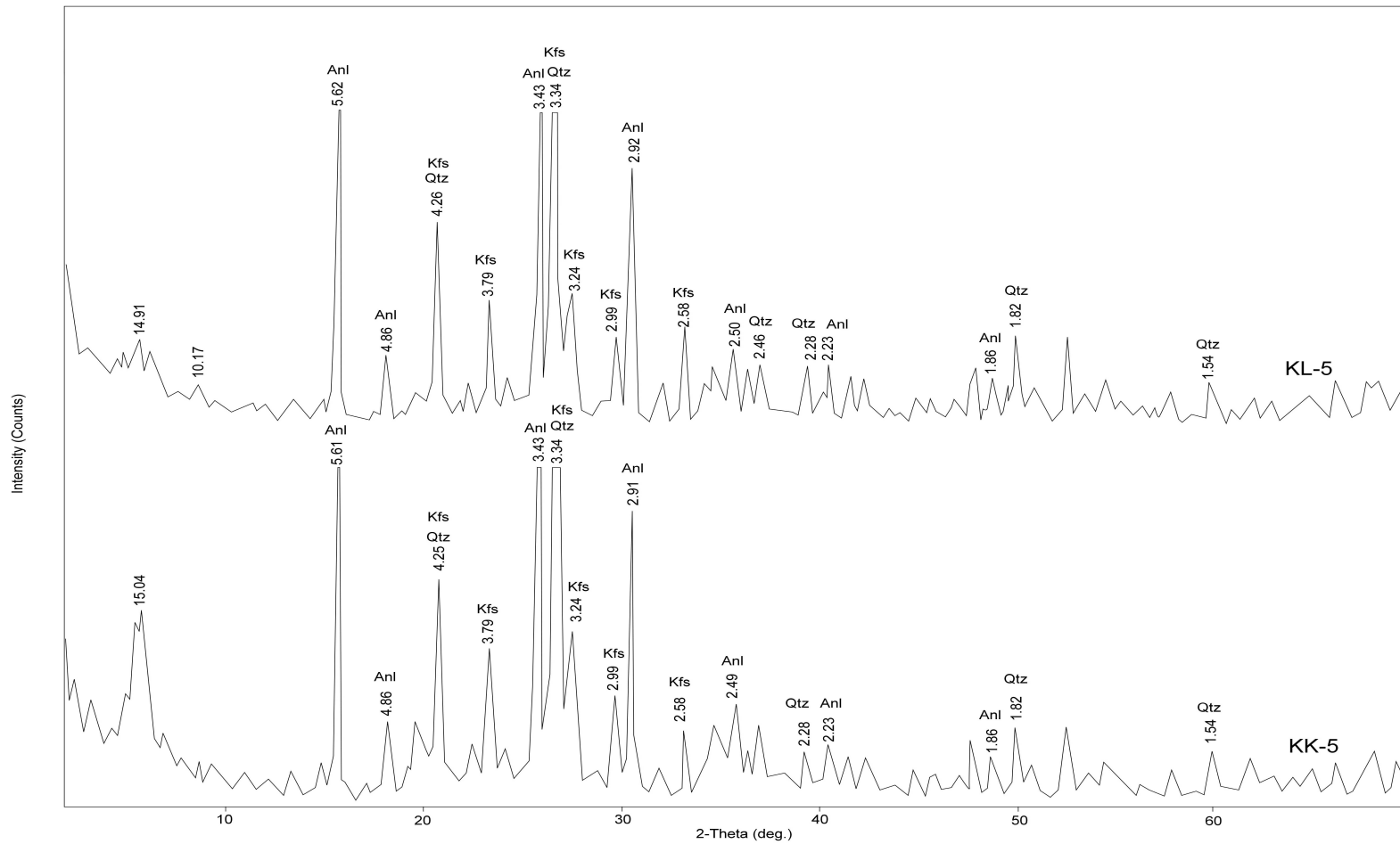
**Figure 59.** Random X-ray diffraction patterns of the KL-5 and KK-5 show analcime peaks.
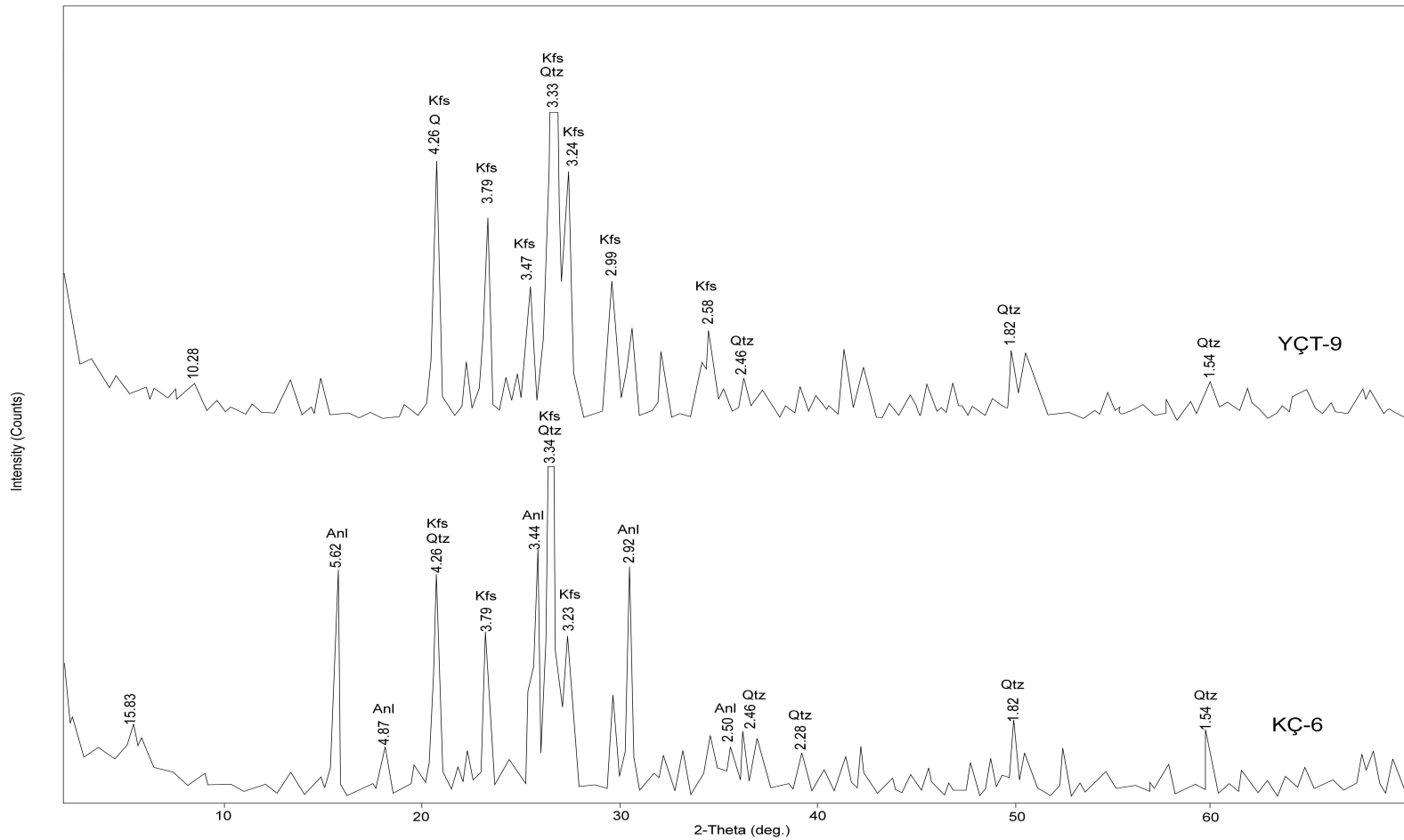
**Figure 60.** Random X-ray diffraction patterns of the YÇT-9 and KÇ-6 show analcime free and analcime bearing samples.

**Dolomite**

Although petrographic examination shows that there is a high abundance of dolomite in some tuff samples (ÇT-8, A-12, A-9), it can hardly be detected by the XRD at first sight. The reason why the main peak of dolomite (2.89 °A) was not seen is, that it is overlapped by the peak of analcime (2.92 °A) (A-12 and ÇT-8 in Figure 61). Whereas, the main peak of dolomite is seen very easily (Figure 62) in the tuff samples, which do not contain analcime (ÇT-14). Dolomite can be easily identified by its 2.91 °A peak in sample ÇT-14.

**Quartz**

It was found in all of the tuff samples and it can be identified by its 3.34, 4.26, 2.46, 2.28, 1.81 °A peaks (Figures 59, 60, 61 and 62). In most tuff samples, except in samples ÇT-6, ÇT-11, ÇT-8, A-12 and A-9, quartz has the dominant peak. In samples ÇT-6, ÇT-11, ÇT-8, A-12 and A-9, however, analcime has the dominant peak. But, this property does not show the exact abundance of these minerals since some K-feldspar peaks overlap with quartz peak as will be explained in K-feldspar. The very high peak of quartz (even though quartz found approximately 3% in tuffs) can be explained with overlaping by K-feldspar. Thus, existence of quartz in XRD patterns was showed with the letter of "S" (Table 8).
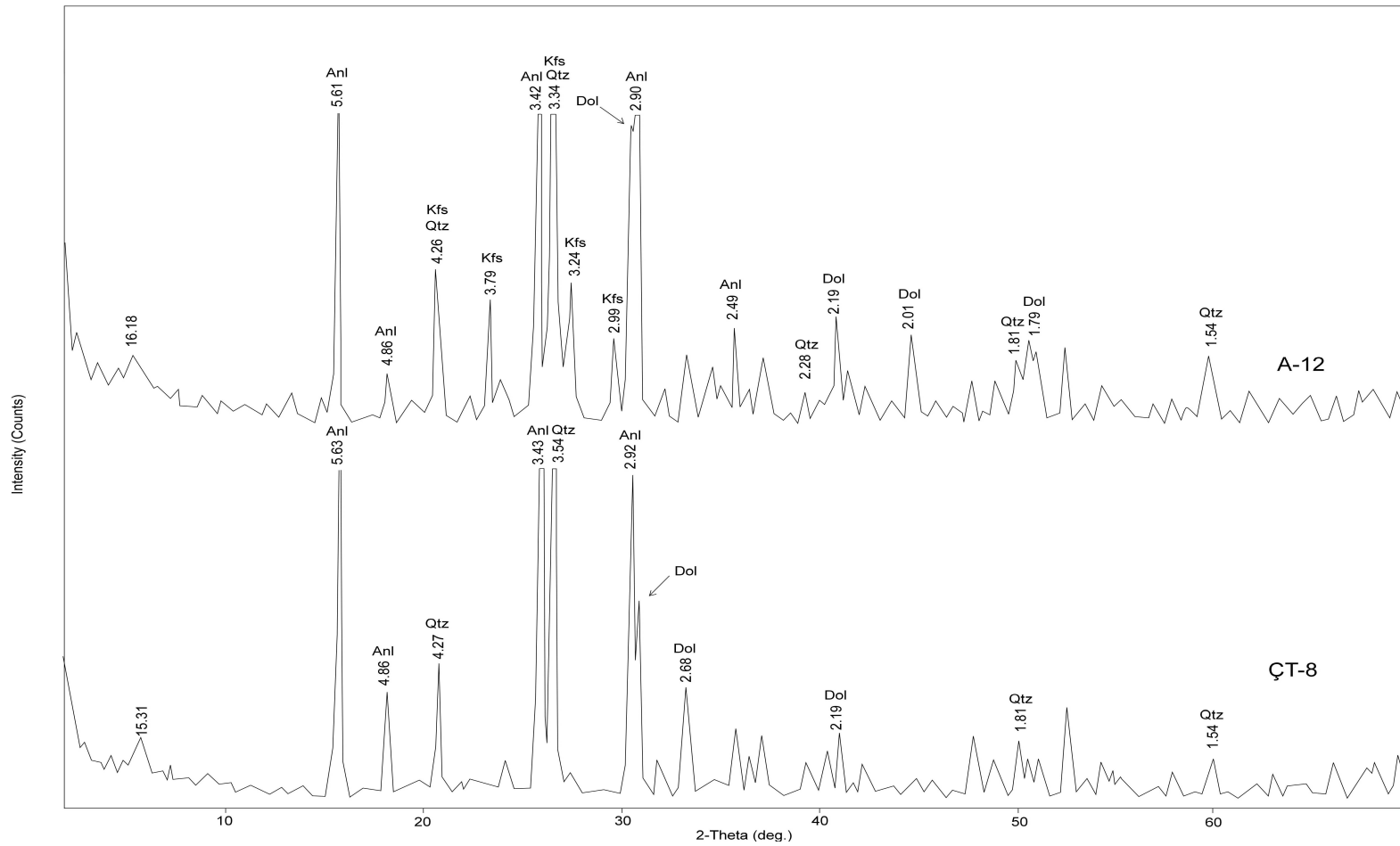
**Figure 61.** Random X-ray diffraction patterns of the A-12 and ÇT-8 show analcime peaks.

101
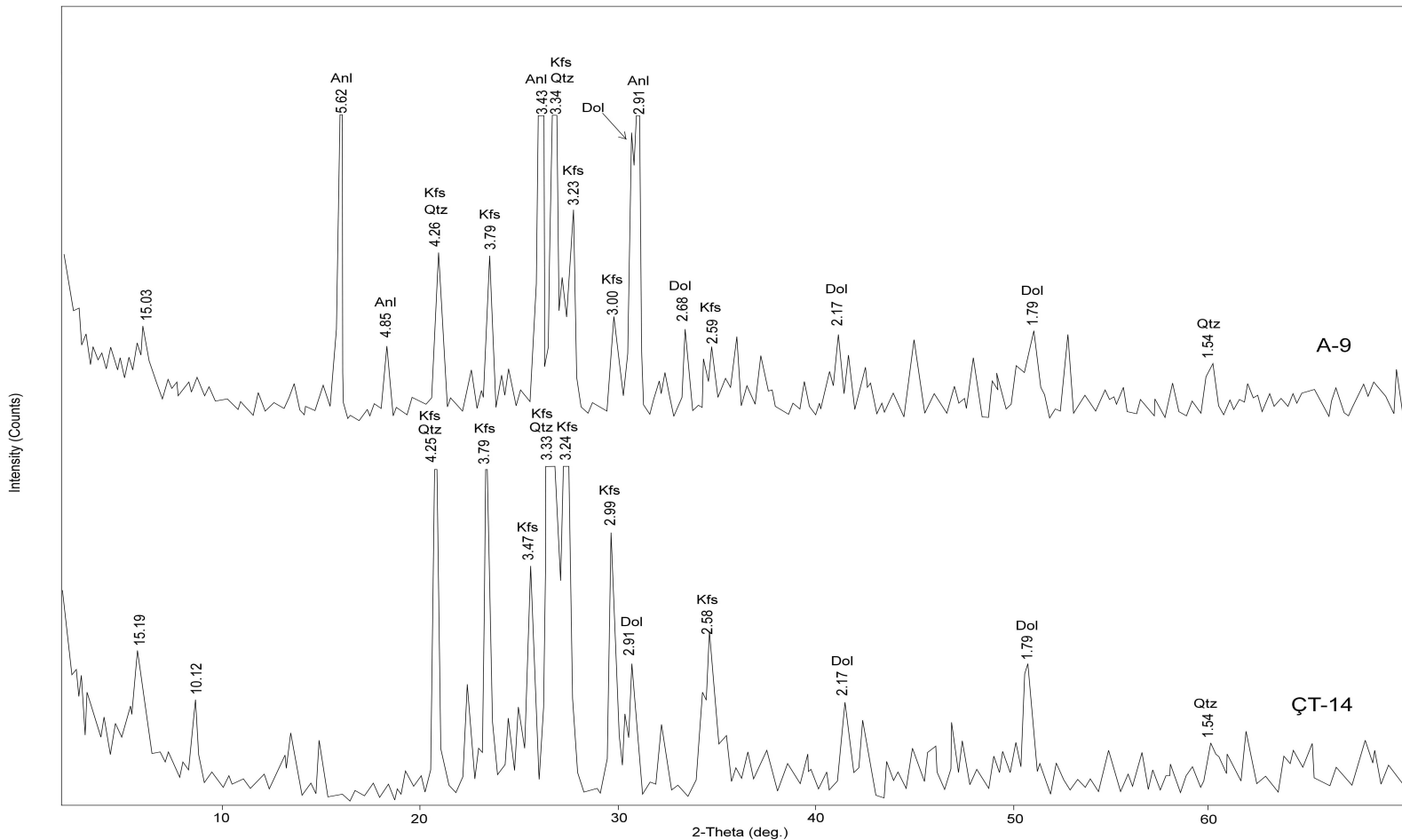
**Figure 62.** Random X-ray diffraction patterns of the A-9 and ÇT-14 show analcime bearing and analcime free samples.

**K-feldspars**

They are designated in all XRD patterns of samples with changing intensities except ÇT-8 which does not contain any K-feldspar peak (Figure 61). By means of matching *d*-spacing and 2θ angles of appropriate minerals, it was not found the exact type of K-feldspar because of overlapping. The approximate *d*-spacing of K-feldspars are 3.33, 3.79, 4.24, 3.23, 3.47 and 3.28 °A with decreasing intensity (Table 7). The peaks of K-feldspar with *d*-spacings at 3.33 and 4.24 °A overlap with quartz's peaks (Figures 59, 60, 61 and 62). The peak of 3.47 °A, on the other hand, overlaps with peak of analcime. In this respect, the determination of K-feldspar is not very easy. The main peaks of K-feldspar (3.33 °A and 4.24 °A) can not be seen, since all samples contain quartz. The peak of 3.28 °A also can not be observed because of overlapping. Merely, A-9 in Figure 62 shows small peak of 3.28 °A of *d*-spacing.

**Clay Minerals**

XRD analyses were performed on Arıklı Tuff samples to asses the types of clay minerals. For this reason, detailed clay analyses were applied to the samples YÇT-8, ÇT-6 and KK-2. Types of clay minerals were identified from five XRD patterns (random, air-dried at 25ºC, ethylene-glycolated, heated at 300ºC for 1 hour and heated 550ºC for 1 hour). Firstly, in random tuff sample (YÇT-8), the very small reflection was observed at 15.069 °A indicating presence of smectite or chlorite. Despite this, a broad and shifted peak occurs at about 14.87 °A. It can not be determined whether this peak belongs to smectite or chlorite since both of them can have a peak around 14.87 °A in the air-dried sample. In the ethylene-glycolated samples, the peak is more shifted toward a lower 2θ (from 15.06 to 17.3 °A). This is due to the grown basal spacing (from 15.06 to 17.3 °A) as the space between the layers become larger with glycolation (Grim, 1968; Borchardt, 1989). That is, the pattern of ethylene-glycolate identified by XRD shows that the clay mineral in the tuff sample is smectite. Heating the specimen to 300ºC and

103

550ºC causes the expanded layers to collapse. The diffraction peak of 10.15 ºA at 300ºC and the diffraction peak of 9.88 ºA at 550ºC also confirmed the presence of smectite. Representative X-ray patterns of air-dried, ethylene-glycolated and heated specimens (at 300ºC and 550ºC 1 hour) are illustrated in Figure 63.

As a result of these analyzes, the presence of smectite was confirmed in the sample YÇT-8. Presence of smectite was also confirmed in the sample ÇT-6, however, smaller peak intensities are less in sampleYÇT-8. Sample KK-2, on the other hand, shows no smectite peak. It was not understood why the smectite peak is not high enough, even though petrographic study showed some tuffs with 30-40% phyllosilicate mineral.

A small reflection at 9.950 ºA indicates the presence of mica or illite in the random YÇT-8 sample (Figure 63). To differentiate illite or mica, we examined XRD patterns of air-dried YÇT-8 sample. Illite is distinguished from mica by a characteristic peak ($d$001=10 ºA). It is unaffected by glycolation and heat treatments. Because no 9.950 ºA peak is observed any more, we can deduce the presence of mica in the sample. Optical microscope examination showed that mica type is biotite and it can be said that a small reflection in random XRD pattern indicates that biotite is present.

To summarize, based on petrographic observations and XRD analyses, the studied Arıklı Tuff samples contain analcime, quartz, feldspar, dolomite, biotite and smectite.
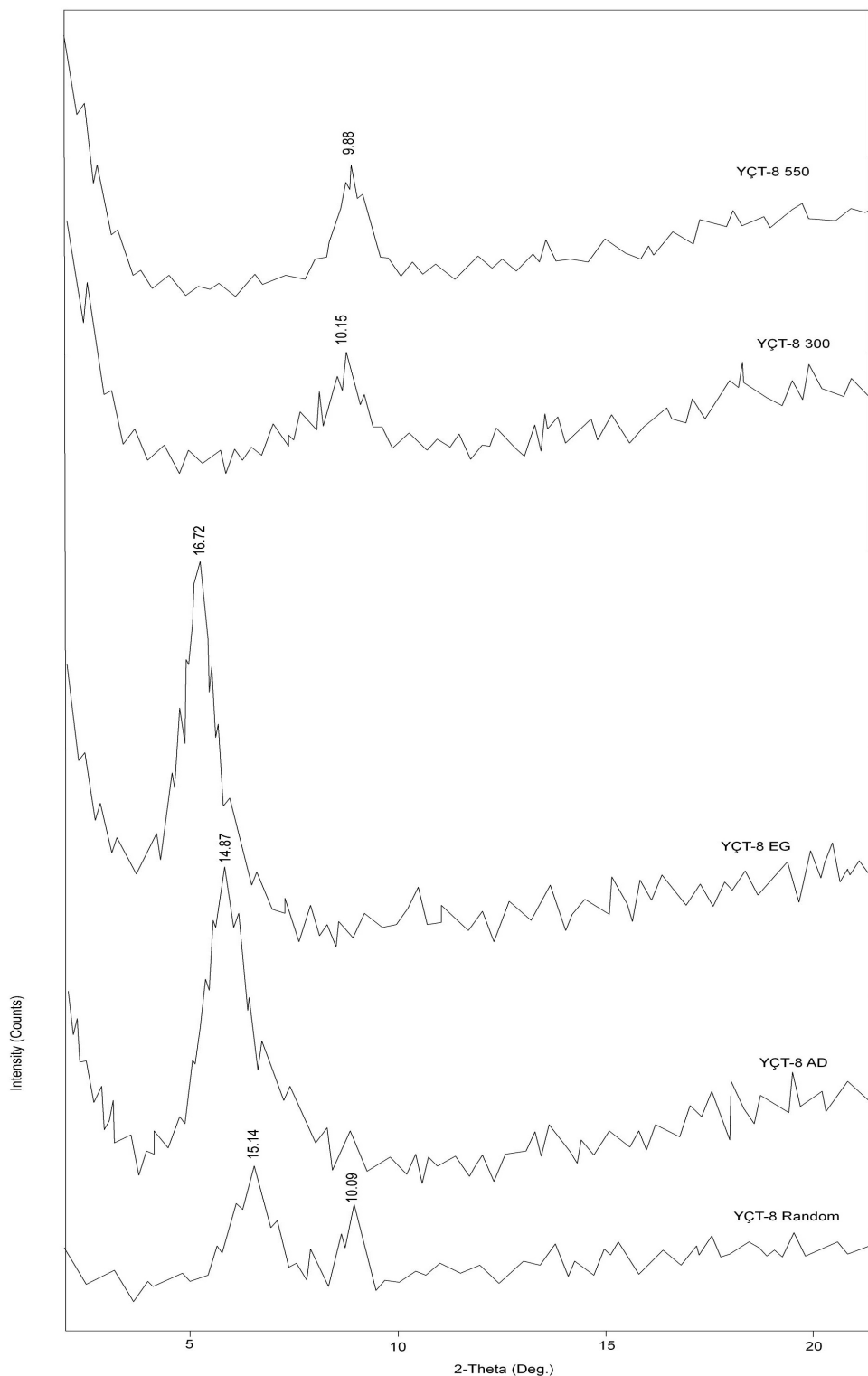
**Figure 63.** X-ray diffraction patterns of the sample YÇT-8. (AD: air-dry, EG: ethylene glycol, heating to 300 ºC and 550 ºC).

## 4.3. Scanning Electron Microscopy (SEM) Analysis

### 4.3.1. Theoretical Background

"The Scanning Electron Microscope (SEM) is an electron beam based microscope that uses electrons to produce high-resolution three dimensional topographic images" (Welton, 1984). Their method of study resemble with petrographic microscope's, however, SEM uses electron beam rather than light. The beam which is created by heating a tungsten filament bombards the sample. When this primary electron beam hits the sample, various forms of radiations (i.e. secondary electrons, characteristic X-rays, backscatter electrons, auger electrons, cathodoluminescence) are ejected from the sample (Figure 64) and these data are used for information about sample. In geologic analysis, secondary electrons (SEM micrograph) and the characteristic X-rays (EDX spectrum) are used .
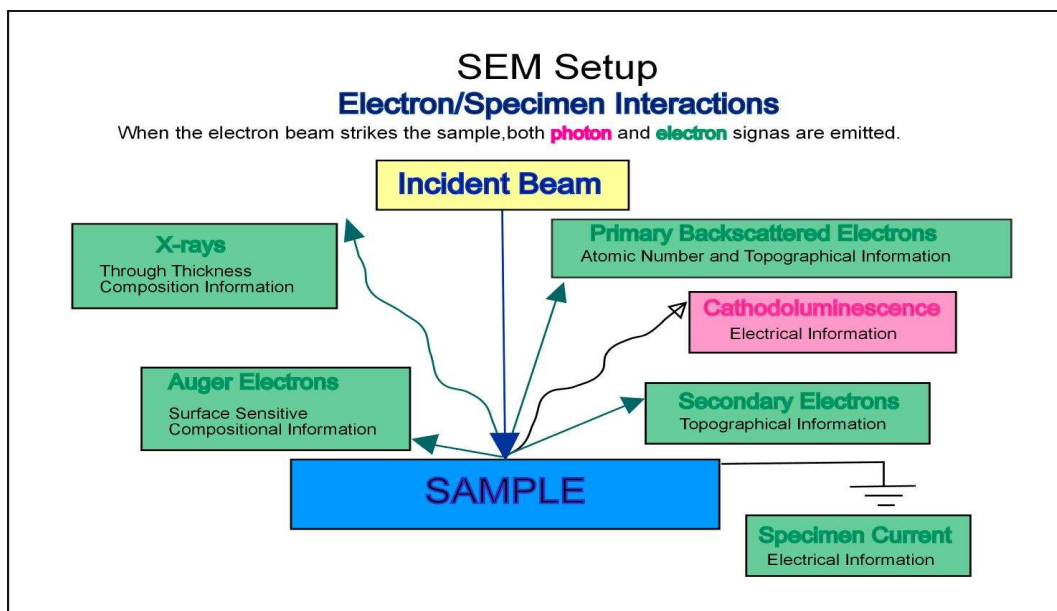


**Figure 64.** Schematic sketch showing the different outputs of the SEM/EDX system (www.uga.edu/caur/BeamSpec.ppt).

### 4.3.2. Preparation of Samples

The sample preparation for SEM is relatively easy. Tuff samples were crushed with hammer for appropriate size and they were fixed to a stub consisting of a metal disc so that they do not fall off easily while handling. Then, they were coated with an extremely thin layer of gold.

However, applying the SEM method to rock-specimens with several different minerals, as it is a common case with geological material, is not always decisive, as there is no optic microscopic control on the samples. To avoid this problem and to be able to image the very small unknown minerals I observed under the normal polarizing microscope, I used thin sections in SEM study of the Arıklı Tuff. However, the main problem with detection, focusing and the optical resolution of the very fine minerals remained unsolved, and the images obtained were not of reproducible quality.

### 4.3.3. Scanning Electron Microscopy Analysis of the Arıklı Tuff

The small particle size of analcime in the studied rocks makes their examination by optical microscopy extremely difficult. Furthermore, thin section analyses of rock samples using polarizing microscope give only two-dimensional data, whereas SEM analyses provide three-dimensional crystal relationships. XRD patterns were helpful to identify the presence of analcime, but they are not sufficient to determine morphology and formation of analcime. The form, habit and size can easily be observed with SEM analysis. The data are also useful for understanding growth mechanism. By this, SEM analysis is an ideal technique for the examination of analcime. The present SEM study focuses on the identification and especially on the formation of the analcime.

In the first instance, samples examined by XRD indicating the presence of analcime were scanned by SEM for confirmation. Eleven samples with analcime were examined and 71 photographs and 8 EDX images were taken. However, only a few images with the most characteristic features were illustrated. In addition, I tried to confirm also the presence of some very fine-grained minerals such as quartz, K-feldspar, smectite and dolomite in the samples, based on their morphology.

Special effort was given to image the neo-formations and replacement structures of the mineral phases, glass and clay minerals, to understand the formation of the diagenetic minerals.

Morphologies of minerals found in tuffs will be briefly explained together with interpretation of the SEM images.

**Analcime**

The very small size of zeolites makes their identification and differentiation from each other by petrographic microscope very difficult. However, zeolites with characteristic morphologies, when examined under the SEM can be easily recognized. For example clinoptilolite generally occurs as euhedral plates and laths, erionite and mordenite occurs as fibers or acicular needles, chabazite occur as cube-like rhombohedra and phillipsite occurs as prism and stubby laths. Like other zeolites, analcime also shows well-formed characteristic morphologies. Before interpreting the morphology of analcime in SEM micrographs, the crystal morphology of analcime will be briefly explained.

Well-developed crystals of analcime are observed in a variety of crystal habits in nature (Figure 65). These crystal forms range from cubic, trapezohedral and cubo-octahedral (Welton, 1984; Mumpton and Ormsby, 1978). Even if analcimes have more than one crystal system (cubic, tetragonal, orthorhombic, monoclinic), they

usually show isometric symmetry. Gottardi and Galli (1985) mentioned that analcimes are usually well-formed trapezohedrons which have a three-dimensional shape bounded by 24 faces.
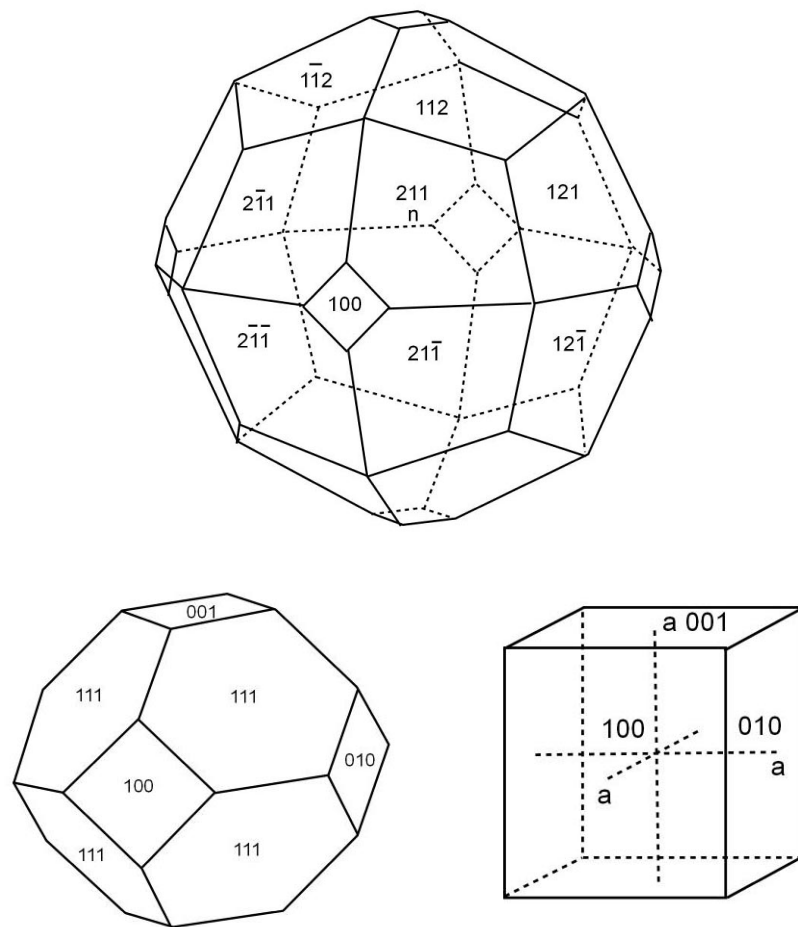


**Figure 65.** Crystal forms of analcime a) trapezohedral b) cubo-octahedral c) cubic morphology (After Gottardi and Galli, 1985; Klein, 2002).

The SEM images of the Arıklı Tuff show usually trapezohedral and cubo-octahedral morphology (Figures 66-71). The crystals with cubic morphology were not determined in this study. The analcime identifications from the Arıklı Tuff

samples were based on comparison of crystal morphology with microscopical observations and X-ray diffraction analysis of several samples. The SEM analyses in most cases confirmed the XRD results that the analcime is found in the Arıklı Tuff.

In Figures 66 and 67, analcimes that show trapezohedral shape are recognized with well-formed faces of (211, 100) as shown in figures.
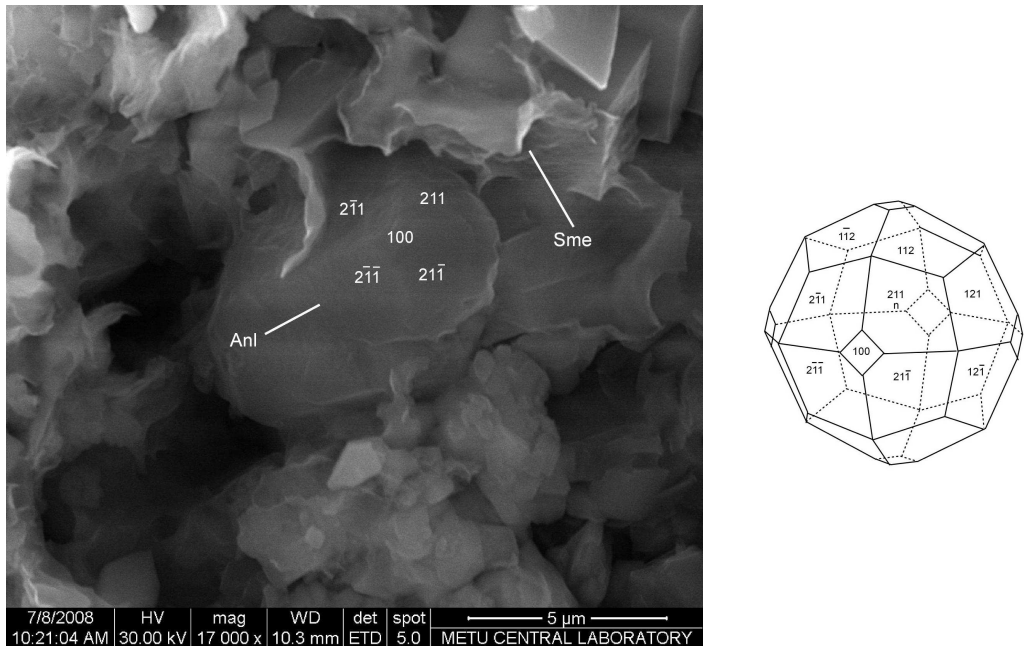


**Figure 66.** Scanning electron micrograph show trapezohedral analcime which is recognized with well-formed 100, 211 faces (Sample KL-5, Anl: analcime, Sme: smectite).
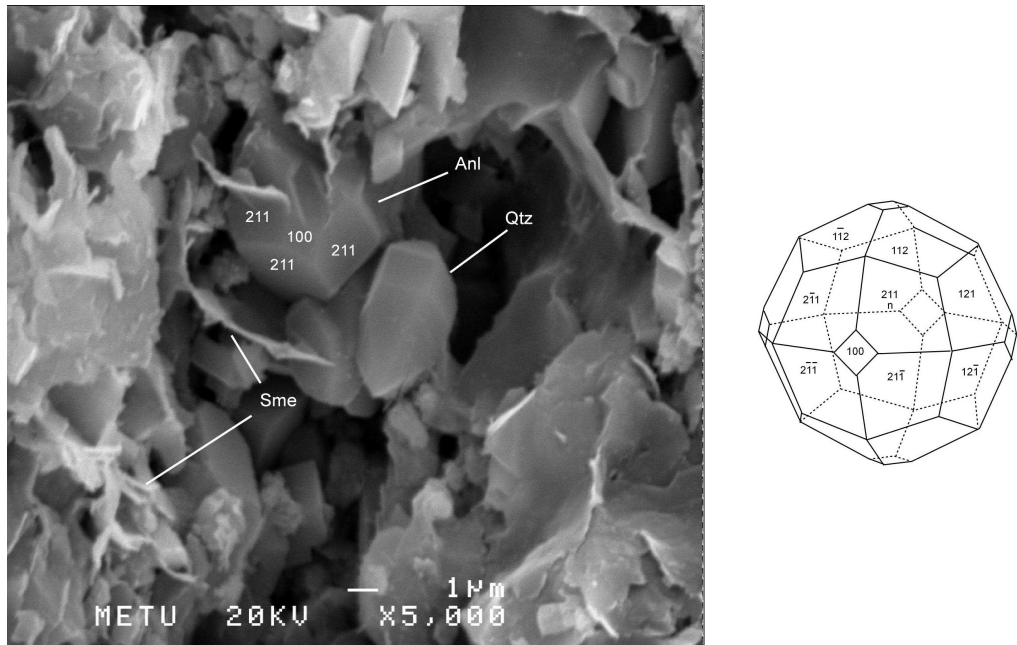
**Figure 67.** Scanning electron micrograph of trapezohedral analcime in void spaces in the tuff. Analcime is recognized with well-formed 211 faces (Sample ÇPT-3, Anl: analcime, Qtz: quartz, Sme: smectite).

In Figure 68, a large analcime occurs with as well-formed cubo-octahedral crystal, which is ~15 μm in diameter and is recognized with well formed 111 face. This analcime grew without being obstructed in a pore and was developed with euhedral faces, as will be evaluated in following chapters. In Figures 66 and 67, analcime takes place as crystals of smaller size, which are ~5 μm in diameter.
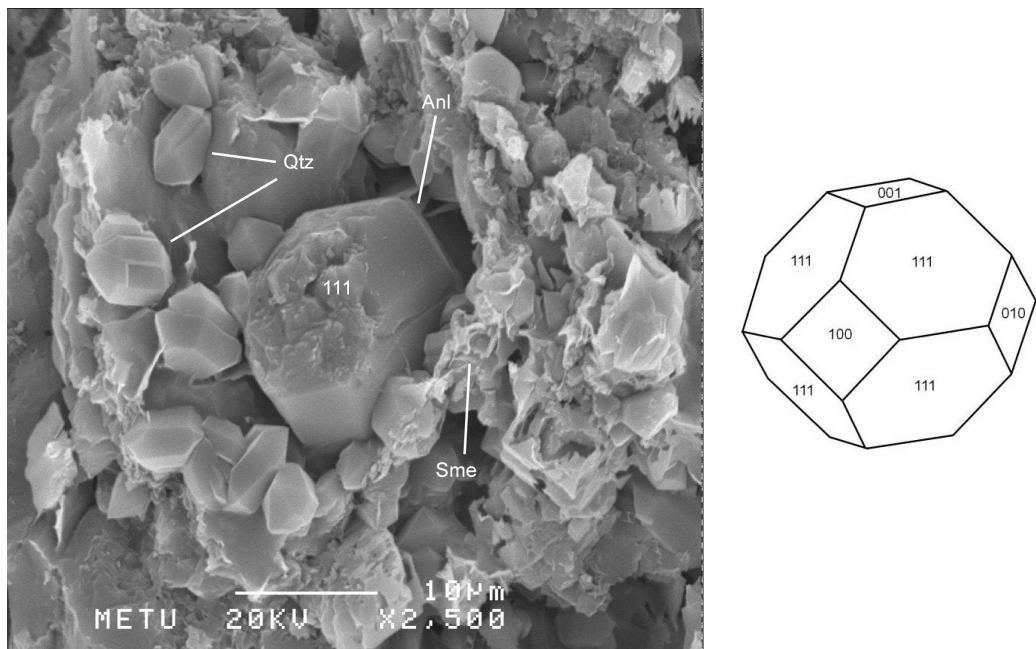
**Figure 68.** Scanning electron micrograph of euhedral analcime from a dolomite rich vitric tuff. Note the characteristic cubo-octahedral symmetry of analcime which is recognized with well-formed 111 face (Sample ÇT-8, Anl: analcime, Qtz: quartz, Sme: smectite).

Most of the analcime occurs as pore-filling subhedral to euhedral crystals as shown in Figures 66-69. The pore-filling character of the analcime indicates that they were formed as chemical precipitates from pore fluids.
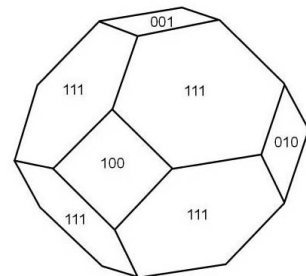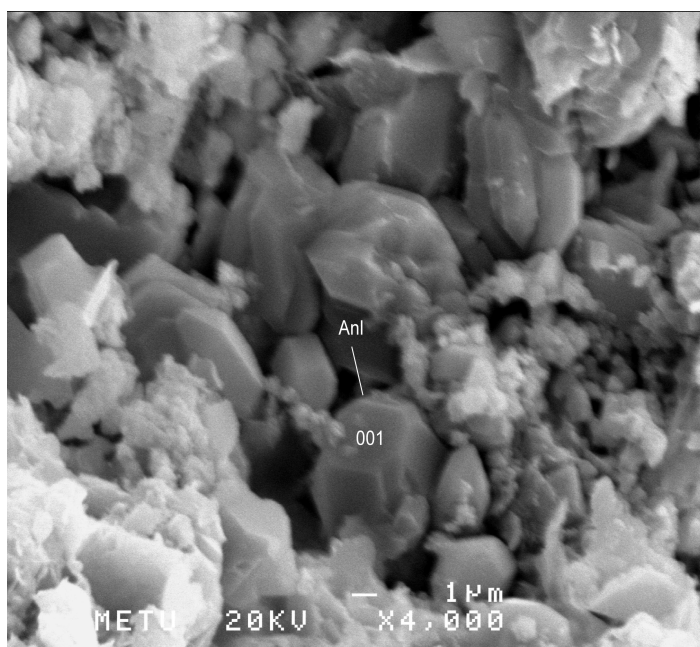
**Figure 69.** Scanning electron micrograph of cubo-octahedral analcime in cavity. Analcime is recognized with well-formed 001 face (Sample ÇPT-3, Anl: analcime).

Idiomorphic analcime crystals were observed in the relatively large pore spaces. Analcime is not only found in pore spaces. They are also observed to form on the edge of volcanic glass that started to be altered to analcime at the edges (Figure 70).
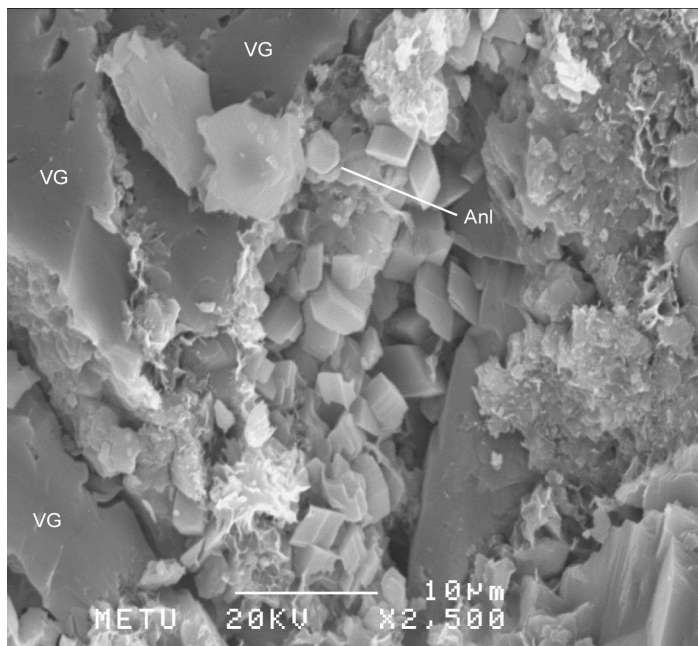
**Figure 70.** Scanning electron micrograph of authigenic analcime overgrowth at the edge of glass (Sample A-12, Anl: analcime, VG: volcanic glass).

The trapezohedral habit of analcime is recognizable even in subhedral grains. In Figure 71, some well-developed crystal faces of (112), (211) and (121) are visible, even though the complete crystal morphology is obscured.
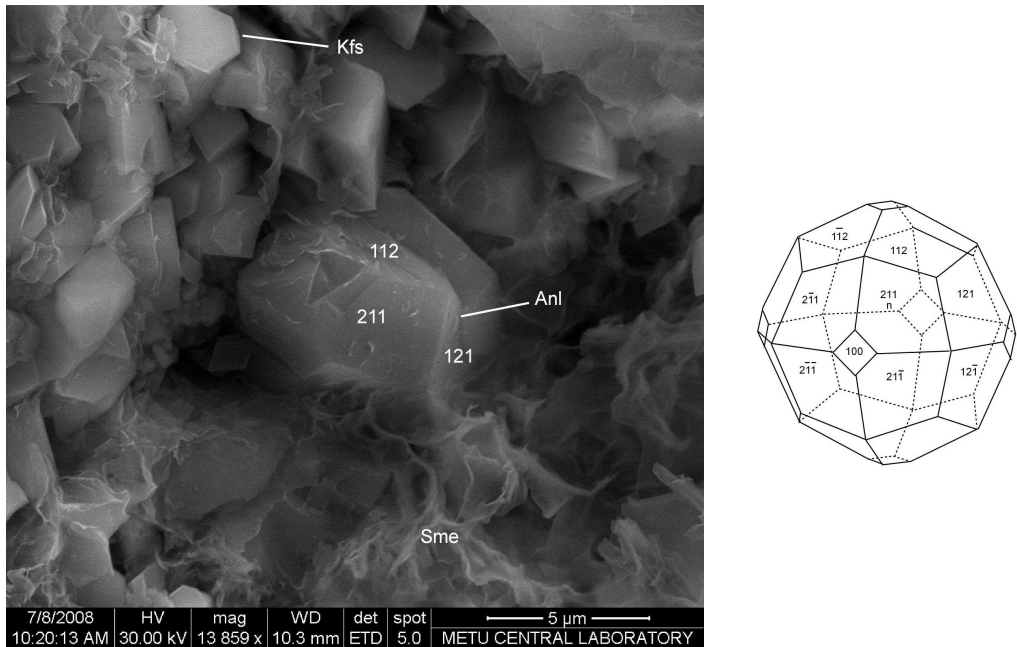
**Figure 71.** Scanning electron micrograph of a large subhedral analcime crystal which is recognized with well-formed (112), (211) and (121) faces (Sample KL-5, Anl: analcime, Sme: smectite, Kfs: K-feldspar).

**Authigenic quartz**

Quartz belongs to the hexagonal crystal system and forms usually hexagonal dipyramids (Figure 72-a) or right and left handed trigonal trapezohedrons (Figure72-b).
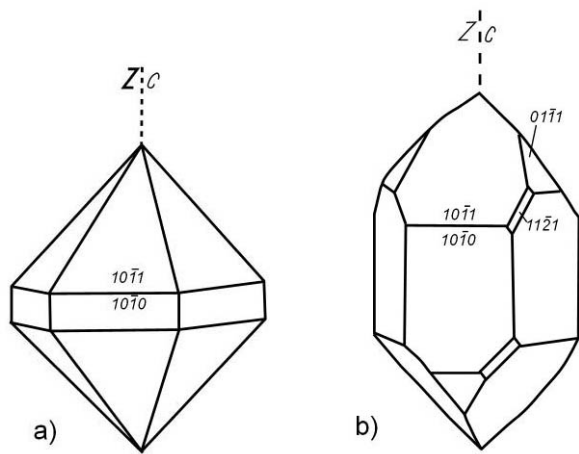
**Figure 72.** Crystal forms of quartz a) hexagonal dipyramid b) trigonal
trapezohedron morphology (After Tröger, 1982).

In Arıklı Tuff, crystal morphology of quartz usually exhibits the right or left
trigonal trapezohedral crystal forms (Figure72-b). So, they can be easily
differentiated by their typical morphology. In Figure 73, quartz is known with
well recognized 1011, 0111 and 1010 faces. They occur as prismatic crystals of
different sizes that commonly are 6-10 μm long and 3-7 μm wide. Clusters of
quartz are often associated with smectites (Figure 73).
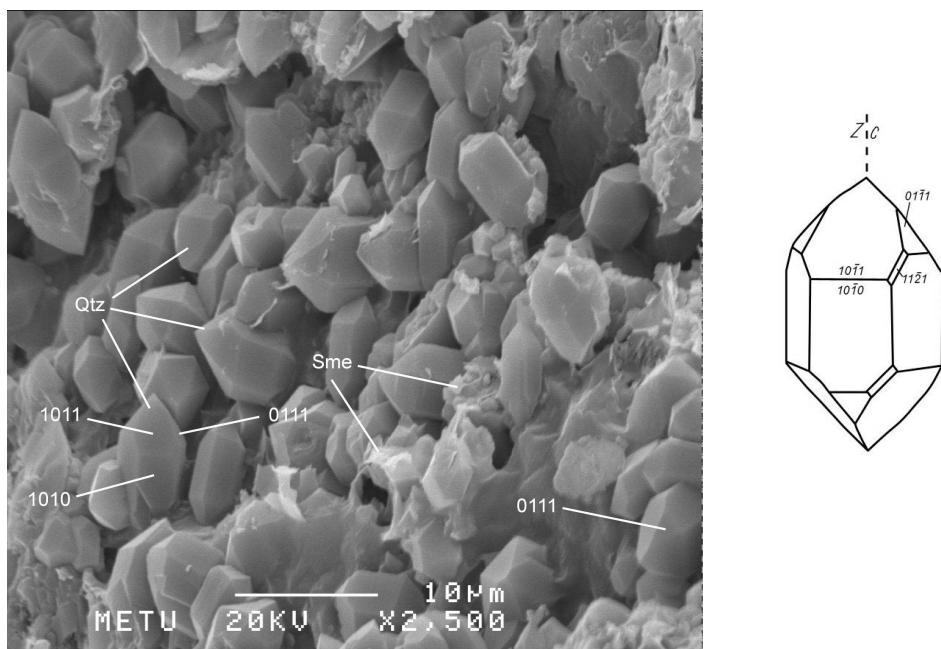
**Figure 73.** Scanning electron micrograph of euhedral quartz grains which is recognized with well-developed 1011, 0111 and 1010 faces (Sample ÇT-8, Qtz: quartz, Sme: smectite).

**Smectite**

Smectite crystals are well developed in YÇT-8 and exhibit a honeycomb arrangement, a typical morphology for the smectites (Figure 74).
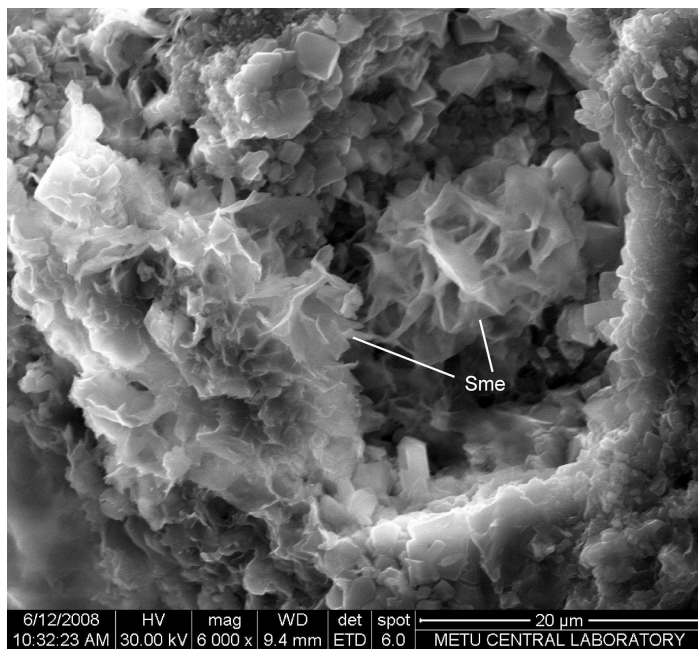
**Figure 74.** Scanning electron micrograph of smectite showing cornflake morphology (Sample YÇT-8, Sme: smectite).

**Dolomite**

Dolomite belongs to the hexagonal crystal system and their crystals display usually the typical unit rhombohedron (Figure 75) form. Some dolomite crystals can display twin growth.
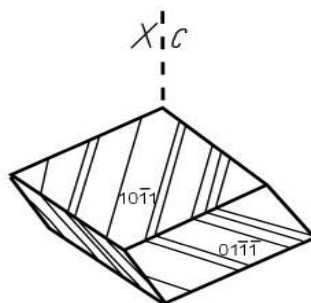


**Figure 75.** Crystal form of rhombohedral dolomite (After Tröger, 1982).

In the SEM images from the studied tuffs, dolomite crystals are seen as euhedral rhombs. Sizes of dolomite crystals range from 2 to 5 μm. Identification of the crystals as dolomite is based on the rhombic morphology. Dolomite is known with well recognizable 1011 and 0111 faces (Figure 76). Petrographical study and XRD analysis confirm the identification. The illustrated Sample A-9 is classified as dolomite-rich vitric tuff in petrography section.
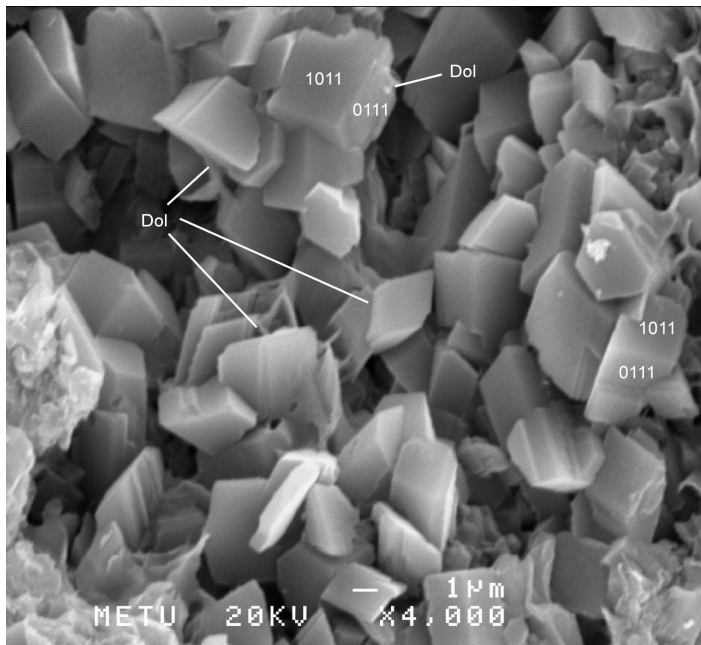


**Figure 76.** Scanning electron micrograph of dolomite with well-formed 1011 and 0111 crystal faces (Sample A-9, Dol: dolomite).

**K-feldspar**

The K-felspars belong to the monoclinic (Figure 77) and rhombohedral crystal system. Crystals are often tabular and display Carlsbad twinning.
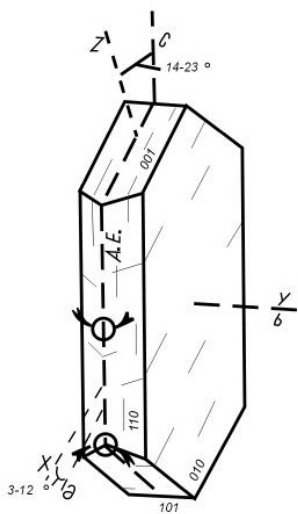
**Figure 77.** Monoclinic crystal form of K-feldspar (After, Tröger, 1982).

K-feldspars in the studied samples was realized on the basis of both SEM and XRD analysis. In the SEM, K-feldspars appear usually as rhombic crystals. Rhomboid K-feldspars can be seen in the middle part of the image (Figure 78). Typical K-feldspar monoclinic morphology, however, can be easily seen in the middle west part of the image (Figure 78). K-feldspars commonly occur as euhedral crystals in pumice fragments (Figure 79).

120
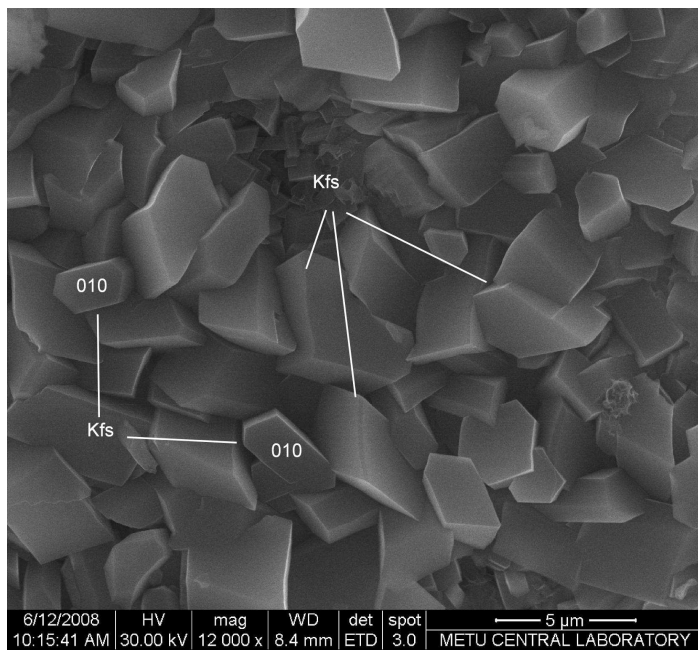
**Figure 78.** Scanning electron micrograph of K-feldspar with well-developed 010 faces (Sample KK-2, Kfs: K-feldspar).

**Pumice Fragment**

Pumice fragments can be differentiated from matrix by their texture. Pumice fragments are generally ranges 20-60 μm wide and 70-130 μm long. They contain euhedral crystals in it. They can be easily differentiated from matrix with texture. Figure 79 shows an elongated pumice fragment which contains euhedral crystal grains. It is 50 μm wide and approximately 100 μm long in diameter.
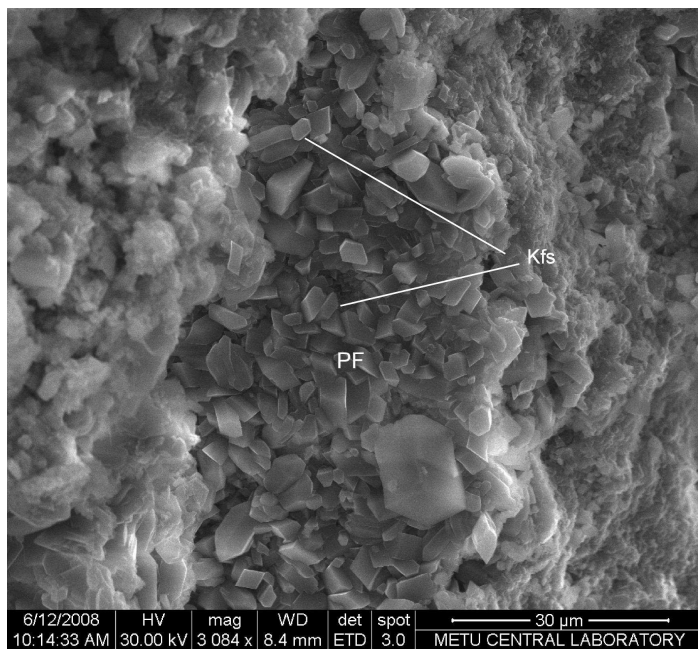
**Figure 79.** Scanning electron micrograph of pumice fragment and well-developed, euhedral, authigenic K-feldspars (Sample KK-2, PF: pumice fragment, Kfs: K-feldspar).

**Glass shard**

SEM images of glass shards is important for present study since they are significant for the formation of analcime (see introduction chapter and Ross, 1928; Bradley, 1928; High and Picard, 1965; Iijima and Utada (1966); Iijima, 1980). In this account, a very careful study was performed for morphology of glass. Most of the glass observed was altered. However, there are also less unaltered ones (Figure 80). This figure shows the typical Y-shaped texture of volcanic glass, which is 20 μm wide and 70 μm long.
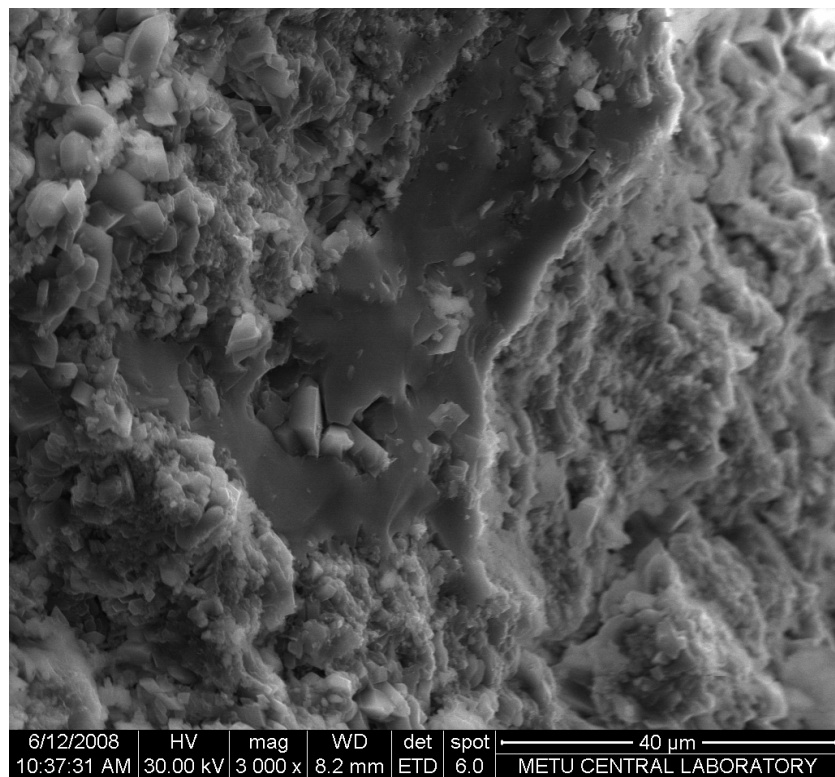
**Figure 80.** Scanning electron micrograph of Y-shaped glass shard (Sample KK-2).

### 4.3.4. Energy Dispersive System Studies

Energy Dispersive System (EDX) measurements were applied to the Arıklı Tuff samples, especially in cases where the crystal morphology was not informative enough to identify the fine grained minerals and for evaluating the chemical composition of unaltered glass.

### 4.3.4.1. Theoretical Background

In EDX analysis, the primary electron beam ionizes the atoms by ejecting electrons in the inner shells of the atoms. To maintain stability, electrons transfer

from outer shell to inner shell. These transitions release energy in form of X-rays. X-rays are used primarily to identify elements. Any major element in the sample corresponds to a peak on a graph (the EDX spectrum) (Welton, 1984).

**4.3.4.2. Energy Dispersive System data of the studied samples**

To evaluate the glass-composition and check whether analcime can be formed from glass or not, EDX was applied on unaltered surface of glass. This measurement was duplicated to be certain.

Subhedral analcime can be seen on edge of the glass (Figure 81). The EDX spectrum contains the elements of Na, Al, Si which are found in analcime. So, it can be said that the composition of glass is suitable for analcime formation. The relative peak height of Na, Al, and Si elements are displayed on the EDX graph (Figure 81).
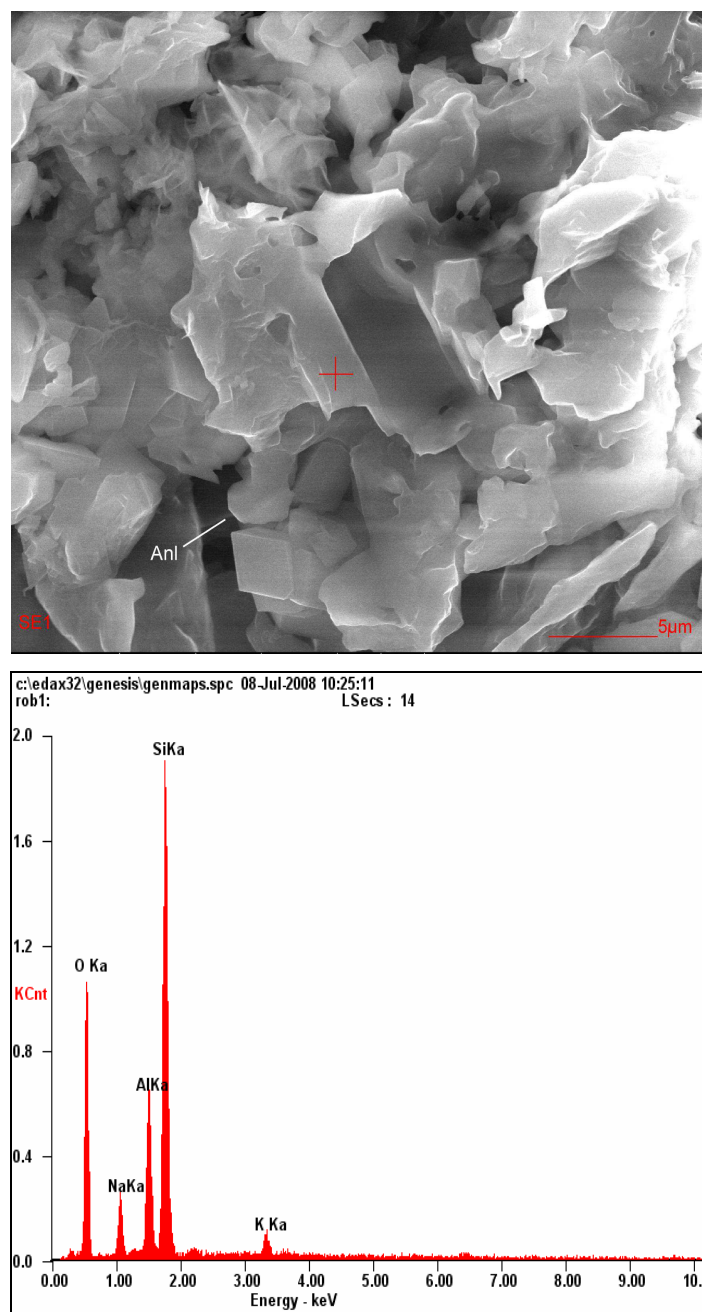
**Figure 81.** SEM photomicrograph and EDX graph from glass with analcime at its edge. EDX spectrum shows the peaks of Na, Al, Si (Sample KL-5, Anl: analcime)

In addition to the evaluating the glass-composition, EDX was used to differentiate fine crystals, especially the K-feldspars. In SEM study, these minerals have three

different morphologies. Crystal morphologies are not sufficient for the exact determination and for identifying these minerals. However, the EDX spectrum of 3 minerals having different morphologies contains similar elements, namely Si, Al and K, which are typical of K-feldspars (Figure 82).
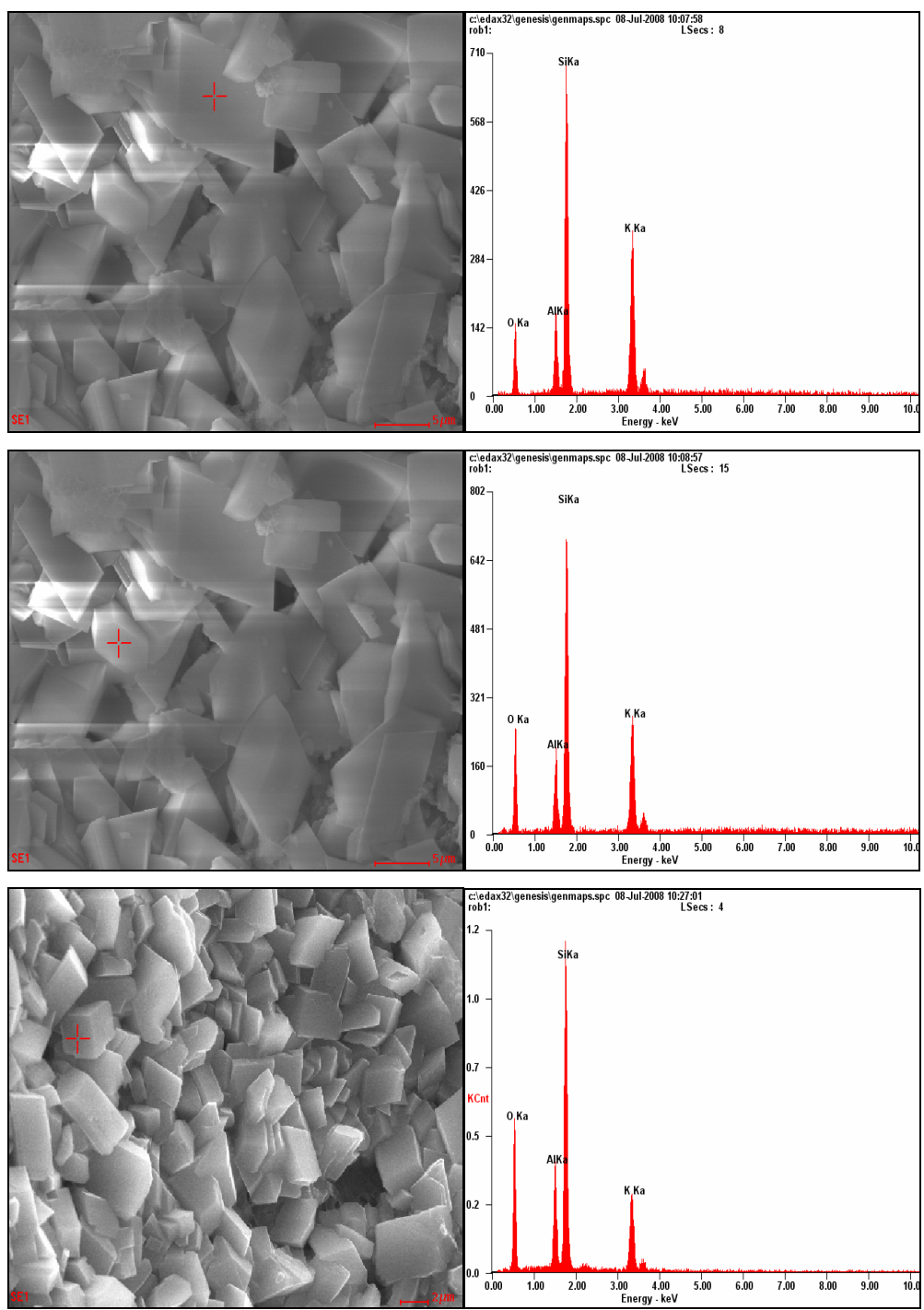
**Figure 82.** SEM photomicrograph and EDX graph from K-feldspar with three different morphologies a, b: (KK-2), c: (KL-5).

## 4.4. Thermal Analysis Methods

### 4.4.1. Theoretical Background

DTA analysis was used for the determination of phase transformations of minerals. The method is appled on samples by heating. When samples are heated, thermal state of sample changes and these changes are transferred as endothermic or exothermic peaks on graph. Minerals which have specific peak temperature ranges can be recognized in such way.

Thermal analysis is a useful tool to provide information about the dehydratation and dehydroxylation temperatures. However, identification of components, either as a group or individually, by differential thermal analysis is not easy since many factors affect the peak temperature such as structure, composition, particle size, nature etc. Besides, when the peaks of two or more different components overlap, the difficulties are higly increased.

Analcimes holding water molecules undergo structural changes when heating and the zeolitic water is removed while giving a thermal effect. Differential thermal analysis curves of several different kinds of zeolites were presented by Koizumi (1953) and he designated that zeolites generally expel water at temperatures from 70 to 550 ºC on heating. Koizumi (1953) revealed that the removal of water takes place as four types of dehydration phenomena in zeolites. From these the Analcime-type shows smooth dehydration phenomena. Koizumi (1953) further stated that since analcime dehydrates so slowly and gradually between 200 ºC and 400 ºC, only a broad endothermic peak is obtained without a sharp endothermic peak in the DTA diagrams (Figure 83).

On this account, first minerals found in tuffs were determined by XRD and optical microscopy. Later, thermal behaviour of these minerals were searched in literature

and finally the obtained DTA and TG curves for the samples of the Arıklı Tuff were interpreted.

The mineralogical composition of two of the Arıklı Tuff samples that were investigated by DTA is given in Tables 4, 8) according to XRD and optical microscopy.

Before interpreting the DTA-TG curves of the analyzed samples, thermal behaviors of analcime, smectite, feldspar, quartz and dolomite will be given in Table 9 and thermal behavior of analcime will be briefly explained.

### 4.4.2. Preparation of Samples

To perform these analyses two tuff samples (samples ÇT-11 and ÇT-8) were grinded to 2 μm by agate mortar.

**Table 9.** Thermal behaviors of smectite, dolomite, quartz, K-feldspar and analcime. (Wilson, 1987; Todor, 1976; Mackenzie, 1957, Smykatz-Kloss, 1974)

| | | |
|---|---|---|
| Smectite<br>endothermic peak<br>endothermic peak<br>endothermic peak<br>(generally followed<br>by small exothermic peak) | 100-300 ºC<br>670-710 ºC<br>800-900 ºC | (loss of adsorbed water)<br>(loss of hydroxyl group)<br>(dehydroxylation) |
| Dolomite<br>endothermic peak<br>endothermic peak | at 745 ºC<br>at 870 ºC | (resolution of Magnesium carbonate)<br>(resolution of Magnesium carbonate) |
| Quartz<br>endothermic peak | at 573 ºC | (transformation of α-Quartz into β-Quartz) |
| K-feldspar<br>endothermic peak | 700-900 ºC | (polymorphous transformation) |
| Analcime<br>endothermic peak | 200-400 ºC | (loss of adsorbed water) |
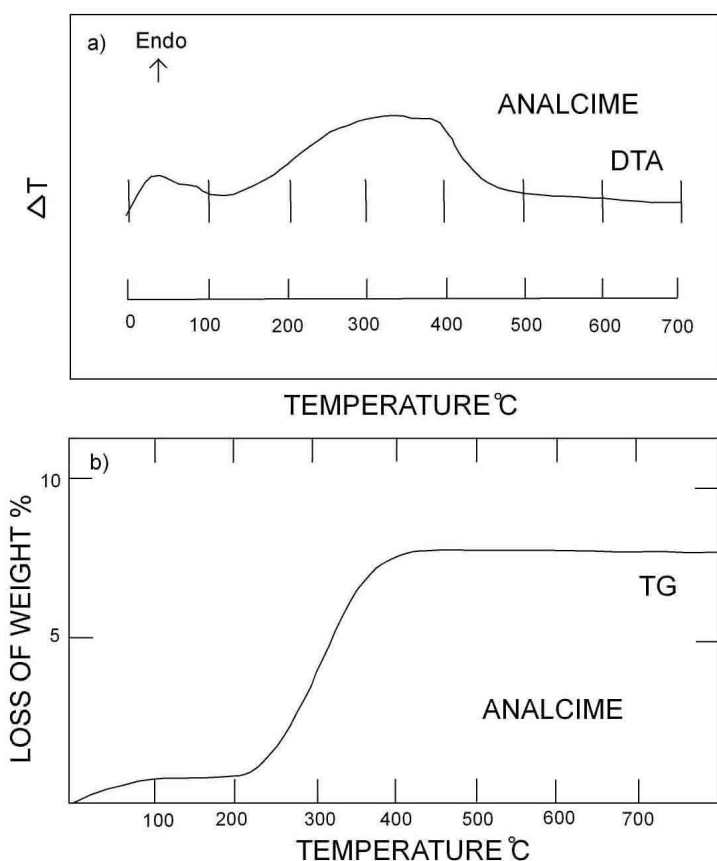
**Figure 83.** a) The differential thermal analysis (DTA) curve of analcime b) the dehydration (TG) curve of analcime. (After Koizumi, 1953).

### 4.4.3. DTA and TG data of Arıklı Tuff

The obtained DTA and TG curves of ÇT-8 are shown in Figure 84. The first mass loss, observed between 50-120 ℃, corresponding to an endothermic peak at 90 ℃ is due to loss of adsorbed water. The amount of water released depends on the relative humidity. The second mass loss that occurs between 200-400 ℃, corresponding to an endothermic peak at 300 ℃ is due to loss of the crystal water of analcime. As indicated by Koizumi (1953), analcime demonstrates broad endothermic peak since it dehydrates slowly and gradually.

130

On further heating, ÇT-8 yields a thermal curve with endothermal effect whose peak is at 760 ℃. Todor (1976) designated that dolomite undergoes two characteristic transformations as it decomposes at 754 ℃ and 870 ℃. The first one consist magnesium carbonate and second one consists calcium carbonate. In terms of this, he classified dolomites in two groups; magnesian dolomites and calcitic dolomite. Sample ÇT-8 showed one peak of dolomite (Figure 84) the other peak corresponding to the 870 ℃ was not observed. On this account, it was also checked whether this peak may correspond to the DTA curve of magnesite ($MgCO_3$). However, no indication to magnesite was found. On the other hand, the presence of dolomite in ÇT-8 was definitely designated with XRD study. Supported by these data, it can be said that ÇT-8 contains magnesian rich dolomite.

Curve of ÇT-11 shows two almost equivalent endothermic effects at 60 ℃ and 285 ℃. Heating of sample ÇT-11 results in a two steps weight loss; from room temperature to 100 ℃ is the first step and 100 to 400 ℃ is the second step. The first mass loss corresponding to endothermic peak at 60 ℃ is due to loss of adsorbed water. The second mass loss that occur 100-400 ℃, corresponding to a broad endothermic peak at 285 ℃ is due to dehydration of analcime. However, it can not be considered as the characteristic peak of analcime, because the sample under investigation contains also smectite, which also has $H_2O$ in its crystal structure. As it was mentioned before, smectite is characterized by the presence of the first endothermic peak between 100-300 ℃, followed by second and third endotherms between 670-710 ℃ and 800-900 ℃ (Todor, 1976; Mackenzie, 1957; Wilson, 1987). Even though the weight loss of smectite was viewed between 100-300℃ the second and third endothermic peaks can not be observed. The reason why no second thermal effect of smectite is observed even though the petrographic study shows presence of 45% smectite (Table 4) in ÇT-11 remains problematic. It is also important to note that no feldspar peak was observed between 700-900 ℃, where the feldspars have their typical endothermal peaks

(Kohler, 1969; Kohler and Wieden, 1954). This can be explained by petrographic study since petrographic study shows 20 % K-feldspar that is small amount.

The peaks at 440 ℃ and 545 ℃ respectively, occuring on Figure 84 have no significance.

Both studied tuff samples show no endothermic quartz peak at 573 ℃ but optical microscope and XRD studies proved quartz presence but in small amount. The reason why no thermal effect of quartz was observed can be explained by small amount.

The DTA diagram of analcime-bearing tuffs shows a broad endothermic peak at around 300 ℃ and 290 ℃. As reported by Koizumi (1953), analcime dehydrates so slowly and gradually between 200-400 ℃ that in the DTA diagrams broad endothermic curve was obtained without a sharp endothermic peak.
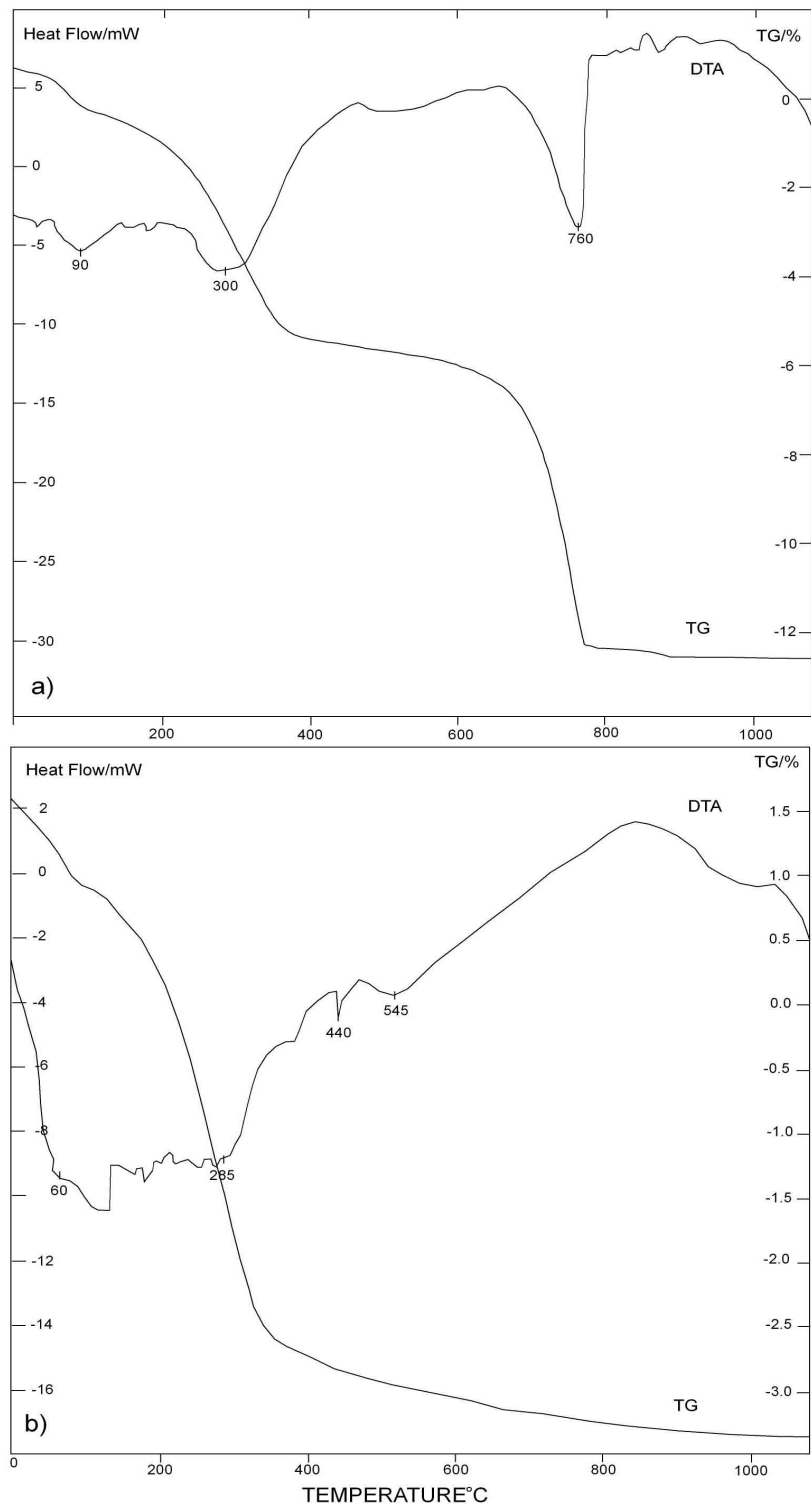
**Figure 84.** a) DTA and TG curve of ÇT-8 b) DTA and TG curve of ÇT-11

# CHAPTER 5

# GEOCHEMISTRY

## 5.1. Introduction

In addition to petrographic and mineralogic study, geochemistry is also a necessary tool to study the tuffs. In this study, total 20 representative samples, which were taken from Arıklı Tuff in the field were evaluated using chemical diagrams based on major and trace elements as well as REE abundances.

Since the tuffs include lithic fragments and have undergone intensive alteration as well as element mobility during diagenesis, the usefulness of geochemistry for the classical chemical classification diagrams (e.g. Cox diagram, etc) is restricted. The actual reason of using such geochemical diagrams is not to characterize specific rock types, but to identify the nature of the parent material that acted as a precursor for the formation of zeolite (e.g. Kitsopoulos et al. 2001) and the role of geochemistry in the zeolitization.

Using elemental analysis, geochemical properties of the Arıklı Tuffs were determined and the behavior of elements along the alteration processes were evaluated.

## 5.2. Geochemical Evaluation

Major, trace and rare earth element (REE) compositions of the analyzed samples from the Arıklı Tuff are given in Table 10.

The mineralogy of the samples is dominated by authigenic minerals such as analcime carbonate and K-feldspar. The evaluation of the geochemical data was done by taking in to account of this system behavior. It was assumed that most of major and trace elements can be removed or enriched by these alteration procedures. Moreover, since zeolitization of the tuffs is related to gains and losses of these elements, especially alkalis, traditional rock-classification diagrams were not used.

Generally, the Arıklı Tuff in the study area is characterized by high $Na_2O$ contents (0.13-5.88) and the concentration of $SiO_2$ ranges between 51.22-68.94%, $Al_2O_3$: 10.63-15.36%, $Fe_2O_3$: 1.74-2.98%, MgO: 0.56-5.03%, CaO: 0.16-8.14%, $K_2O$: 0.80-12.19%. The values of Na, K, Mg and Ca oxides vary widely, but, the values of Al, Si and Fe oxides vary little (Table 10). For example, the value of $Na_2O$ is 0.13 in A-2, but 5.88 in Sample ÇT-8. The concentrations of the remaining oxides ($TiO_2$, $P_2O_5$, MnO and $Cr_2O_3$) are lower than 1%. The concentrations of some trace elements vary widely too. The content of Sr changes between 37.9-231.4 ppm, Ba: 205-1887, Cs: 1.5-77.0 and the amounts of Ni, Hf, Y and Nb are less then 50 ppm.

Variation diagrams of the major element oxides versus silica are not appropriate for such tuff samples. As shown in Figure 85, $Na_2O$ concentrations show considerably scattered pattern, possibly due to original rock compositions, differential alteration and affect of permeability of the original rock, that facilitated the circulation of diagenetic fluids.
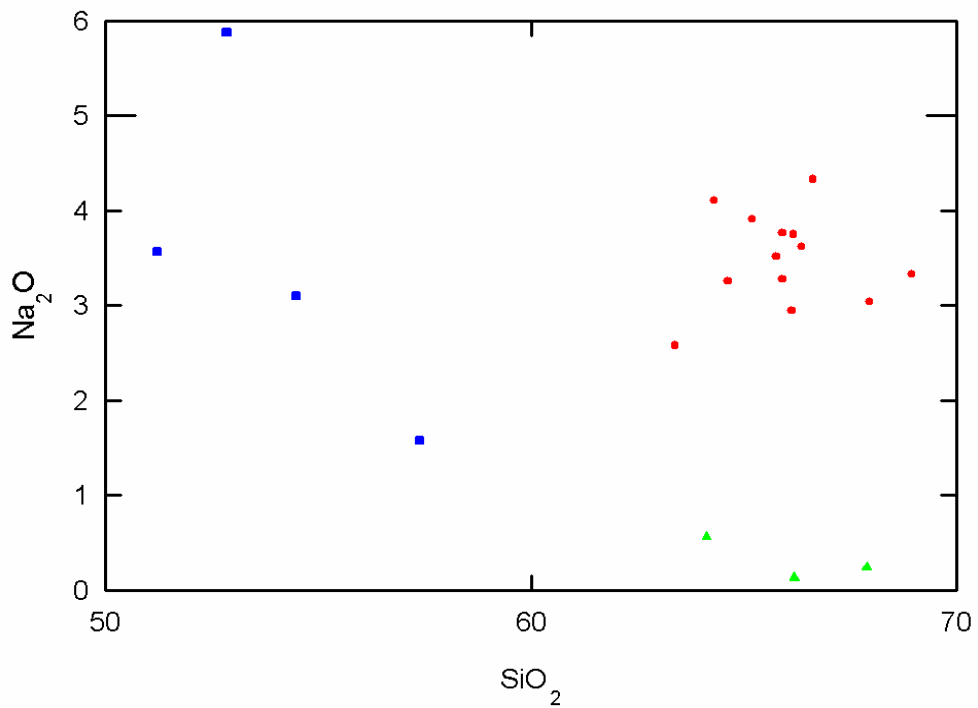
**Figure 85.** Variation of the $Na_2O$ with silica (blue squares represent dolomite rich vitric tuff, red circles represent phyllosilicate-bearing vitric tuffs, green triangles represent analcime-free vitric tuffs).

**Table 10.** Major (wt%) and trace element (ppm) values of Arıklı Tuff.

| | $SiO_2$ | $Al_2O_3$ | $Fe_2O_3$ | MgO | CaO | $Na_2O$ | $K_2O$ | $TiO_2$ | $P_2O_5$ | MnO | $Cr_2O_3$ | Ni | Sc |
|---|---|---|---|---|---|---|---|---|---|---|---|---|---|
| KK-5 | 63.39 | 15.06 | 2.49 | 1.38 | 0.82 | 2.58 | 4.46 | 0.36 | 0.07 | 0.03 | <0.002 | <20 | 6 |
| A-2 | 66.19 | 14.04 | 1.78 | 1.15 | 1.72 | 0.13 | 9.47 | 0.32 | 0.061 | 0.05 | 0.002 | <20 | 5 |
| A-9 | 54.49 | 12.91 | 1.93 | 3.83 | 5.37 | 3.1 | 5.58 | 0.29 | 0.061 | 0.11 | 0.003 | 22 | 5 |
| A-12 | 51.22 | 10.63 | 1.85 | 5.03 | 8.14 | 3.57 | 3.32 | 0.26 | 0.045 | 0.18 | <0.002 | <20 | 5 |
| Y-12 | 57.38 | 13.28 | 2.98 | 3.06 | 3.62 | 1.58 | 7.47 | 0.38 | 0.132 | 0.08 | 0.004 | <20 | 8 |
| YCT-9 | 67.89 | 14.31 | 2.4 | 0.56 | 0.16 | 0.24 | 11.84 | 0.33 | 0.051 | 0.02 | <0.002 | <20 | 5 |
| KC-1 | 66.17 | 14.65 | 2.33 | 0.98 | 0.27 | 3.75 | 6.68 | 0.34 | 0.06 | 0.03 | <0.002 | <20 | 4 |
| KL-5 | 65.91 | 15.09 | 1.74 | 0.63 | 0.44 | 3.28 | 6.05 | 0.31 | 0.072 | 0.03 | <0.002 | <20 | 6 |
| CPT-1 | 64.63 | 13.85 | 2.13 | 1.4 | 0.77 | 3.26 | 6.6 | 0.33 | 0.07 | 0.03 | <0.002 | <20 | 5 |
| CPT-3 | 66.36 | 14.54 | 2.24 | 0.8 | 0.5 | 3.62 | 6.74 | 0.34 | 0.056 | 0.05 | <0.002 | <20 | 6 |
| CPT-7 | 67.96 | 13.65 | 2.27 | 0.86 | 0.51 | 3.04 | 6.45 | 0.33 | 0.066 | 0.04 | <0.002 | <20 | 5 |
| CPT-10 | 68.94 | 13.18 | 2.26 | 0.7 | 0.33 | 3.33 | 5.51 | 0.31 | 0.052 | 0.02 | <0.002 | <20 | 5 |
| CT-6 | 64.3 | 15.36 | 1.99 | 0.91 | 0.6 | 4.11 | 5.33 | 0.35 | 0.06 | 0.04 | <0.002 | <20 | 5 |
| CT-7 | 65.77 | 14.33 | 2.36 | 1.18 | 0.56 | 3.52 | 6.11 | 0.33 | 0.069 | 0.02 | 0.003 | <20 | 4 |
| CT-8 | 52.85 | 12.11 | 1.91 | 4.7 | 5.92 | 5.88 | 0.8 | 0.27 | 0.143 | 0.1 | <0.002 | <20 | 5 |
| CT-11 | 66.62 | 14.29 | 2.47 | 0.58 | 0.28 | 4.33 | 5.1 | 0.33 | 0.057 | 0.04 | <0.002 | <20 | 5 |
| CT-14 | 64.12 | 15 | 2.87 | 1.1 | 0.63 | 0.56 | 12.19 | 0.5 | 0.11 | 0.01 | <0.002 | <20 | 6 |
| CT-15 | 65.2 | 14.64 | 2.17 | 1.25 | 0.45 | 3.91 | 5.18 | 0.32 | 0.054 | 0.03 | <0.002 | <20 | 5 |
| CT-16-A | 65.91 | 14.43 | 2.06 | 1 | 0.69 | 3.77 | 5.19 | 0.33 | 0.049 | 0.05 | <0.002 | <20 | 6 |
| CT-17 | 66.13 | 13.96 | 2.24 | 1.17 | 0.69 | 2.95 | 6.16 | 0.32 | 0.057 | 0.03 | <0.002 | <20 | 4 |

**Table 10** (continued)

|  | LOI | Sum | Ba | Be | Co | Cs | Ga | Hf | Nb | Rb | Sn | Sr | Ta |
|---|---|---|---|---|---|---|---|---|---|---|---|---|---|
| KK-5 | 9.1 | 99.76 | 1309 | 4 | 2 | 15.4 | 19.1 | 11 | 23.3 | 188.7 | 4 | 85.8 | 1.3 |
| A-2 | 5 | 99.86 | 205 | 5 | 2.6 | 1.5 | 16.5 | 9.8 | 20 | 266.2 | 4 | 231.4 | 1.1 |
| A-9 | 12.1 | 99.81 | 524 | 5 | 3.2 | 26.9 | 13.4 | 8.7 | 16.8 | 195.5 | 4 | 177.1 | 1 |
| A-12 | 15.5 | 99.75 | 353 | 5 | 2.4 | 24.9 | 9.8 | 7.3 | 14.5 | 110 | 3 | 212.3 | 0.8 |
| Y-12 | 9.6 | 99.53 | 1887 | 4 | 3.8 | 27.4 | 15.1 | 8.2 | 16.3 | 270 | 3 | 200.7 | 0.9 |
| YCT-9 | 2 | 99.77 | 421 | 5 | 1.4 | 6.2 | 17.6 | 12.5 | 21.6 | 365.6 | 4 | 37.9 | 1.2 |
| KC-1 | 4.6 | 99.82 | 308 | 4 | 1.7 | 77 | 16.5 | 11.8 | 21.1 | 194.3 | 5 | 48.7 | 1.2 |
| KL-5 | 6.4 | 99.91 | 1403 | 4 | 2.1 | 34.9 | 15.3 | 11.6 | 17.3 | 175.2 | 4 | 72.3 | 1.2 |
| CPT-1 | 6.9 | 99.93 | 299 | 4 | 2.1 | 33.9 | 16.7 | 12 | 21.3 | 218.2 | 5 | 74.5 | 1.3 |
| CPT-3 | 4.7 | 99.93 | 363 | 4 | 1.9 | 24.6 | 15.7 | 11.9 | 21 | 195.5 | 5 | 51.5 | 1.2 |
| CPT-7 | 4.7 | 99.86 | 328 | 4 | 1.9 | 16 | 16.4 | 11.8 | 21.5 | 213.5 | 4 | 56.7 | 1.2 |
| CPT-10 | 5.2 | 99.84 | 419 | 4 | 2.3 | 20 | 16.4 | 11.4 | 21.1 | 191.7 | 3 | 54.5 | 1.1 |
| CT-6 | 6.7 | 99.78 | 475 | 5 | 2 | 51 | 16.3 | 11.4 | 22.1 | 174.6 | 3 | 85.5 | 1.2 |
| CT-7 | 5.4 | 99.65 | 807 | 5 | 1.5 | 26.8 | 18 | 11.8 | 21.2 | 197.9 | 4 | 71.3 | 1.1 |
| CT-8 | 15.2 | 99.89 | 212 | 3 | 1.6 | 56.8 | 10.7 | 8.7 | 17.3 | 45.7 | 3 | 198.2 | 1 |
| CT-11 | 5.7 | 99.79 | 820 | 4 | 2.3 | 51.5 | 17.6 | 11.6 | 21.8 | 179.7 | 5 | 61.1 | 1.2 |
| CT-14 | 2.7 | 99.81 | 878 | 4 | 3.3 | 2.3 | 16 | 9.7 | 17.9 | 293 | 3 | 55.3 | 0.9 |
| CT-15 | 6.7 | 99.91 | 365 | 4 | 1.4 | 48.9 | 14.9 | 10 | 20.4 | 185.8 | 3 | 67.9 | 1.1 |
| CT-16-A | 6.5 | 99.95 | 264 | 4 | 1.7 | 45.1 | 15.6 | 11 | 20.1 | 163 | 3 | 78.1 | 1.1 |
| CT-17 | 6.2 | 99.91 | 448 | 4 | 2.2 | 23.4 | 17.4 | 10.4 | 20.5 | 198.2 | 4 | 82.4 | 1.1 |

**Table 10** (continued)

| | Th | U | V | W | Zr | Y | La | Ce | Pr | Nd | Sm | Eu | Gd |
|---|---|---|---|---|---|---|---|---|---|---|---|---|---|
| KK-5 | 53.6 | 10.3 | 22 | 2.6 | 355.7 | 27.1 | 89.1 | 165.9 | 17.96 | 62 | 8.77 | 1.39 | 6.51 |
| A-2 | 49.1 | 3.5 | 20 | 1 | 323.5 | 24.4 | 77.4 | 146.9 | 15.67 | 54.3 | 7.8 | 1.28 | 5.76 |
| A-9 | 43.2 | 8.9 | 23 | 0.7 | 286.5 | 23.2 | 72.3 | 135.5 | 14.65 | 50 | 7.54 | 1.27 | 5.43 |
| A-12 | 36.2 | 6.3 | 20 | 0.9 | 233.9 | 22.6 | 62.2 | 117.8 | 12.63 | 43.4 | 6.43 | 1.09 | 4.89 |
| Y-12 | 39.5 | 8.3 | 62 | 2.2 | 276.2 | 23.5 | 69.3 | 131.2 | 14.36 | 48.4 | 7.12 | 1.06 | 5.27 |
| YCT-9 | 52.4 | 6 | 21 | 1.8 | 406 | 25.2 | 91.7 | 169.6 | 18.06 | 61.7 | 8.37 | 1.09 | 6.02 |
| KC-1 | 49.7 | 5.3 | 17 | 1.3 | 380.4 | 25.5 | 88.7 | 167.6 | 17.55 | 59.8 | 8.74 | 1.08 | 6.02 |
| KL-5 | 45.9 | 5.9 | 15 | 1.2 | 434.7 | 22.2 | 83 | 156.4 | 16.61 | 57.6 | 8.14 | 1.08 | 5.8 |
| CPT-1 | 52.6 | 7.3 | 12 | 3.1 | 398.7 | 21.6 | 93.1 | 172.9 | 18.47 | 63 | 9.02 | 1.1 | 6.31 |
| CPT-3 | 50.8 | 5 | 13 | 3.7 | 410.5 | 22.4 | 88.3 | 168 | 18.06 | 62 | 8.8 | 1.12 | 6.19 |
| CPT-7 | 52.1 | 7.8 | 13 | 3.7 | 406.4 | 27.7 | 88.1 | 166.8 | 17.73 | 61.6 | 9.09 | 1.17 | 6.5 |
| CPT-10 | 48.5 | 7.1 | 15 | 3.3 | 394 | 29.8 | 89.3 | 166.9 | 17.91 | 61.8 | 9.01 | 1.15 | 6.83 |
| CT-6 | 53.5 | 9.1 | 13 | 1.7 | 388.6 | 22.8 | 94.6 | 173.5 | 18.38 | 61.8 | 8.6 | 1.09 | 6.02 |
| CT-7 | 50.9 | 5.3 | 14 | 1.6 | 390.6 | 20.8 | 89 | 165.5 | 17.64 | 59.7 | 8.4 | 1.06 | 5.73 |
| CT-8 | 43.6 | 5.7 | 30 | 2.3 | 292 | 21.6 | 74.6 | 137.8 | 14.92 | 51.8 | 7.28 | 0.98 | 5.43 |
| CT-11 | 50 | 8.3 | 16 | 1.5 | 401.1 | 25.7 | 90.3 | 169.3 | 17.91 | 62.5 | 8.65 | 1.13 | 6 |
| CT-14 | 38.8 | 4.3 | 31 | 2.1 | 350.1 | 21.8 | 75.2 | 138.1 | 14.68 | 50.6 | 7.52 | 1.25 | 5.43 |
| CT-15 | 47.9 | 8.8 | 12 | 1.7 | 316.7 | 18.8 | 85.9 | 157.6 | 16.91 | 58.4 | 7.94 | 0.94 | 5.32 |
| CT-16-A | 47.5 | 3 | 15 | 1.5 | 377.9 | 19.7 | 84.9 | 161 | 16.97 | 57.8 | 7.8 | 0.96 | 5.18 |
| CT-17 | 46.8 | 6.2 | 12 | 2.2 | 352 | 19.8 | 85.3 | 157.4 | 16.69 | 56.4 | 7.99 | 0.96 | 5.41 |

**Table 10** (continued)

|  | Tb | Dy | Ho | Er | Tm | Yb | Lu | Mo | Cu | Pb | Zn | Ni | As |
|---|---|---|---|---|---|---|---|---|---|---|---|---|---|
| KK-5 | 0.85 | 4.89 | 0.92 | 2.56 | 0.41 | 2.64 | 0.39 | 0.3 | 23.6 | 65.7 | 57 | 2 | 40 |
| A-2 | 0.82 | 4.28 | 0.82 | 2.3 | 0.39 | 2.48 | 0.38 | 3.3 | 25 | 69.2 | 45 | 3.4 | 318.7 |
| A-9 | 0.76 | 4 | 0.77 | 2.21 | 0.35 | 2.32 | 0.36 | 0.8 | 18 | 65.6 | 33 | 10.1 | 89 |
| A-12 | 0.69 | 3.76 | 0.74 | 2.1 | 0.35 | 2.33 | 0.35 | 0.8 | 26.2 | 46.8 | 29 | 2.5 | 95.3 |
| Y-12 | 0.73 | 4.16 | 0.81 | 2.29 | 0.36 | 2.48 | 0.36 | 9.9 | 48.6 | 53.1 | 60 | 17.1 | 162.7 |
| YCT-9 | 0.81 | 4.23 | 0.82 | 2.36 | 0.39 | 2.53 | 0.36 | 1.8 | 22.6 | 65.6 | 53 | 2.3 | 234.7 |
| KC-1 | 0.82 | 4.47 | 0.86 | 2.29 | 0.38 | 2.26 | 0.34 | 1.4 | 30.2 | 62.3 | 55 | 2.6 | 82 |
| KL-5 | 0.78 | 4.3 | 0.77 | 2.07 | 0.3 | 1.91 | 0.26 | 0.1 | 31.6 | 67.7 | 39 | 2.1 | 58 |
| CPT-1 | 0.81 | 4.08 | 0.76 | 1.98 | 0.3 | 1.88 | 0.26 | 0.6 | 36.7 | 62.7 | 55 | 3.4 | 96.8 |
| CPT-3 | 0.83 | 4.24 | 0.79 | 2.16 | 0.34 | 2.07 | 0.3 | 1.7 | 29.5 | 77.1 | 54 | 3.4 | 140.3 |
| CPT-7 | 0.91 | 4.92 | 0.91 | 2.51 | 0.41 | 2.55 | 0.37 | 1 | 19.8 | 68.8 | 50 | 3.3 | 56.4 |
| CPT-10 | 0.94 | 5.37 | 1.02 | 2.87 | 0.44 | 2.86 | 0.41 | 1.1 | 15.5 | 67.7 | 49 | 3.1 | 46.4 |
| CT-6 | 0.82 | 4.3 | 0.8 | 2.12 | 0.33 | 2.18 | 0.32 | 0.2 | 24.2 | 65.2 | 47 | 4.5 | 49.3 |
| CT-7 | 0.76 | 4.24 | 0.73 | 1.86 | 0.29 | 1.8 | 0.27 | 1 | 23.4 | 63.6 | 33 | 7.2 | 174.4 |
| CT-8 | 0.73 | 4.02 | 0.76 | 2.06 | 0.33 | 2.22 | 0.34 | 2.9 | 12.4 | 54.7 | 39 | 2.4 | 48 |
| CT-11 | 0.84 | 4.46 | 0.88 | 2.46 | 0.41 | 2.69 | 0.4 | 2.5 | 25.1 | 71.7 | 55 | 3.1 | 38.8 |
| CT-14 | 0.74 | 3.99 | 0.77 | 2.16 | 0.33 | 2.13 | 0.31 | 0.8 | 28.2 | 66.2 | 56 | 5.2 | 313.6 |
| CT-15 | 0.71 | 3.65 | 0.67 | 1.74 | 0.26 | 1.7 | 0.25 | 0.2 | 21.3 | 65.7 | 58 | 3.1 | 47.2 |
| CT-16-A | 0.68 | 3.75 | 0.67 | 1.9 | 0.32 | 1.92 | 0.28 | <0.1 | 24.5 | 68.3 | 38 | 2.7 | 80.9 |
| CT-17 | 0.72 | 3.79 | 0.71 | 1.87 | 0.3 | 2.03 | 0.29 | 0.3 | 25 | 72.1 | 30 | 6 | 106.9 |

**Table 10** (continued)

|         | Cd    | Sb  | Bi  | Ag    | Au    | Hg    | Tl  | Se    |
|---------|-------|-----|-----|-------|-------|-------|-----|-------|
| KK-5    | <0.1  | 1   | 0.3 | <0.1  | <0.5  | <0.01 | 0.3 | 0.5   |
| A-2     | <0.1  | 2.5 | 0.4 | <0.1  | <0.5  | <0.01 | 0.6 | <0.5  |
| A-9     | 0.1   | 0.5 | 0.4 | <0.1  | <0.5  | <0.01 | 0.2 | <0.5  |
| A-12    | <0.1  | 0.9 | 0.3 | <0.1  | <0.5  | <0.01 | 0.2 | <0.5  |
| Y-12    | <0.1  | 2.6 | 0.4 | 0.1   | 0.9   | 0.07  | 0.6 | <0.5  |
| YCT-9   | <0.1  | 3   | 0.3 | <0.1  | 0.7   | <0.01 | 0.4 | <0.5  |
| KC-1    | <0.1  | 1.3 | 0.2 | <0.1  | <0.5  | 0.01  | 0.7 | <0.5  |
| KL-5    | <0.1  | 0.6 | 0.3 | <0.1  | <0.5  | <0.01 | 0.6 | <0.5  |
| CPT-1   | <0.1  | 0.8 | 0.3 | <0.1  | <0.5  | <0.01 | 0.4 | <0.5  |
| CPT-3   | <0.1  | 1.3 | 0.3 | <0.1  | <0.5  | <0.01 | 0.7 | <0.5  |
| CPT-7   | <0.1  | 1.1 | 0.3 | <0.1  | <0.5  | <0.01 | 0.7 | <0.5  |
| CPT-10  | <0.1  | 1.2 | 0.2 | <0.1  | <0.5  | 0.01  | 0.5 | <0.5  |
| CT-6    | <0.1  | 0.7 | 0.3 | <0.1  | <0.5  | <0.01 | 0.5 | <0.5  |
| CT-7    | <0.1  | 1.3 | 0.3 | <0.1  | <0.5  | 0.01  | 1   | <0.5  |
| CT-8    | <0.1  | 0.8 | 0.2 | <0.1  | <0.5  | <0.01 | 0.3 | <0.5  |
| CT-11   | <0.1  | 1.3 | 0.3 | <0.1  | <0.5  | <0.01 | 0.7 | <0.5  |
| CT-14   | <0.1  | 1.8 | 0.2 | <0.1  | <0.5  | 0.01  | 0.4 | <0.5  |
| CT-15   | <0.1  | 0.8 | 0.3 | <0.1  | <0.5  | <0.01 | 0.4 | <0.5  |
| CT-16-A | <0.1  | 0.6 | 0.2 | <0.1  | <0.5  | <0.01 | 0.6 | <0.5  |
| CT-17   | <0.1  | 1.1 | 0.3 | <0.1  | <0.5  | <0.01 | 0.5 | <0.5  |

Chemical differences of Arıklı tuff samples are clearly shown in the triangular diagram, Na$_2$O-K$_2$O-(CaO+MgO) (Figure 86). Plotted in the triangular diagram three groups were discriminated clearly. Group 1 is Cao+MgO rich, Group 2 is relatively Na$_2$O rich and Group 3 is K$_2$O rich. Group 1 differentiated geochemically corresponds to the dolomite-rich vitric tuff in petrography section. These samples plot where the values of CaO+MgO are highest (Figure 86). Their Na$_2$O values are variable; from lower to higher Y-12: 1.58; A-9: 3.10; A-12: 3.57; ÇT-8: 5.88 (Table 10).
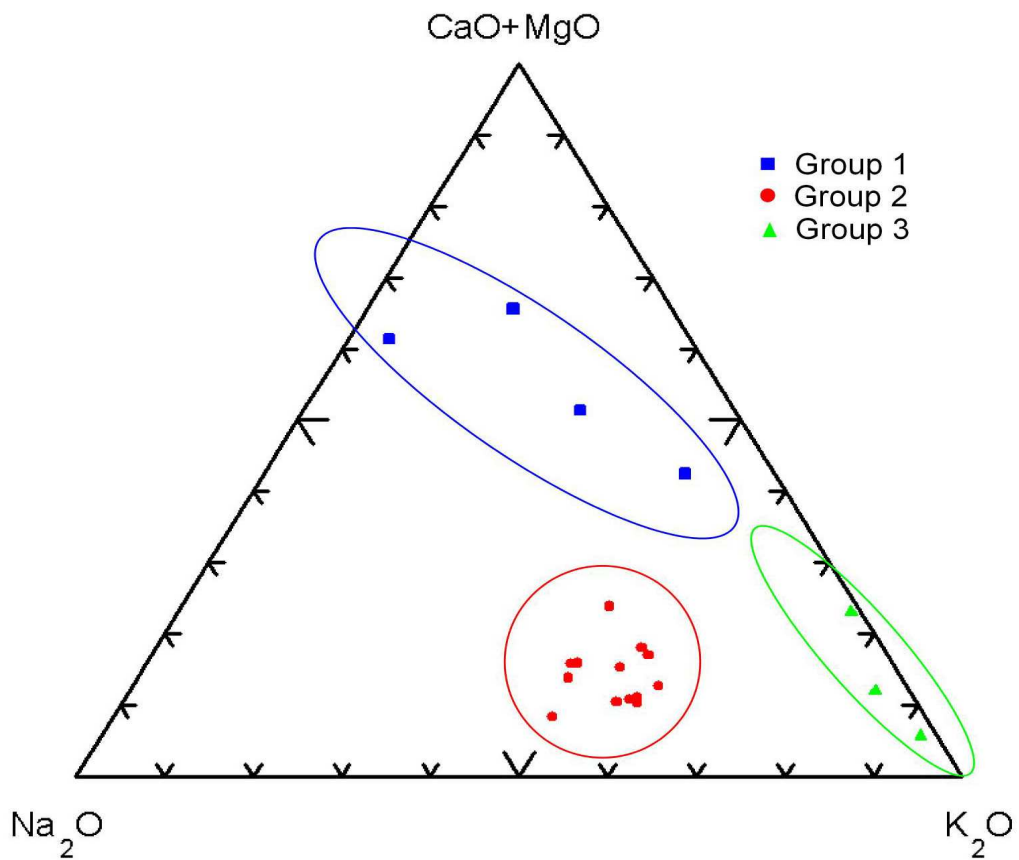


**Figure 86.** Arıklı tuff samples plotted on a triangular Na2O-K2O-(CaO+MgO) composition diagram (The symbols for samples are given on Figure 85).

In the triangular diagram (Figure 86), it can be seen that the analcime-rich tuffs (Group 1 and Group 2) discriminate from the analcime-free tuffs (Group 3) with higher Na2O contents. In addition, analcime rich tuffs are discriminated between each other. All the samples with moderate to low CaO+MgO and higher Na2O form a distinct group, coinciding with the phyllosilicate mineral dominated vitric tuff (Group 2) in petrography section.

The third group with the highest $K_2O$ and lowest $Na_2O$ values consists of analcime-free samples. Even if two samples of this group (A-2, YÇT-9) were differentiated as K-feldspar dominated vitric tuffs, the third sample (ÇT-14) is not confirmable with this generalization. However, as mentioned in the petrography section ÇT-14 is a crystal tuff with a high crystal content. It contains authigenic K-feldspar in matrix. But it can not be differentiated as K-feldspar dominated tuff since it contains also a very high amount of phyllosilicate minerals. The reason that it has the highest $K_2O$ value can be explain that it contains both authigenic K-feldspar and primary K-feldspar minerals.

Even though the studied samples with higher $K_2O$ usually contain less $Na_2O$, there is no reverse relationship between $K_2O$ and $Na_2O$ in all samples. Namely, KK-5 contains 4.46% $K_2O$ and 2.58% $Na_2O$, but ÇT-6 with higher $K_2O$ content (5.33%) also contains more $Na_2O$ (4.11%). Still, the general trend is that $K_2O$ decreases with increasing $Na_2O$ as shown in Figure 87.
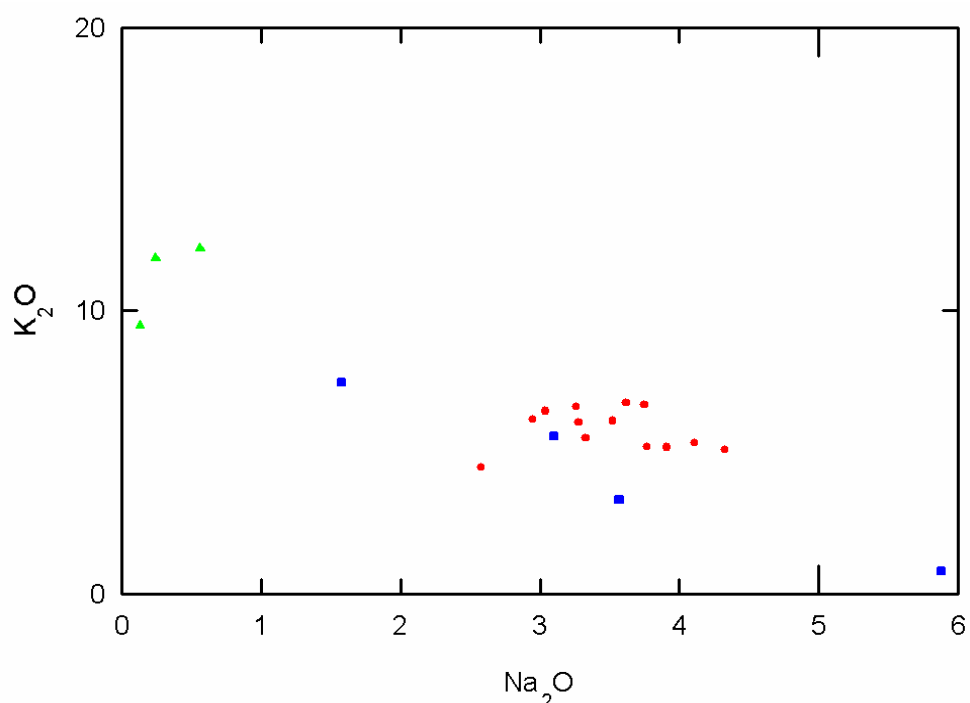
**Figure 87.** Variation of K₂O with Na₂O in Arıklı Tuff samples (The symbols for samples are given on Figure 86).

To observe more apparently the relationship between K and Na, an elemental variation diagram for all samples is given in Figure 88. Here, it can be easily noticed that analcime-free samples (A-2, YÇT-9, ÇT-14) having lower Na, have higher K contents. On the other hand, the richest analcime sample (ÇT-8) has the lowest K content. But still, it can not be said that the reverse relationship between K and Na is valid. For example, Sample ÇT-11 having the highest Na (3.21) after ÇT-8 is also higher in K (4.36) as seen in Figure 88.
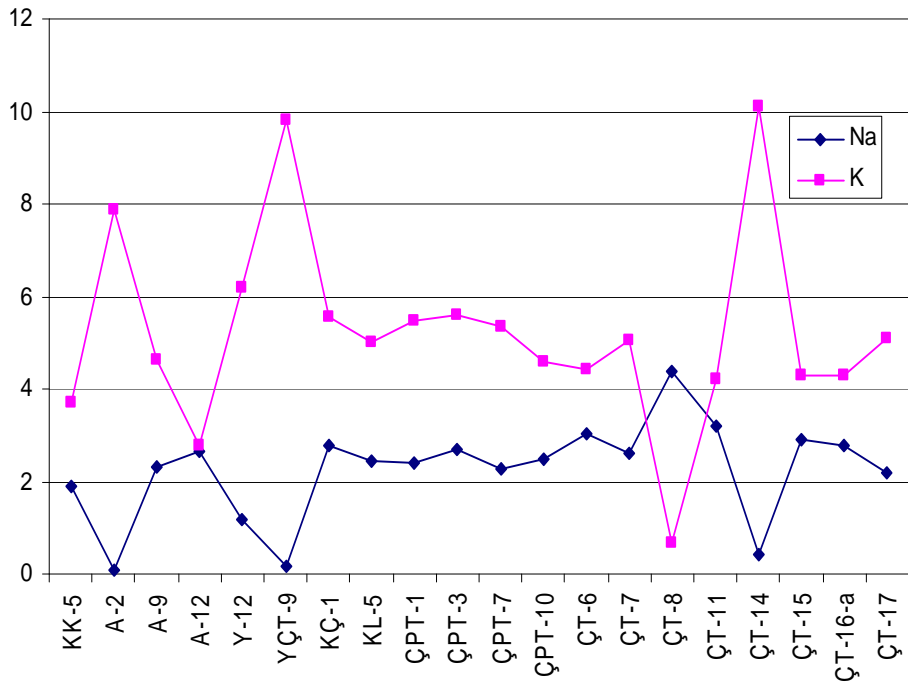
**Figure 88.** Elemental relationship of all Arıklı Tuff samples.

The values of LOI are usually higher in samples that contain analcime, compared with the analcime-free (ÇT-14, YÇT-9) tuffs (Table 10). This is reasonable because analcimes adsorb water. That is, there is a correlation between LOI and analcime. One analcime-free tuff sample (A-2), however, has higher LOI value than other analcime-free tuffs even if it has still lower LOI value than analcime-rich ones. The point that should be taken into account with this sample is that it has a higher CaO content than samples ÇT-14 and YÇT-9. By this, sample A-2 was petrographically grouped as K-feldspar dominated vitric tuff, but it contains a higher amount of dolomite (Table 4). In addition to this, all samples with highest LOI values (ÇT-8, A-12, Y-12 and A-9) contain the highest CaO contents and all of these samples were grouped as dolomite-rich vitric tuff. Consequently, correlation can also be made between LOI and CaO, as clearly seen in samples A-2, ÇT-8, A-12, Y-12 and A-9 (Table 4), meaning that their LOI value may be

attributed to the presence of dolomite because of the large amount of CaO (i. e. Kaçmaz and Köktürk, 2004).

The geochemical nature of the host rock is extremely difficult to establish because of the absence of preserved volcanic glass in these tuffs. Altered ones exposed mobilization and redistribution of silica, alkali and alkaline earth cations and water during alteration (Slaughter and Earley, 1965; Kitsopoulos et al., 2001). That is, some elements left and some elements enter in the system.

The some problem involved with the mobilization of the alkalis is seen by plotting the $SiO_2$ versus total alkali ($Na_2O+K_2O$) diagram (TAS) of Le Bas et al. (1986) for the chemical classification of the host rock (Figure 89). This is a classical diagram which is used to classify common volcanic rocks. In petrography chapter, it was said that tuffs mainly consist of quartz, biotite and sanidine. So, the samples might then be expected to plot around the rhyolite-dacite fields. Arıklı Tuff, on the other hand, plot in the basaltic trachyandesite and trachyandesite field while the majority of the samples plot in the trachyte-trachyandesite field. The spread of the points is much wider than expected and it is not possible that the parent material really includes all these different type of rocks. Namely, the use of this chemical classification diagram with altered rocks could lead to incorrect conclusions. However, the Winchester and Floyd (1977) diagram (Figure 90) which uses immobile elements is more efficient.
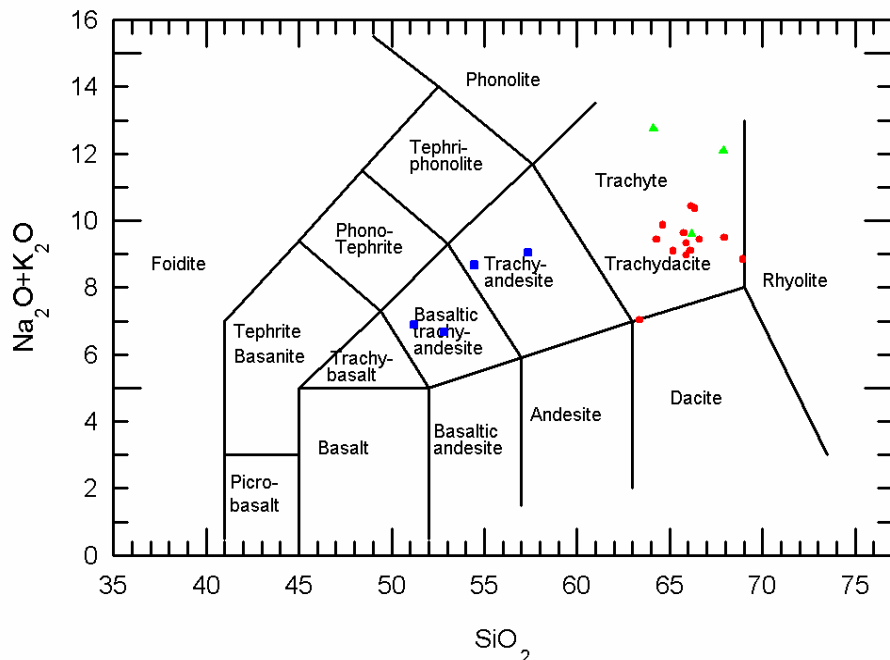
**Figure 89.** The SiO$_2$ versus total alkali (Na$_2$O+K$_2$O) diagram (TAS) of Le Bas et al. (1986) (The symbols for samples are given on Figure 86).

According to the Winchester and Floyd (1977), Nb, Y, Ti and Zr are immobile during alteration processes. For this reason, immobile trace element classification diagram, Zr/TiO$_2$ versus Nb/Y was used in Figure 90. By using immobile elements, the Arıklı Tuff samples plot in the field of trachyandesite/ rhyolite. Even if this diagram based on immobile elements such as Nb, Zr, Ti and Y are much more dependable, they must be used with care for rocks that have undergone alteration, because, even immobile elements can be removed under intense alteration. Classification of the studied tuff samples by immobile trace elements is given in Table 11.
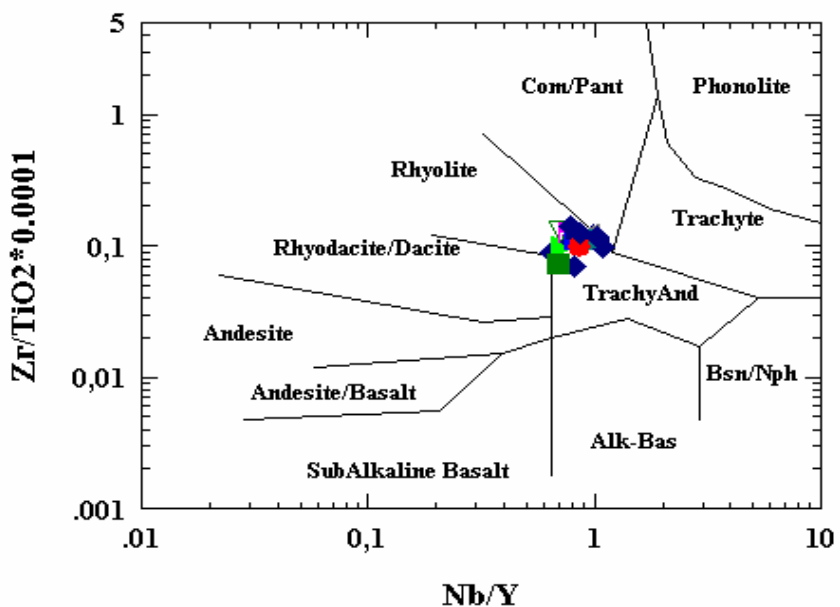
**Figure 90.** The Zr/TiO$_2$ vs Nb/Y discrimination diagram (Winchester and Floyd ,1977) and the locations of Arıklı Tuff samples.

**Table 11.** Chemical classification of Arıklı Tuff samples.

| Rhyolite | Trachyandesite | Rhyolite and Trachyandesite |
|---|---|---|
| A-12 | A-2 | A-9 |
| ÇPT-10 | ÇPT-1 | ÇPT-11 |
| ÇPT-7 | ÇPT-3 | YÇT-9 |
| KL-5 | ÇT-15 | |
| | ÇT-14 | |
| | ÇT-16-a | |
| | ÇT-17 | |
| | ÇT-6 | |
| | ÇT-7 | |
| | ÇT-8 | |
| | KÇ-1 | |
| | KK-5 | |
| | Y-12 | |

In Figure 91, elemental abundances of samples from the Arıklı Tuff are graphed to correlate element abundances of analcime-free and analcime-bearing samples.

Looking at this graph, the point to notice is that the decreasing or increasing values are only reflected in some of the samples (ÇT-14, ÇT-8, YÇT-9, Y-12, A-12, A-9 and A-2). Remaining samples demonstrate a rather smooth lines (Figure 91). The graph of Si and Al are rather alike. The values of Si and Al are low in A-12, ÇT-8, A-9 and Y-12 respectively (Figure 91). These samples are grouped as dolomite-rich vitric tuff (only Y-12 grouped as dolomite) in petrography section (Table 5). The graph of Ca and Mg are also similar and shows a smooth pattern except for samples ÇT-8, A-12, A-9 and Y-12. The values of Ca and Mg are high in samples A-12, ÇT-8, A-9, and Y-12 and all of them are grouped as dolomite-rich vitric tuff, except sample Y-12. The graphs of Na and K show a smooth pattern except for sample ÇT-14, YÇT-9, A-2 and ÇT-8. The values of Na are low in A-2, YÇT-9 and ÇT-14, which are zeolite-free samples. The Na value is very high in ÇT-8. Remaining samples contain same Na except sample Y-12. The values of K are high in ÇT-14, YÇT-9 and A-12, but it is low in ÇT-8 (Figure 91). The values of Fe are high in Y-12 and ÇT-14.

Samples ÇT-8, A-12 and A-9 are differentiated from others by their Si, Al, Ca and Mg contents. All of them are low in Si and Al contents and high in Ca and Mg contents. The high content of Ca and Mg can be explained with the presence of dolomite. The lower content of Si and Al can be explained by two different ways. The first one is that Si and Al were removed during alteration. The second one is that the original composition of the studied samples was different. If Si and Al were removed during alteration, it should be explained why other tuff samples were not affected by this event, although they have also undergone alteration. Consequently, a difference in original compositions is more reasonable. Besides, all of these dolomite-rich virtic tuffs are classified as a different group in petrography section.

Another striking point, however, is related to the Na and K contents. Even though samples A-12 and A-9 resemble each other very much petrographically and were taken from the same outcrop (distance between them is less than 1m) the Na contents are quite different. Sample A-12 includes high Na and low K in sample A-12 but vice versa in sample A-9. ÇT-8 has higher Na content than A-12 and A-9 and lower K content than A-12 and A-9. Hence it can be said that Na and K have reverse relationship. This might be related to analcime formation because all of them contain analcime.

SampleY-12 is grouped as dolomite petrographycally. It contains lower Si and Al but higher Ca and Mg than the average. High Ca and Mg contents are caused by the presence of dolomite. The difference in Si and Al can be explained by differences in rock group, as sample Y-12 is not a tuff. It does not contain glass shards or pumice fragment. As a result of this the formation of analcime can only be due to precipitation and the result might be the low Na content. The reverse relationship between K and Na is also observed in sample Y-12.
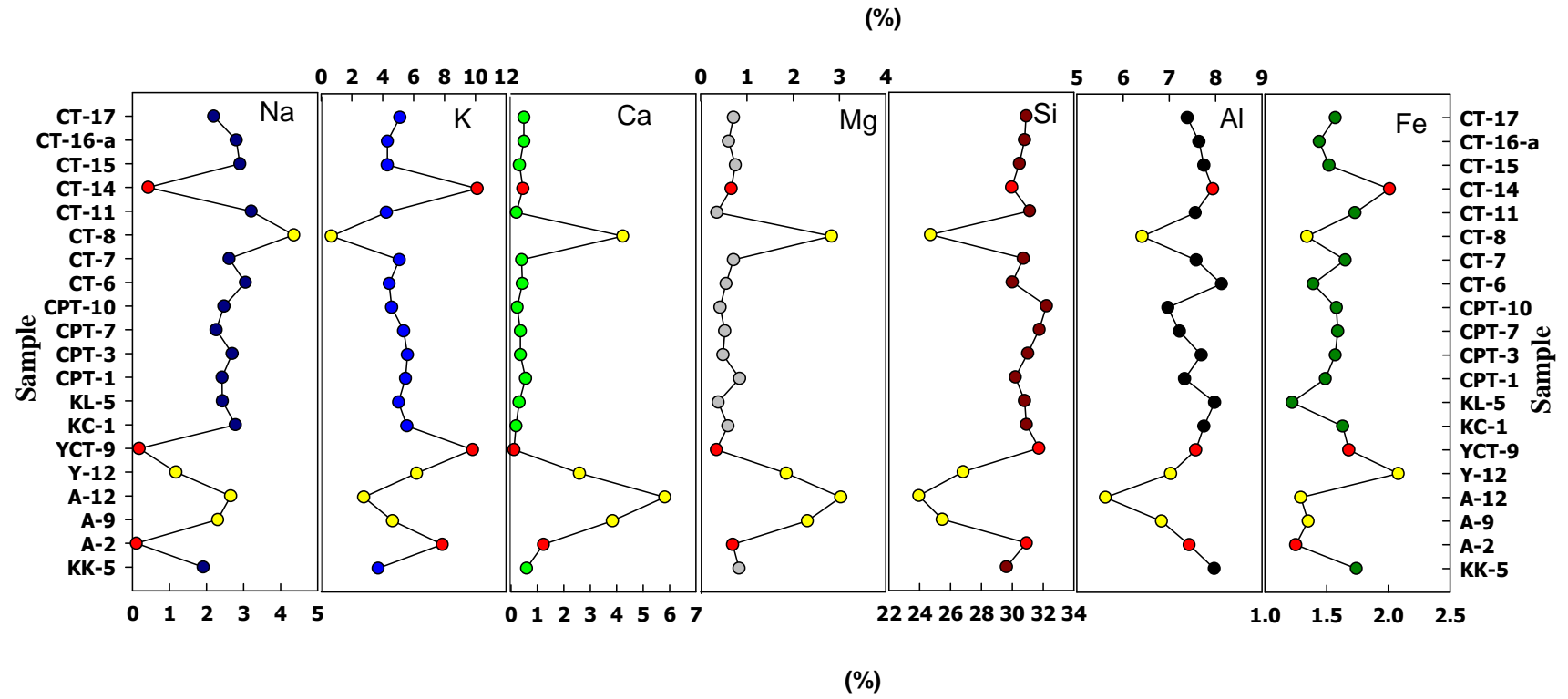
**Figure 91.** Major element abundances of samples from Arıklı Tuff.

Samples ÇT-14, YÇT-9 and A-2 have similar Si, Al, Ca and Mg contents with the average values. They, on the other hand, have the lowest Na and highest K contents. Sample YÇT-9 is petrographically rather similar to the phyllosilcate-bearing ones, except its high content in sanidine in the matrix. Disregarding this, it is chemically almost the same with the phyllosilicate-rich samples. The reason it is differentiated from others must be related to alteration. Reverse relationship between Na and K can be observed in A-2 and ÇT-14. ÇT-14 is quite different from others since it is a crystal tuff. Still it contains very high K.

Phyllosilicate-bearing tuffs are characterized by average plots in diagram (Figure 91). All samples of this group display nearly similar Na, K, Ca, Mg, Si and Al contents.

There are two important points that should be emphasized. The first one is; even though ÇT-8, A-9 and A-12 are different originally, the Na content can be similar or higher than those in the phyllosilicate-bearing ones. The second one is; even though YÇT-9 and A-2 are similar originally, their Na content is lower than those samples with phyllosilicate mineral.

The mobility of the major elements is normally accompanied by the mobility of trace and REE during the diagenetic events. Hence, the correlation of the abundances of these elements with respect to the major ones within the Arıklı Tuff is important. For this we considered the classical approach for alteration.

It is known that when a rock is subjected to alteration, it shows element mobility. Trace element mobility is controlled by the mineralogical changes during alteration. In general, incompatible elements (Sr, K, Rb, Ba) are mobile whereas compatible elements are immobile (Zr, Y, Hf). In addition, the transition metals (Zn, Cu) tend to be mobile, whereas Ni and V are immobile.

When plotted on the variation diagram (Figure 92) the trace element patterns of the studied samples, except some, define an average value, characterized by the median line, as it was the case in Figure 91, and shows enrichments and depletions with regard to this mean value. Since Rb substitutes K, its pattern in Figure 92 is just like K on Figure 92. Rb content increases in analcime-free samples (Çt-14, YÇT-9, A-2), but it decreases in samples ÇT-8, A-12 and A-9 which are dolomitic ones. As Sr substitutes Ca it behaves like Ca, except in sample A-2. Even though Ca is constant in A-2, Sr increases in A-2 significantly. Other two analcime-free samples display constant Sr contents. In samples ÇT-8, Y-12 and A-9, however, Sr content increases together with increasing Ca. Ba values are constant in all analcime-free and dolomite-rich vitric tuffs. It increases only in samples KL-5, Y-12 and KK-5. There is no significant change in Ni and Cu except in sample Y-12, which displays increased values. Dolomite–rich samples (ÇT-8, Y-12, A-12 and A-9) show decreasing behavior in their Zr content, which increases significantly in analcime-free ones.
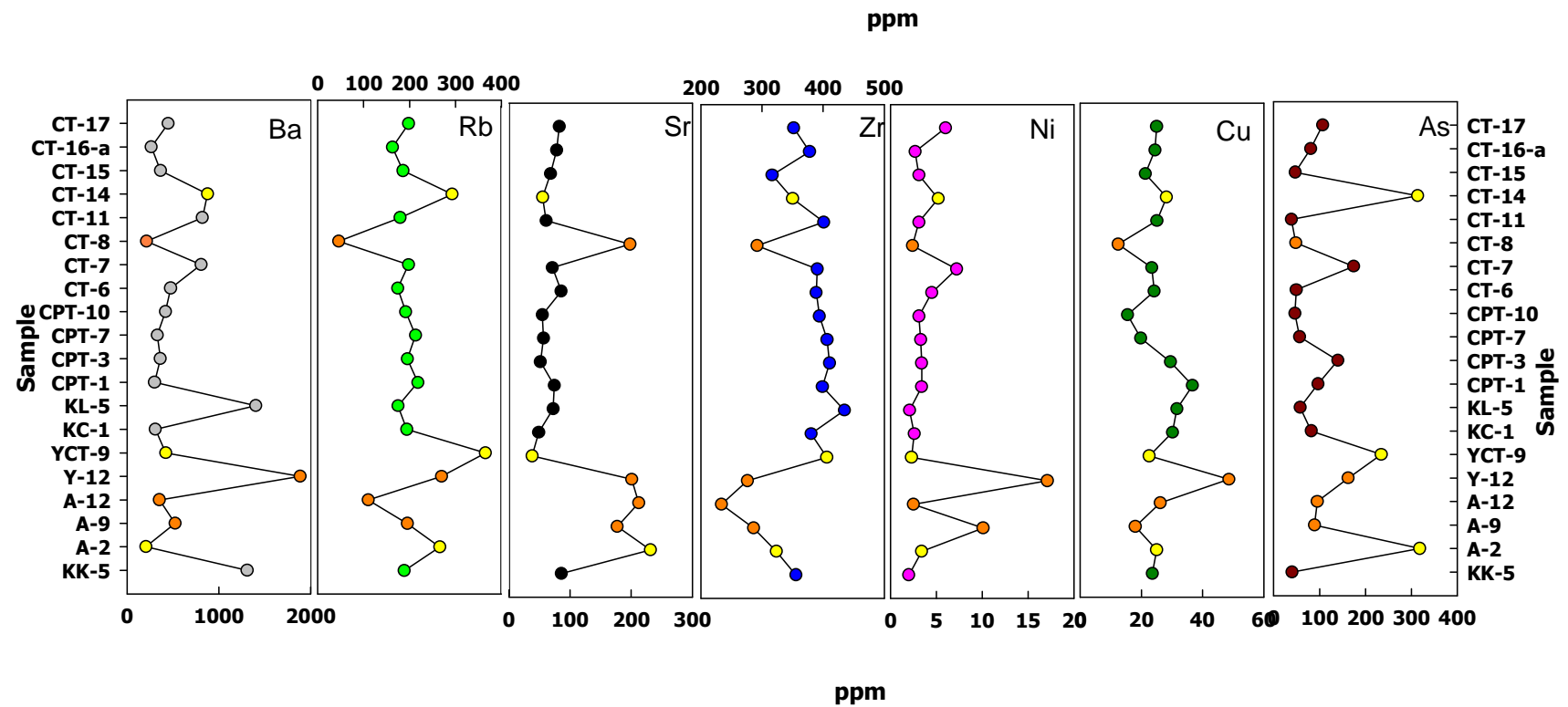
**Figure 92.** Trace element abundances of samples from Arıklı Tuff.

After correlation elemental abundances between analcime-rich and analcime-free tuffs, an attempt was made to compare the compositions of the altered Arıklı Tuff samples with a theoretical rhyolitic tuff (TRT) composition. This supposed rhyolitic composition was based mainly on the Winchester and Floyd (1977) diagram on Figure 90. The average rhyolite composition is from Raymond (1995). Samples were normalized with respect to this TRT average composition. Since phyllosilicate-bearing samples displayed minimum variation on Figure 91 the normalization graph with respect to rhyolite was applied only to these samples. That is, ÇT-8, Y-12, A-12 and A-9 were not used for normalization diagram because of different original composition.

In Figure 93, two tuff samples were selected, analcime-free (YÇT-9) and analcime rich (ÇT-11) and compare with the TRT composition. In sample YÇT-9, Ca and Na are depleted with respect to TRT. K, Al, Fe and Mg, however, are enriched. Si does not vary very much. In ÇT-11, a depletion in Ca obvious, and Al, Fe, Mg and Na are enriched in the system. K and Si did not change much in the sample ÇT-11.

155
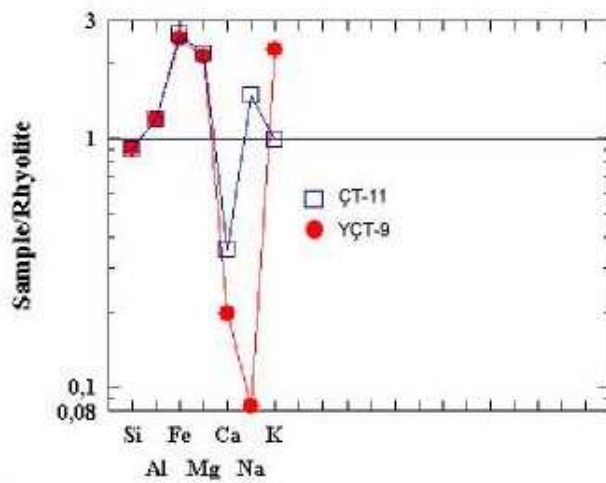
**Figure 93.** Major element concentrations normalized to the composition of the theoretical rhyolitic tuff (TRT) for YÇT-9 (analcime-free), ÇT-11 (analcime-bearing). Normalizing values are from Raymond (1995).

YÇT-9, ÇT-14 and A-2 normalized with respect to TRT to examine the behavior of elements of analcime-free samples together (Figure 94). All analcime-free samples show the same enrichment and depletion except Ca. The system is considerably depleted in Na. K, on the other hand, has entered to the system. Si is not affected too much. Al, Fe and Mg enriched in the system. Ca is depleted in YÇT-9 and ÇT-14, but enriched in A-2.
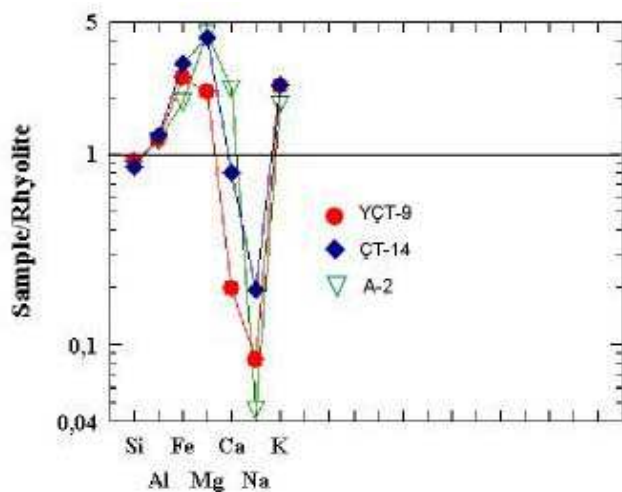
**Figure 94.** Major element concentrations normalized to the composition of the theoretical rhyolitic tuff (TRT) for analcime-free tuff. Normalizing values are from Raymond (1995).

The behavior of analcime bearing samples was also evaluated with respect to TRT (Figure 95). For this, samples ÇT-6, ÇT-11 and ÇT-16-a were selected, which were grouped petrographically as phyllosilicate-bearing samples. The three samples display the same enrichment and depletion. There is a distinct increase in the Na content. K content does not vary much. A limited loss in Si content was observed. Al, Fe and Mg behave just like the analcime-free equivalents. The altered rock system dramatically depleted in Ca content during the alteration.
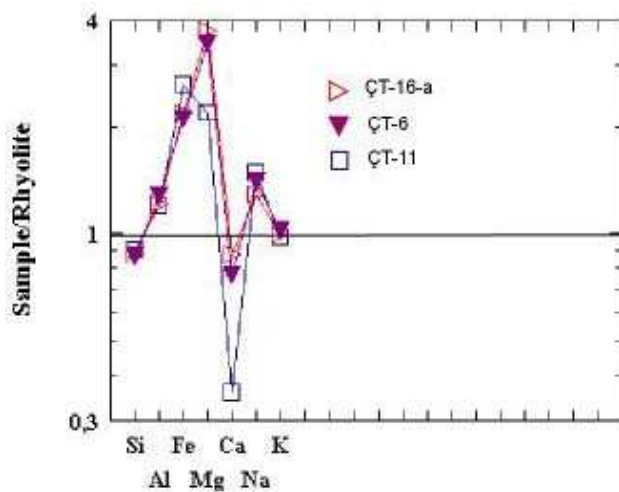
**Figure 95.** Major element concentrations normalized to the composition of the theoretical rhyolitic tuff (TRT) for analcime-bearing tuff. Normalizing values are from Raymond (1995).

It can be generally said that Si content of altered tuffs was not changed much with respect to Si of TRT. However, Na and K contents changed significantly. Na was depleted and K was enriched in analcime-free tuffs. Na was enriched and K was not changed in analcime-bearing present samples. Al, Fe and Mg were enriched in all tuff samples.

The possible causes of this empirical approach will be evaluated in the Discussions on the formation of analcime in the Arıklı Tuff.

# CHAPTER 6

# DISCUSSION

In this chapter, the data presented in the previous chapters will be evaluated and the origin and formation of analcime will be discussed on the basis of field and laboratory work.

Zeolitization and the formation of analcime is controlled by many significant factors. Hence, it is very important to understand the factors of zeolitization to answer the question why some tuffs are zeolitized and others are not even if they have same original composition and texture.

The species and amount of zeolite depend on many factors such as texture and composition of the host rock, composition of interstitial water, geological environment, age, pH, time, salinity, temperature and pressure (Hay, 1978; Hay, 1966; Surdam, 1978; Hall, 1998; Cas and Wright, 1987). However, the principal conditions are 1) a high proportion of volcanic glass content, 2) high internal surface area (porosity), and 3) favorable hydrological conditions. Hall, 1998 mention that "because of high volcanic glass content and porosity, the pyroclastic rocks have appropriate conditions for formation of zeolites".

The pH of the circulating fluids during the diagenetic stage is the most important chemical parameter of zeolitization. The experiments proved that volcanic glasses are altered most rapidly by alkaline conditions (Mariner and Surdam, 1970). "The rate of dissolution of rhyolitic glasses increases 20 times when the pH is raised from 8.5 to 11.5" (Mariner and Surdam, 1970). Zeolitization therefore takes place under alkaline conditions. It was designated that substantial amounts of zeolites

159

can form in a few thousand years at a pH of 9.5 (Hay, 1978). The reaction of volcanic glass with water also cause an increase in pH. This is because of dissolution mechanism, where $H_3O^+$ enters the glass from the solution while $Na^+$ and $K^+$ enter the solution from the glass (Casey and Bunker, 1990). Barth-Wirsching and Höller (1989) showed that high temperature (at least higher than earth-surface atmospheric) causes the alteration of volcanic glasses. Pressure appears less important than temperature, but its effect increases if temperature and pressure are in combination.

The different types of zeolite formation were already mentioned in Chapter 1 (introduction). The saline-alkaline lake condition is the most important one, since analcimes are formed in this environment more commonly. In saline alkaline lake deposits zeolites form from volcanic glass (Surdam and Sheppard, 1978). The authigenic minerals make up lateral zonation from outer to inner: unaltered glass→alkali zeolites mostly clinoptilolite→analcime→K-feldspar (Figure 2).

Analcime in sedimentary rocks may form by reaction of volcanic glass, aluminosilicate minerals, clays or gel and they may be also chemically precipitated (Bradley, 1928, Ross, 1928; High and Picard, 1965; , Iijima and Utada, 1966 ;Iijima, 1980; Surdam and Sheppard, 1978; Surdam and Parker, 1972; Surdam and Eugster, 1976; Brobst and Tucker, 1973; Keller, 1952; Hay and Moiola, 1963; Sheppard, 1971; Van Houten, 1962; Hay, 1966; Hay, 1986; Wu, 1970). These different types for analcime-formation will be explained below.

**1) Alteration of volcanic glass**

Analcime can be formed as an alteration product of volcanic glass (Ross, 1928; Bradley, 1928; Iijima, 1980; Iijima and Utada, 1966; Tyrell and Peacock, 1926). Ross (1928) described small isotropic crystal grains with perfect trapezohedrons as analcime in playa lake deposit in Yavapai County, Arizona. He also showed

that many of these analcimes are free individual crystals but some may appear together as groups or irregular chains (Figure 96-a).
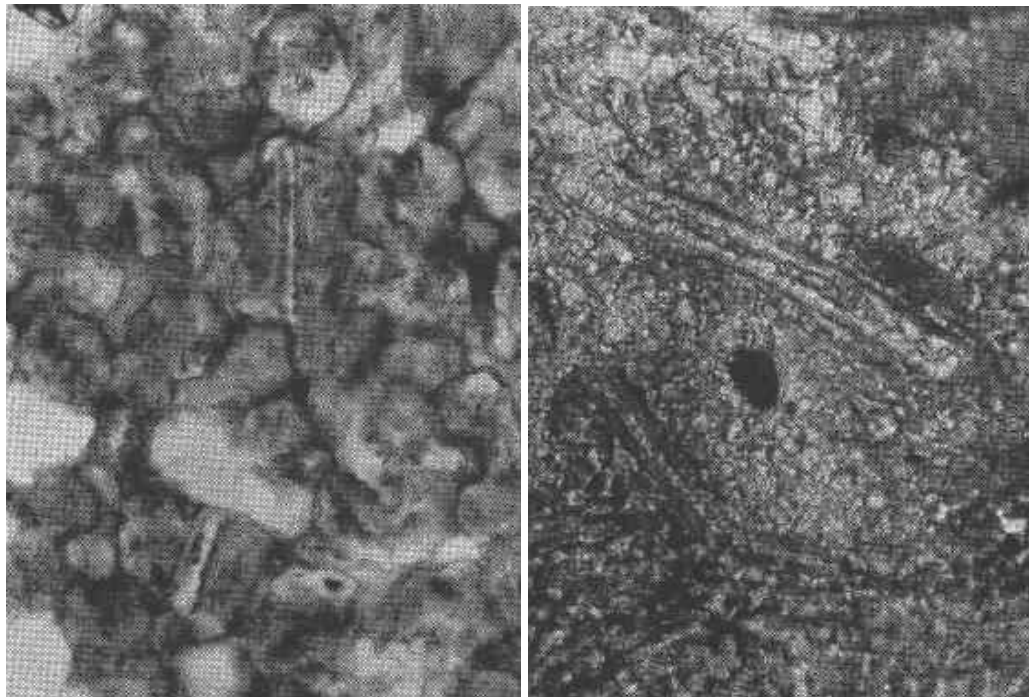


**Figure 96.** Photomicrographs showing a) free or grouped individual analcime crystals b) analcime formation from volcanic glass (Ross, 1928).

Ross (1928) further claimed that the tuff structure in altered material is generally not well preserved but traces of it occur as ghost-structures with analcime (Figure 96-a). He also showed that analcime grains were formed within altered glass shard as shown in Figure 96-b. Thus, it was put forward that the reaction of glassy volcanic ash and sodium salts formed analcime rather than bentonite, the normal product when glassy volcanic ash breaks down.

Bradley (1928) also described similar occurrence of analcime and mentioned that analcime is formed as a result of interactions between various salts dissolved in lake water and dissolution products of volcanic ash. It was also mentioned that

analcime is formed by reaction of volcanic glass with Na-rich water (Iijima, 1980; Iijima and Utada, 1966; Tyrell and Peacock, 1926).

## 2) Precipitation from saline alkaline water

Some saline alkaline lake deposits contain analcime but lack significant volcanic material (e.g. glass shards). This suggests that analcime may precipitate directly from saline-alkaline lake water in arid regions (Hay, 1966; Van Houten; Iijima and Utada, 1966; Wu, 1970). According to Wu (1970) factors that affect chemical precipitation of analcime are mainly high pH, salinity and sodium availability. Wu (1970) also stated that an increase in salinity would lower the activity of water. If activity of water decreases, less hydrous phases will be preferred. That is, if the salinity increases less hydrous phases (such as analcime) precipitate rather than more hydrous phases (Table 1). High proportion of Na cations is also important for the formation of analcime. Evaporation in moderately saline alkaline-lake water provides Na-rich brines and this causes the formation of analcime (Remy and Ferrel, 1989).

## 3) Formation from precursor zeolite

Surdam and Sheppard (1978), however, claimed that analcime does not form directly from glass. It forms from alteration of volcanic glass and alkali zeolite precursor; silicic glass + saline alkaline lake water → alkali zeolite + saline alkaline lake water → analcime (Surdam and Parker, 1972). Here analcime forms from precursor zeolite by increase in salinity and alkalinity. If salinity and alkalinity increases, the activity of water and Si/Al ratio decrease which causes the formation of analcime (Surdam and Sheppard, 1978).

## 4) Formation from gel and clay

In addition to alkali zeolites, gels (Surdam and Eugster, 1976; Surdam and Sheppard, 1978; Mariner and Surdam, 1970) derived from glass are considered as starting points for the formation of analcime in saline alkaline lakes. Surdam and Eugster (1976) studying the sediments at Lake Magadi, demonstrated that some analcime was formed from a hydrous sodium aluminosilicate gel. He proved the relationship between gel and analcime with XRD patterns, as shown in the XRD patterns (Figure 97). This finding was confirmed by Mariner and Surdam (1970) and Surdam and Sheppard (1978). The gels were not only formed in the solutions but also found adhering to some glass fragments as gelatinous precipitates.

Some other researchers (Keller, 1952; Hay and Moiola, 1963; Pipkin, 1967; Remy and Ferrell, 1989) suggested that analcime may have formed as an alteration product of clays deposited in saline-alkaline lakes. Keller (1952) described that the analcime originated from by the interaction of hydrous aluminium silicate (clay) minerals with sodium-rich waters. He concluded this result from the observation that no volcanic glass was available to form analcime. According to the Keller (1952), absence of volcanic glass indicates that aluminium and silica can only derive from aluminium silicate clay minerals.
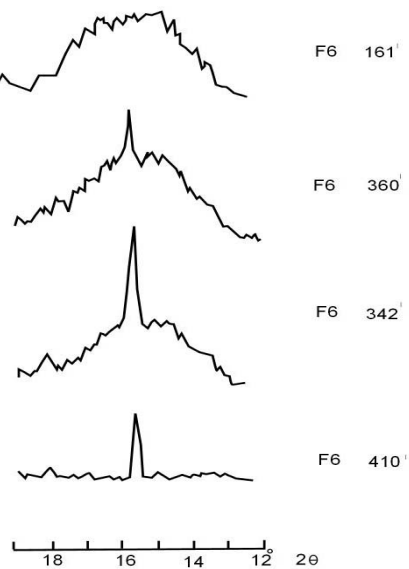
**Figure 97.** Diffractometer patterns glass and analcime from drill core of Lake Magadi, Kenya (After Surdam and Eugster, 1976).

*Analcime Formation in the Study Area*

## 1. Geological and Mineralogical constraints for the existence of saline-alkaline lake conditions

Analcimes in Arıklı Tuff are formed in lacustrine environment based on primary studies (Yılmaz et al, 2001; Çiftçi et al, 2004). Çiftçi et al. (2004) analyzed early-middle Miocene paleogeography of Küçükkuyu basin and he claimed that "the basin margin was probably defined by fault controlled elevated block at the north of the gulf of Edremit, whereas topographical highlands formed by volcanic eruption centers marked the margin at the south of the gulf". The imaginary figure of the Küçükkuyu basin are seen in Figure 98. Yılmaz et al (2001) also stated that the volcanic activity began about 20 million years ago in the Biga Peninsula. The volcanoes errupted not only lavas, but also pyroclastic ash as a result of huge

164

explosions. Important point is that the pyroclastic rocks were transported further away and were interbedded with lake deposits. Lake water is acidic at the time of eruption but later it changes to the alkaline conditions, being appropriate for the formation of analcime. Diatoms observed in some tuffs in petrographical study (i.e. ÇT-8) also indicate that the tuffs deposited in lacustrine environment (Figure 43).
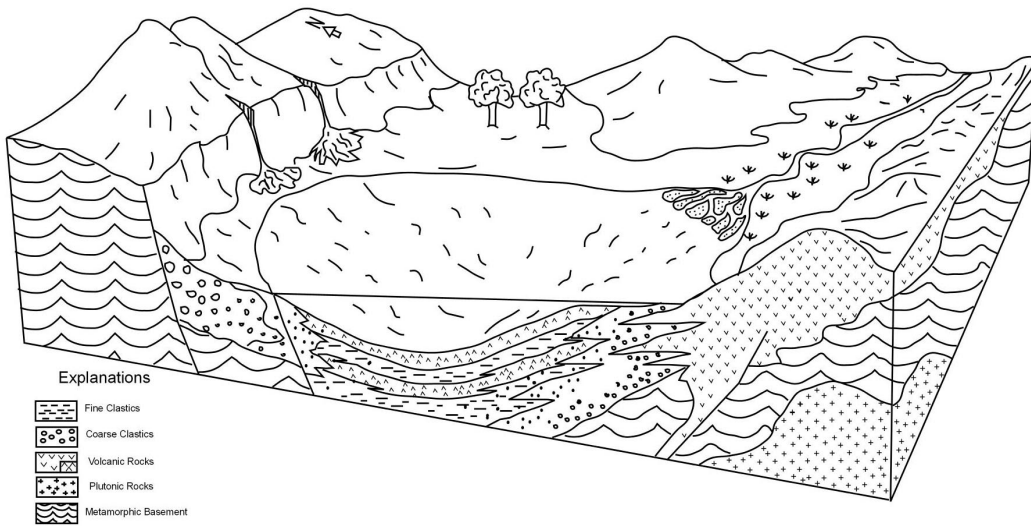


**Figure 98.** Early-middle Miocene paleogeography of the Küçükkuyu basin (After Çiftçi et al. 2004).

It was assumed that the studied analcimes were formed from moderately saline-alkaline lake part based on two observations;

1) Dolomite forms in high pH and alkaline lakes (Kelts and Hsü, 1978) and generally does not precipitate in freshwater lakes (Jones and Bowser, 1978). As dolomite can not precipitate in freshwater lakes, the occurrence of analcime confirm the alkaline lake conditions, where analcime can only be formed. Hence, it is obvious that the lake is not fresh but saline.

2) Carbonates in saline-alkaline lakes exhibit salinity-controlled zonations like zeolites, with calcite occurring near lake margins and dolomite ocurring in lake centers (Dyni, 1976). Although dolomite occurs towards lake centers, analcime can not form exactly in the lake center because in highly saline-alkaline environments analcime alters to K-feldspar (Surdam and Sheppard, 1978). In addition, no halite or other evaporite minerals that form under high saline environment were found in the studied samples. Although salinity and alkalinity of the lake at the time of analcime formation can not be measured directly, observations mentioned above suggest that the lake was only moderately saline and alkaline.

Alkaline environments having low Si/Al ratio are very suitable for the formation of analcimes (Table 1), because the solubility of rhyolitic glass increases and the ratio of silicon to aluminium decreases with increasing alkalinity. It was understood that the Si/Al ratio of analcimes in the Arıklı Tuff is low because dolomite is generally associated with low-silica analcime (Iijima and Hay, 1968).

## 2. Mineralogical and chemical constraints for the formation of analcime

One of the aims of this thesis is to understand the formation of analcime. This will be done by evaluation of the existing but limited field and laboratory data and observations, based on numerous theories about the formation of analcime in literature. For this account thin sections were investigated carefully, XRD data checked many times, lots of SEM images in literature were compared and DTA results were studied very carefully.

Prior to explaining the favorable modes of analcime formation, it will be discussed, why the two other formation types are not appropriate for formation of analcimes in Arıklı Tuff.

**1) Formation from precursor zeolite**

Surdam and Sheppard (1978) suggest that analcime in the saline-alkaline lake conditions forms from precursor alkali zeolites. A number of evidences, however, strongly suggest that analcime in Arıklı tuffs did not form from precursor alkali zeolites, derived from volcanic glass. First of all, thin section, XRD, SEM and DTA analyses show that analcime is the only zeolite in the Arıklı tuffs. There is no any evidence or even clue about the presence of other alkali zeolites except analcime. In addition, SEM studies must show alkali zeolites together with analcime, if it was formed from precursor zeolite. Besides Çelik *et all.* (1999) studied 500 rock samples, taken just from this thesis study region petrographically and mineralogically based on optical microscope and XRD method and they also did not find zeolites other than analcime type.

**2) Formation from gel and clay**

Surdam and Eugster (1976) proved the formation of analcime realized from hydrous aluminoslicate gel based on the XRD data (Figure 97). In this figure, amorphous material and analcime peaks can be easily observed in diffractometer patterns. The XRD patterns of all 30 Arıklı Tuff samples, however, indicated that there is no amorphous material in these tuffs. So, it is very difficult to interpret that analcime was formed from gel.

It was supposed that formation of analcime from clay is not appropriate. Firstly, there is no any of petrographic or SEM data about formation of analcimes from clay minerals. Secondly, since derivation of analcime from clay is not easy for chemically as mentioned by Keller (1952), the formation type from clay is excluded.

Finally, the following two modes of occurrence that were preferred for the formation of analcimes from the Arıklı Tuff will be discussed.

## 3) Analcime formation from volcanic glass

Many of authors suggested that analcime forms from volcanic glass (Ross, 1928; Bradley, 1928; Iijima, 1980; Iijima and Utada, 1966; Tyrell and Peacock, 1926). Volcanic glass is highly unstable and generally can not be protected in saline-alkaline lake waters. In the Arıklı Tuff, volcanic glass is usually absent except in two tuff samples (KK-2, KK-5), other types of volcanic fragments such as pumice fragments and rock fragments are found nearly in all tuffs. This is indicative for glass content previous to the alteration in the tuffs.

Surdam and Eugster (1976) supported that analcime does not form directly from the alteration of glass. He concluded this because analcimes he studied in the tuffaceous Magadi sediments in Kenya were commonly associated with alkali zeolite and there was no association of analcime with glass. Although the glass shards are usually not well preserved in Arıklı Tuff, two tuff samples (KK-2, KK-5) contain glass shards and these are associated with analcime as shown in Figure 99. Moreover, there is no association between analcime and other types zeolites. Since analcime crystals are very small size, it is generally difficult to observe analcime formations with petrographic study. SEM studies, on the other hand, are more useful to understand of analcime formation. For this reason, analcimes in the tuffs were investigated more carefully under SEM study for understanding formation mechanism.

To recognize the formation from glass not only SEM images, but also EDX spectrum of the samples were examined. EDX studies showed that volcanic glass found in tuffs is chemically suitable for the formation of analcime (Figure 81, 100). This is evidenced by the rich Na, Al and Si elements in the volcanic glass, which corresponds to the chemical composition of analcime too.
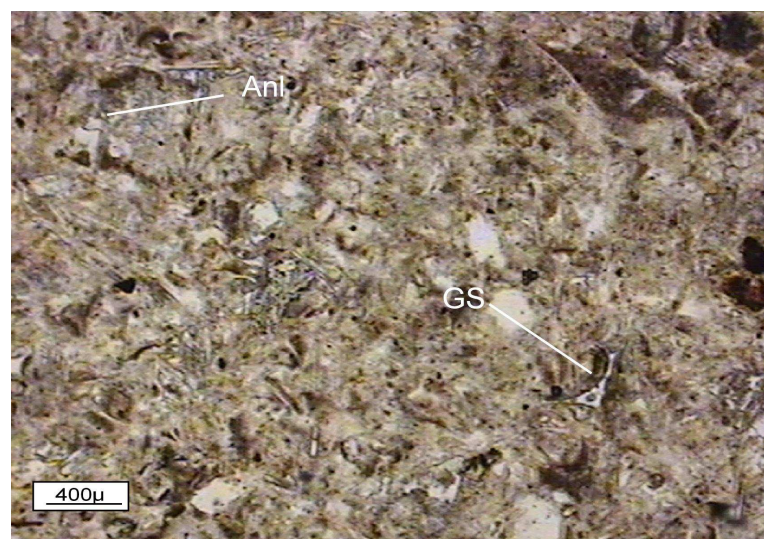
**Figure 99.** Photomicrograph showing glass shards and analcime (KK-2, PPL, Anl: analcime, GS: glass shard).
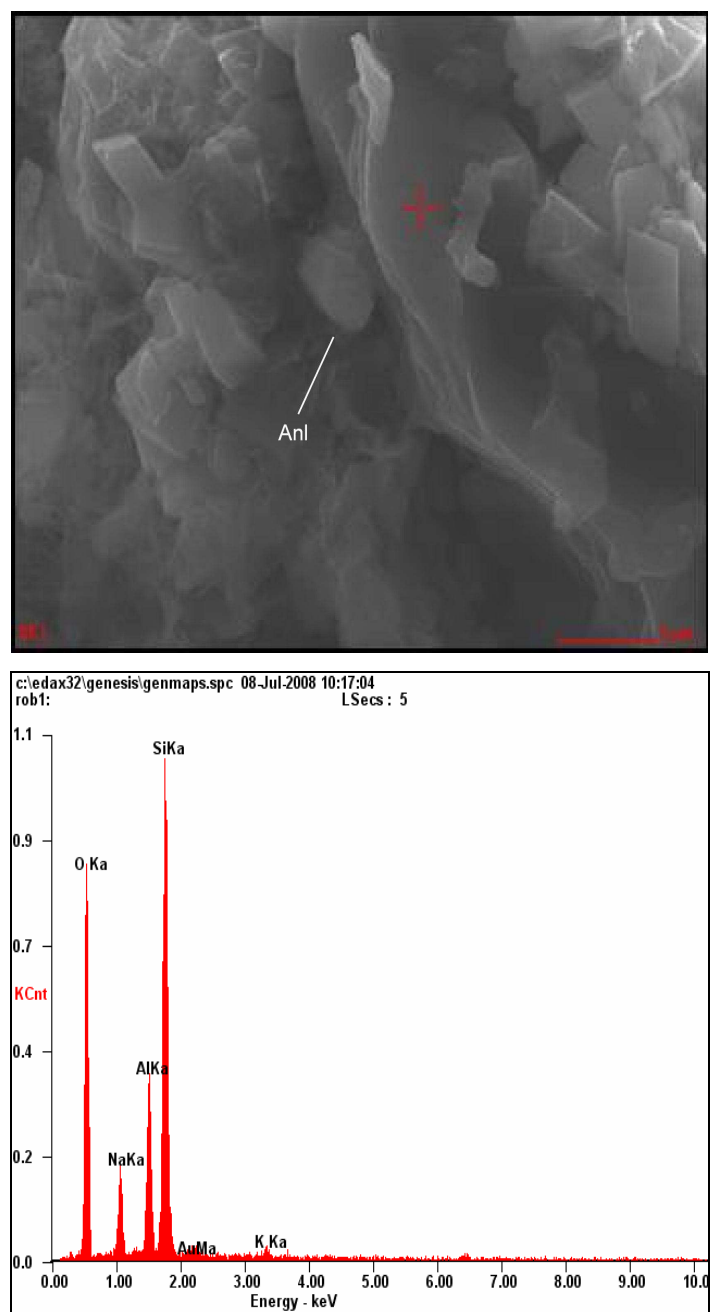
**Figure 100.** SEM photomicrograph and EDX graph from glass with analcime at its edge (KL-5, Anl: analcime).

In addition to EDX spectrum, SEM photomicrograps clearly indicate that analcime is formed from glass (Figures 70, 101) Figure 101 shows the best view that the authigenic analcime overgrows from the edge of glass.
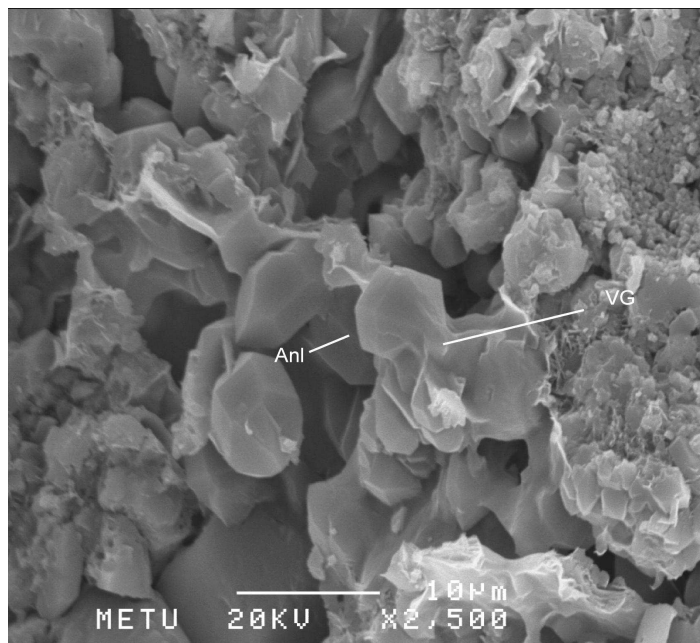


**Figure 101.** Scanning electron micrograph of authigenic analcime overgrowth at the edge of glass (ÇT-8, Anl: analcime, VG: volcanic glass).

By this, it was concluded that analcime was formed from volcanic glass. It was said that in petrography chapter there are analcimes in the matrix. That is, these analcimes founding in the matrix were formed from volcanic glass. This explains why there is some circular isotropic clusters observed in the matrix because of cryptocrystalline analcimes formed from glass in the matrix (Figure 32).

## 4) Analcime formation by precipitation

According to the Eugster and Hardie (1978) sodium is one of the most abundant ions in saline-alkaline lakes. During evaporative concentrations this sodium ions are precipitated together with dolomite.

Alkaline solutions include high amount of $Na^+$ ions because of own dissolution mechanism of glass (Casey and Bunker, 1990). The tuffaceous rocks have generally porous texture, which appropriate to circulate water in it. On this account, the circulating water which have $Na^+$ ions are easily precipitated in cavities of tuffs and form euhedral analcimes in cavities.

Thin section studies of the Arıklı Tuff proved that analcime is also found in the form of cement (Figure 27, 46). Analcime associated with dolomite might be directly precipitated from dissolved silica-rich alkaline lake water. It is not clear whether the dissolved silica has originated from detrital silicate grains or has originally concentrated in water.

Geochemistry studies showed that high amount of Na element is found in analcime-bearing tuffs with respect to analcime-free equivalents (Figure 91). In addition, Figure 94, 95 demonsrates the correlation of composition of Arıklı tuffs with theoretical rhyolitic tuff (TRT) and this figure showed that addition of Na+ ions in analcime-bearing tuffs with respect to TRT composition and loss of Na+ ions in analcime-free equivalents. It can be said that water, which reacts with volcanic glass resolves the Na+ ions from glass with dissolution mechanism and water enriched with Na+ ions. The residue glass composition is not enough to formation of analcime if water flows away. That is, tuffs, which were depleted by Na+ ions do not contain analcime. However, tuffs in which Na+ rich water precipitated, contain analcime.

Thus, it is suggested that the analcime crystals were directly precipitated from dissolved silica rich alkaline lake water.

To conclude, with the preliminary data we obtained by petrographic, mineralogic and geochemical studies there are two modes of occurrence for the formation of analcimes in Arıklı tuffs. These are formation from volcanic glass and precipitation.

# CHAPTER 7

# CONCLUSIONS

In terms of stratigraphy, the study area to the west of Biga peninsula between Ayvacık and Küçükkuyu comprises pre-Eocene basement rocks, volcanic unit, lacustrine sediments and alluvium. Behram Volcanics above the Eocene volcano-sedimentary units includes Arıklı Tuff, andesite, andesitic tuff and andesitic agglomerate. It is laterally and vertically transitional to the Miocene lacustrine sediments (Küçükkuyu Formation). Quaternay alluvium, on the other hand, forms the uppermost unit.

The dacitic-rhyolitic Arıklı Tuff, which is the main objective of this study, is Early-Middle Miocene in age and occurs as mainly massive and rarely bedded rocks which are generally yellow to white, whitish green in color. The thickness of single beds varies from 2 mm to 1 m. The Arıklı Tuff is overlain by andesitic agglomerate and lies conformably over the Küçükkuyu Formation.

The Arıklı Tuff is petrographically composed of varying amounts of quartz, biotite, plagioclase and sanidine as primary phenocrysts, analcime, dolomite, K-feldspar and phyllosilicate as authigenic minerals, pumice fragments, glass shards and rock fragments as lithic components. Based on the dominance of authigenic minerals in the matrix, the tuffs are petrographically separated into three main groups. These groups are phyllosilicate-, dolomite- and K-feldspar-dominant types. Glass shards are mainly altered but may be observed in some samples (e.g. sample KK-5) which are grouped as phyllosilicate-bearing vitric tuff or as K-feldspar-dominated vitric tuff (e.g. KK-2).

174

Fine-grained and coarse-grained analcime crystals were determined by their typical optical properties. They are colorless, isotropic, trapezohedral and have low relief. Analcime crystals are mainly euhedral or subhedral in pumice fragments or cavities and anhedral in the matrix. Even though presence of analcimes with very minute size in the matrix can not been observed petrographically even with very high mignification (x40), some predictions were made based on the similarity of isotropic coarse-grained clusters which are observed petrographically in the matrix. Still, the abundance of analcime can not be exactly measured (as volume %) due to very fine grain size, but the visual estimations in different samples range between 10-35 %.

Two modes of occurrences of analcime are noticed; coarse-grained euhedral or anhedral crystals in cavities and pumice fragments and clusters or single crystals of fine-grained analcimes embedded in the matrix. Analcime associates with phyllosilicate, dolomite and K-feldspar. Petrographically five thin sections do not contain analcime. From these, samples KK-8, KK-2, A-2 and YÇT-9 are grouped as K-feldspar-bearing tuffs and YÇT-8 is grouped as phyllosilicate- rich ones. All of dolomitic samples (A-9, A-12, ÇT-8, Y-12, ÇT-10, ÇT-19, Çt-20) on the other hand, contain analcimes.

XRD analyses confirmed the presence of analcime. The characteristic peaks of analcime were found on the XRD patterns of 25 samples. No other zeolite type was determined by XRD analysis. Detailed clay mineral analysis confirmed the presence of smectite. Quartz, dolomite and K-feldspar were also observed in XRD analyses.

Scanning Electron Microscopy (SEM) studies also confirmed the presence of analcime crystals of approximately 5-10 μm diameter with characteristic cubo-octahedral and trapezohedral morphology. Two types of analcime occurrences were determined by SEM-analyses. Subhedral to euhedral analcime crystals in pore spaces indicate that precipitation of analcime from alkaline lake water and

analcimes at the edge of volcanic glass indicate that analcime formation by alteration of volcanic glass. EDX spectrums of glasses with analcime on their edges display a relative peak height of Na, Al, Si elements, that also proved the formation from glass.

DTA method also confirmed the presence of analcime by displaying a typical broad endothermic peak between 200-400 ℃ indicating the loss of adsorbed water.

Rock types of Arıklı Tuff could not be specifically characterized because of alteration. To identify the nature of parent material and to understand the formation of analcime trace element diagrams were used. Tuffs plotted in rhyolite, trachyandesite and just on the border of ryholite-trachyandesite fields by using immobile elements as discriminators. Arıklı Tuff plotted in triangular diagrams were also discriminated as three groups; phyllosilicate present, dolomite rich and analcime-free ones, confirming the petrographical classification. LOI values are shown to be higher in samples that contain analcime. Elements correlation diagrams show the depletion of Na in analcime-free samples. All phyllosilicate-bearing samples show average element values except analcime-free and dolomite rich tuffs. Diagrams based on an empirical calculation, analcime-free tuffs show Na depletion and K enrichment, analcime-bearing ones, however, display reverse relations.

There are two modes of occurrences for the formation of analcimes. These are formation from volcanic glass and precipitation from alkaline lake water. Formation from glass was proved both petrographical and SEM studies. Petrographical study showed the presence of analcime together with volcanic glass. This association indicated possible formation from glass but, the SEM study, the most reliable method for interpretation, proved that analcime was formed from glass. Precipitation from alkaline solutions can easily be determined with petrographical examinations.

176

In addition to all these conclusions, it is recommended for future work to investigate the analcimes by more detail mineralogical (e.g. atomic arrangements, crystal structure, etc) and geochemical (crytal chemistry) methods.

# REFERENCES

Adatte, T., Stinnesbeck, W., and Keller, G., 1996. Lithostratigraphic and mineralogic correlations of near K/T boundary clastic sediments in northeastern Mexico: Implications for origin and nature of deposition. Geological Society of America Special Paper 307, 211-226.

Ataman, G., 1977. Batı Anadolu zeolit oluşumları. Yerbilimleri 3, 85-95.

Ataman, G., and Beseme, P., 1972. Decouverte de Analcime sedimentaire en Anatolie du Nord-Ouest (Turquie). Mineralogie, Genese, Paragenese. Chem. Geol., 9, 203-225.

Ataman, G., and Gündoğdu, N., 1981. Anadolu tersiyerinde analsimli zonlar ve bunların jeolojik konumu. Yerbilimleri 7, 9-14.

Baldar, N. A., and Whittig, L. D., 1968. Occurrences and synthesis of soil zeolites. Proc. Soil. Sci. Amer. 32, 235-238.

Bates, R, L., and Jackson, J.A. 1980. Glossary of Geology. Virginia.

Bingöl, E., Akyürek, B., and Korkmazer, B. 1973. Biga yarımadasının jeolojisi ve Karakaya formasyonunun bazı özellikleri. Cumhuriyetin 50.Yılı Yerbilimleri Kongresi Tebliğler Kitabı, MTA Enstitüsü, 70-76.

Borchardt, G., 1989. Smectites. In minerals in Soil Environments. J. B. Dixon and S. B. Weed (eds.), SSSA Book Series, Madison, 675-727.

Borsi, S., Ferrara, C., Innocenti, F., and Mazzudi, R. 1972. Geochronoly and petrology of recent volcanics of Eastern Aegean Sea. Bull. Volcan., 36, 473-496.

Bradley, W.H., 1928. Zeolite beds in the Green River Formation. Science 67, 73-74.

Brobst, D. A., and Tucker, J. D., 1973. X-ray mineralogy of the Parachute Creek Member, Green River Formation, in the northern Piceance Creek basin, Colorado. U. S. Geol. Surv. Prof. Pap. 803, 55pp.

Çelik, E., Ayok, F., and Demir, N. 1999. Ayvacık-Küçükkuyu (Çanakkale) Bölgesi fosfat cevherleşmesi maden jeolojisi raporu. MTA Raporu 10228.

Çiftçi, N. B., Temel, R. Ö., and Terzioğlu, M.N., 2004. Edremit Körfezi civarının Neojen stratigrafisi ve hidrokarbon sistemi. TPJD Bülteni 16(1), 81-104.

Coombs, D. S., 1971. Present status of zeolite facies, In: Molecular Sieve Zeolites-I, Advances in Chemistry Series 101. Amer. Chem. Soc., Washington D. C., 317-327.

Cooms, D. S., 1955. X-ray observations of wairakite and non-cubic analcime. Miner. Mag., 30, 699-708.

Cronstedt, A. F., 1756. Observation and description of an unknown kind of rock to be named zeolites (in Swedish) . Kongl. Vetenskaps Acad. Handl. Stockh., 17, 120-123.

Dönmez, M., Akçay, A. E., Genç, Ş. C., and Acar Ş., 2005. Biga yarımadasında orta-üst eosen volkanizması ve denizel ignimbritler. MTA Dergisi 131, 49-61.

Ercan, T., 1979. Batı Anadolu, Trakya ve Ege adalarındaki Senozoyik volcanizması. Jeo. Müh. Derg., 9, 23-46.

Ercan, T., 1996. Biga ve Gelibolu Yarımadaları ile Gökçeada, Bozcaada ve Tavşan adalarının jeolojik, arkeolojik ve tarihi özellikleri. MTA Genel Müdürlüğü, Yerbilimleri ve Kültür Serisi, No: 1.

Ercan, T., Satır, M., Sevin, D., and Türkecan, A., 1996. Batı Anadolu'daki tersiyer ve kuvaterner yaşlı volkanik kayaçlarda yeni yapılan radyometrik yaş ölçümlerinin yorumu. MTA Dergisi 119, 103-112.

Ercan, T., Satır, M., Steınıtz, G., Dora, A., Sarıfakıoğlu, E., Adis, C., Walter, H. J., and Yıldırım, T., 1995. Biga yarımadası ile Gökçeada, Bozcaada ve Tavşan Adalarındaki ( KB Anadolu) tersiyer volkanizmasının özellikleri. MTA Dergisi 117, 55-86.

Ercan, T., Türkecan, A., Gullou, H., Satır, M., Sevin, D., and Saroğlu, F., 1998. Features of the tertiary volcanism around sea of Marmara. Mineral Res. Expl. Bull., 120, 97-118.

Ertürk, O., Dinçöz, E., and Alaygut, D., 1990. Petrology of the Cenozoic volcanics in the Biga Peninsula, NW Turkey. International Earth Sciences Congres on Aegean Region Proceedings, II, 368-384.

Esenli, F., Uz, B., Suner, F., Esenli, V., Ece, Ö. I. and Kumbasar, I. 2005. Zeolitization of tuffaceous rocks in the Keşan region, Thrace, Turkey. Geologia Croatica 58/2, 151-161.

Eskola, P., 1936. A paragenesis of gedrite and cummingtonite from Isopaa in Kalvola, Finland. Bull. Comm. Geol. Finlande 115, 475-487.

Fenner, C. N., 1936. Bore-hole investigations in Yellowstone Prak. J. Geol. 44, 225-315.

Ferraris, G., Jones, D. W., and Yerkess, J. 1972. A neutron diffraction study of crystal structure of analcime $NaAlSi_2O_6.H_2O$. Zeitschrift für Kristallographie 135, 240-252.

Fisher, R. V., and Schmincke, R. V., 1984. Pyroclastic Rocks. Springer-Verlag, Berlin, 472 pp.

Gevrek, A.İ., Şener, M., and Ercan, T., 1984-1985. Çanakkale -Tuzla jeotermal alanının hidrotermal alterasyon etüdü ve volkanik kayaçların petrolojisi. 103-104, 55-82.

Gottardi, G., 1978. Mineralogy and crystal chemistry of zeolites: in Natural Zeolites: Occurrence, Properties, Use, Sand, L. B., and Mumpton, F. A., eds., Pergamon Press, Elmsford, New York, 31-44.

Gottardi, G., and Galli, E., 1985. Natural Zeolites. Springer-Verlag, Berlin, Germany.

Gözler, M. Z. 1986. Kazdağ batısı mıhlı dere vadisinin jeolojik ve petrografik incelenmesi. Türkiye Jeoloji Kurumu Bülteni C.29, 133-142.

Grim, R. E., 1968. Clay Mineralogy. McGraw-Hill, New York, 596 pp.

Haüy, R. J., 1801. Traite de mineralogie, Vol 3. Ches Louis, Paris, p. 180.

Hay, R, L., 1963b. Zeolitic weathering in Olduvai Gorge, Tanganyika. Geol. Soc. Amer. Bull. 74, 1281-1286.

Hay, R. L. 1978. Geologic occurrence of zeolites: in Natural Zeolites: Occurrence, Properties, Use, L. B. Sand and F. A. Mumpton, eds., Pergamon Press, Elmsford, New York, 135-143.

Hay, R. L., 1966. Zeolites and zeolitic reactions in sedimentary rocks. Geol. Soc. Amer. Spec. Paper 85, 130.

Hay, R. L., 1970. Silicate reactions in three lithifacies of a semiarid basin, Olduvai Gorge, Tanzania. Mineral. Soc. Amer. Spec. Papers 3, 237-255.

Hay, R. L., 1977. Geology of zeolites in sedimentary rocks. In Mineralogy and Geology of Natural Zeolites. F. A. Mumpton, ed., Reviews in Mineralogy 4, Mineralogical Society of America, Washington, D. C., 53-64.

Hay, R. L., and Moiola, R. J., 1963. Authigenic silicate minerals in Searles Lake, California. Sedimentology 2, 312-332.

Hazen, R. M., and F,nger, L. W., 1979. Polyhedral tilting: a common type of pure displacive phase transition and its relationship to analcite at high pressure. Phase Transitions 1, 1-22.

High, L. R. and Picard, M. D. 1965. Sedimentary petrology and origin of analcime-rich Popo Agie member, Chugwater (triassic) formation, west-central Wyoming. Journal of Sedimentary Petrology 35(1), 49-70.

Iijima, A. and Utada, M. 1966. Zeolites in sedimentary rocks, with reference to the depositional environments and zonal distribution. Sedimentology 7, 327-357.

Iijima, A., 1980. Geology of Natural Zeolites and Zeolitic Rocks. Pure and Appl. Chem. 52, 2115-2130.

İnci, U., 1984. Demirci ve Burhaniye bitumlu şeyllerinin stratigrafisi ve organik özellikleri. Türkiye Jeoloji Kurumu Bülteni 5, 27-40.

İşseven, T., Tapırdamaz, M.C., Özçep, F., Hisarlı, M., Orbay, N. and Sanver, M. 1995. Kuzeybatı Anadolu'nun tectoniği ve paleomanyetik sonuçlar. Jeofizik 9, 10, 201-212.

Jackson, M. L. 1975. Soil Chemical Analysis-Advance Course. $2^{nd}$ Edition, $10^{th}$ printing. Published by Author: Madison, Wisconsin, 53705.

Johannsen, A., 1914. Petrographic analysis of the Bridger, Washikie and other Eocene Formations of the Rocky Mountains. Bull. Amer. Mus. Nat. Hist., 33-209-222.

Kacmaz, H. and Kokturk, U. 2004. Geochemsitry and mineralogy of zeolitic tuffs from the Alacatı (Cesme) area, Turkey. Clays and Clay Minerals 52(6), 705-713.

Karacık, Z., and Yılmaz, Y., 1995. Geology of the ignimbite eruptions of Ezine-Ayvacık region NW Anatolia. Int. Earth Sci. Colloquium on the Aegean Region (IESCA) Proceedings, pp. 415-427.

Karacık, Z., and Yılmaz, Y., 1998. Geology of ignimbrites and the associated volcano-plutonic complex of the Ezine area, northwestern Anatolia. Journal of Volcanology and Geothermal Research 85, 251-264.

Keller, W. D. 1952. Analcime in the Popo agie member of the Chugwater formation. Journal of Sedimentary Petrology 22 (2), 70-82.

Kitsopoulos, K. P., Scott, P. W., Jeffrey, C. A., and Marsh, N. G., 2001. The minerraloy and and geochemistry of zeolite-bearing volcanics from Akrotiri (Santorini İsland) and polyegos (Milos group of islands), Greece. Implications for

geochemical classification diagrams. Bulletion of the Geological Society of Greece 34(3), 859-865.

Klein, C., 2002. The 22$^{nd}$ Edition of the Manual of Mineral Science (after J. D. Dana). John Wiley and Sons, Inc., New York, 641 pp.

Koizumi, M., 1953. The differential thermal analysis curves and the dehydration curves of zeolites. Mineralogical Journal 1 (1), 36-47.

Kubler, B., 1987. Cristallinite de illite, methods normalisees de preparation, methodes normalisees de measures. Neuchatel, Suisse, Cahiers Inst. Geologie, Ser ADX 1, 13 pp.

Le Bas, M. J., Le Maitre, R. W., Streckeisen, A., and Zanettin, B., 1986. A chemical classification of volcanic rocks based on the total alkali-silica diagram. Journal of Petrology 27, 745-750.

Mackenzie, R. C., 1957. The differential thermal investigation of clays. Mineralogical Society, London, 456 pp.

Mazzi, F., and Galli, E., 1978. Is each analcime different? Am. Miner., 63, 448-460.

Mumpton, F. A., 1978. Natural zeolites: a new industrial mineral commodity: in Natural Zeolites: Occurrence, Properties, Use, Sand, L. B., and Mumpton, F. A., eds., Pergamon Press, Elmsford, New York, 3-27.

Mumpton, F. A., and Ormsby, W. C., 1978. Morphology of zeolites in sedimentary rocks by scanning electron microscopy: in Natural Zeolites: Occurrence, Properties, Use, Sand, L. B., and Mumpton, F. A., eds., Pergamon Press, Elmsford, New York, 113-132.

Munson, R. A., and Sheppard, R. A., 1974. Natural zeolites: their properties, occurrences, and uses: Minerals Sci. Engng 6, 19-34.

Murray, J., and Renard, A. F., 1891. Report on the scientific results of the voyage of "HMS Challenger" during the yeras 1873-1876. Neill, Edinburg.

Okay, A. İ. and Göncüoğlu, M. C. 2004. The Karakaya complex: A review of data and concepts. Turkish Journal of Earth Sciences 13, 77-95.

Okay, A. İ., and Satır, M., 2000(a). Upper cretaceous eclogite-facies metamorphic rocks from the Biga Peninsula, Northwest Turkey. Turkish Journal of Earth Sciences 9, 47-56.

Okay, A. İ., and Satır, M., 2000(b). Coeval plutonism and metamorphism in a latest Oligocene metamorphic core complex in northwest Turkey. Geol. Mag. 137(5), 495-516.

Okay, A. İ., Siyako, M., and Bürkan, K. A., 1990. Biga Yarımadası'nın jeolojisi ve tectonic evrimi. TPJD Bülteni C.2/1, 83-121.

Öngür, T., 1973. Çanakkale-Tuzla yöresinin volcanolojisi ve jeotermal enerji olanakları. MTA Raporu, 5510.

Pettijohn, F. J., 1975. Sedimentary Rocks. 2$^{nd}$ ed., New York, Harper and Row, 718 p.

Raymond, L. A., 1995. Petrology: The study of igneous, sedimentary and metamorphic rocks. WCB/McGraw-Hill, 742 p.

Ross, C. S., 1928. Sedimentary analcite. American Mineralogist 13, 195-197.

Sheppard, R. A., 1971. Zeolites in sedimenatry deposits of the United States. A review in Molecular Sieve Zeolites-I,R. F. Gould, ed., Amer. Chem. Soc. Advances in Chemistry Series 101, 2790-310.

Sheppard, R. A., 1973. Zeolites in sedimentary rocks. U. S. Geol. Surv. Profess. Paper 820, pp. 689-695.

Sheppard, R. A., and Gude, A. J., 1968. Distribution and genesis of authigenic silicate minerals in tuffs of Pleistocene Lake Tecopa, Inyo County, California. U. S. Geol. Surv. Profess. Paper 597, p. 38.

Sheppard, R. A., and Gude, A. J., 1969a. Diagenesis of tuffs in the Barstow Formation, Mud Hills, San Bernardio County, California. U. S. Geol. Surv. Profess. Paper 634, p. 35.

Siyako, M., Burkan, K. A., and Okay, A.I., 1989, Biga ve Gelibolu yarımadalarının Tersiyer jeolojisi ve hidrokarbon olanakları. TPJD Bülteni C. 1/3, 183-199.

Slaughter, M., and Earley, J. W., 1965. Mineralogy and geological significance of the Mowry bentonites, Wyoming. Geol. Soc. Am. Spec. Pap., 83, 95 p.

Smykatz-Kloss, W., 1974. Differential Thermal Analysis: application and results in mineralogy. Springer-Verlag, Berlin, 185 pp.

Surdam, R. C. and Eugster, H. P. 1976. Mineral reactions in the sedimentary deposits of the lake Magadi region, Kenya. Geological Society of America Bulletin 87, 1739-1752.

186

Surdam, R. C. and Sheppard, R. A. 1978. Zeolites in saline, alkaline-lake deposits: in Natural Zeolites: Occurrence, Properties, Use, L. B. Sand and F. A. Mumpton, eds. Pergamon Press, Elmsford, New York, 145-174.

Surdam, R. C., and Parker, R. D., 1972. Authigenic aluminosilicate minerals in the tuffaceous rocks of the Green River Formation, Wyoming. Geological Society of America Bulletin 83, 689-700.

Taylor, W. H., 1930. The structure of analcite. Z Kristallogr., 74, 1-19.

Todor, D. N., 1976. Thermal analysis of minerals. Abacus Press, England, 256 pp.

Tröger, W. E., 1982. Optische Bestimmung der gesteinsbildenden Minerale. E. Schweizerbart'sche Verlagsbuchhandlung, Stutgart, Germany.

University of Georgia, www.uga.edu/caur/BeamSpec.ppt, last visited on September 2008.

Van Houten, F. B., 1962. Cyclic sedimentation and the origin of analcime-rich Upper Triassic Lockatong Formation, west-central New Jersey and adjacent Pennsylvanie. Amer. J. Sci. 260, 561-576.

Walton, A. W., 1975. Zeolitic diagenesis in Oligocene volcanic sediments, Trans-Pecos, Texas. Geol. Soc. Amer. Bull. 86, 615-624.

Welton, E. J., 1984. SEM Petrology Atlas The American Association of Petroleum Geologist, USA, 237 pp.

Williams, H., Turner, F, J., and Gilbert, C. M., 1982. Petrography: an introduction to the study of rocks in thin sections. 2nd Edition, W. H. Freeman and Company, San Francisco, 624 pp.

Wilson, M. J., 1987. A handbook of determinative methods in clay mineralogy. Chapman and Hall, New York, 308 pp.

Winchester, J. A., and Floyd, P. A., 177. Geochemical discrimination of different magma series and their differentiation products using immobile elements. Chem. Geol., 20, 325-343.

Wu, D. C., 1970. Origin of mineral analcite in the upper flowerpot shale, nortwestern Oklahoma. Transactions of the Kansas Academy of Science 73 (2), 247-251.

Yılmaz, Y., Genç, Ş. C., Karacık, Z., and Altunkaynak, Ş., 2001. Two contrasting magmatic associations of NW Anatolia and their tectonic significance. Journal of Geodynamics 31, 243-271.